A novel day/night-technique for area-wide precipitation retrieval over Central Europe using MSG SEVIRI data

kumulative
Dissertation
zur Erlangung des Doktorgrades
der Naturwissenschaften
(Dr. rer. nat.)

dem Fachbereich Geographie
der Philipps-Universität Marburg
vorgelegt von

Boris Thies
aus Hadamar

Marburg/Lahn, 8. Mai
2008

Vom Fachbereich Geographie
der Philipps-Universität Marburg als Dissertation am 15.05.2008
angenommen.

Erstgutachter: Prof. Dr. Jörg Bendix

Zweitgutachter: Prof. Dr. Georg Miehe

Tag der mündlichen Prüfung am 22.10.2008

Preface

At the end of my thesis I would like to thank all those people who made this thesis possible and a valuable experience for me.

First of all I wish to express my sincere gratitude to my supervisor Jörg Bendix, who guided this work and helped whenever I was in need. He at all times met my requests with open ears and was always ready to provide any support needed.

I am grateful to my colleagues at the Laboratory for Climatology and Remote Sensing for their support and their comradeship. I especially thank Thomas Nauß for many fruitful exchanges and scientific discussions as well as for his generous assistance during this time. He has been a source of enthusiasm and encouragement over the last years. Special thanks also to Christoph Reudenbach for his support and valuable comments especially during the early stages of this thesis. Moreover, I thank Jan Cermak for his help and assistance. The final thesis prepared by Andreas Turek was of great use in the context of this study. I thank Maik Dobbermann for his support and patience in providing the satellite data for this study.

I am very thankful to my colleagues within the GLOWA-Danube project for their co-operation. Especially I thank Barbara Früh (University of Karlsruhe, formerly University of Mainz), Andreas Pfeiffer (University of Munich), Hans Schipper (University of Karlsruhe, formerly University of Munich) as well as the project leader Wolfram Mauser (University of Munich).

I gratefully acknowledge the financial support by the Federal Ministry of Education and Research (BMBF) within the GLOWA-Danube project as well as by the German Research Council (DFG) within the SORT project.

Finally, I would like to express my deepest gratitude for the constant support and encouragement that I received from my parents and my sister. Moreover, I thank my partner Kerstin for her understanding and patience as well as for reminding me of the real priorities in life whenever needed.

Boris Thies

Marburg, Mai 2008

Contents

List of Figures

List of Tables

List of Acronyms and Symbols

ACT	Advective Convective Technique
a_{ef}	effective particle radius
AVHRR	Advanced Very High Resolution Radiometer
BT	Brightness Temperature
Cb	Cumulonimbus
CGMS	Coordination Group for Meteorological Satellites
Ci	Cirrus
CP	Cloud Phase
CSI	Critical Success Index
CSS	Cloud Classification System
CST	Convective Stratiform Technique
CTT	cloud Top Temperature
CWP	Cloud Water Path
CYCLES	CYCLonic Extra-tropical Storms
D_e	mean effective diameter of ice crystals
ΔT	Temperature Difference
DISORT	discrete ordinate solver
DWD	Deutscher Wetterdienst
ECST	Enhanced Convective Stratiform Technique
ESA	European Space Agency
ETS	Equitable Threat Score
EUMETSAT	European Organisation for the Exploitation of Meteorological Satellites
FAR	False Alarm Ratio
GARP	Global Atmosphere Research Programme
GATE	GARP Atlantic Tropical Experiment
GEO	Geostationary Orbit
GOES	Geostationary Operational Environmental Satellite
GPCP	Global Precipitation Climatology Project

GPI	GOES Precipitation Index
HKD	Hansen Kuipers discriminant
HSS	Heidke Skill Score
IPWG	International Precipitation Working Group
IR	Infrared
IWC	Ice Water Content
JAXA	Japanese Space Agency
LEO	Low Earth Orbit
LT	Local Time
LWC	Liquid Water Content
MFG	Meteosat First Generation
MODIS	Moderate Resolution Imaging Spectroradiometer
MSG	Meteosat Second Generation
MSS	Marburg Satellite Station
MVIRI	Metesoat Visible and Infra-Red Imager radiometer
NASA	National Space Agency
NIR	Near Infrared
NOAA	National Oceanic and Atmospheric Administration
Ns	Nimbostratus
PERSIANN	Precipitation Estimation from Remotely Sensed Information using Artificial Neural Networks
POD	Probability Of Detection
POFD	Probability Of False Detection
PR	TRMM Precipitation Radar
PMW	Passive Microwave
RADS-D	Rain Area Delineation Scheme during Day-time
RADS-N	Rain Area Delineation Scheme during Night-time
RAO	Research Announcement of Opportunity
R_e	effective radius of water droplets
ROC	Relative Operation Characteristic
SACURA	Semi-Analytical Cloud Retrieval Algorithm
SEVIRI	Spinning Enhanced Visible and InfraRed Imager

SRF	spectral response functions
SSM/I	Special Sensor Microwave Imager
SSP	Sub Satellite Point
τ	optical cloud thickness
TOGA-COARE	Tropical Ocean Global Atmosphere Coupled Ocean Atmosphere Response Experiment
TRMM	Tropical Rainfall Measurement Mission
UTC	Universal Time Code
VIS	Visible
VISSR	Visible and Infrared Spin Scan Radiometer
WCRP	World Climate Research Programme
WGDM	Working Group on Data Management
WGNE	Working Group on Numerical Experimentation
WMO	World Meteorological Organisation
WV	Water Vapour
WWRP	World Weather Research Program

CHAPTER 1

Motivation, Objectives and Structure

1 Motivation, Objectives and Structure

1.1 Motivation

Precipitation is a key parameter of the global water cycle and effects all aspects of human life and ecosystem processes. Area-wide information on its distribution in a high spatial and temporal resolution is indispensable for a proper determination of the local, regional and global water cycle and thus, for all climatological and hydrological studies (TRENBERTH et al. 2003; NEW et al. 2001; RODELL et al. 2004; MAURER et al. 2002). Furthermore, information about the spatio-temporal rainfall distribution is very important for now-casting and very short-change forecasting purposes warranting a surveillance of disastrous rainfall events and thus, the application of protection measures, but also the estimation of potential damages in risk management (e.g. MÜNCHNER RÜCK 2003; EVANS 2001; PORCÙ et al. 1997).

Despite the demand for area-wide precipitation information, its monitoring and forecasting in a sufficiently high spatial and temporal resolution is still a challenging task. This is mainly due to the high spatial and temporal variability of precipitation (DE GONCALVES et al. 2006; NEW et al. 2001), which hampers its correct detection and quantification.

Especially in the absence of a dense ground-based weather radar network, a strong demand for an alternative spatial precipitation detection system sufficient for the applications mentioned above exists. In this context, geostationary (GEO) weather satellite systems with their high spatial and temporal resolution offer a high potential for area-wide precipitation detection and monitoring.

Due to the poor spectral resolution of first generation sensors, most of the rainfall retrieval techniques based on optical satellite data of GEO systems developed so far, rely on a relationship between cloud top temperature measured in an infrared (IR) channel and the rainfall probability and intensity (e.g. ADLER & MACK 1984; ARKIN & MEISNER 1987; VICENTE et al. 1998). These so-called IR retrievals are based on the assumption that highly convective, precipitating clouds are characterized by a large vertical extension with a cloud top rising high into the atmosphere. As a consequence, cold cloud tops are assumed to be connected with high rainfall intensities. These precipitating cloud regions are divided into different sub-areas, to which different rainfall intensities are assigned by more enhanced IR retrieval techniques (e.g. REUDENBACH et al. 2001; REUDENBACH 2003;

REUDENBACH et al. 2007; HONG et al. 2004; HSU et al. 2002; PORCÙ et al. 1999; ADLER & NEGRI 1988; TSONIS 1987; O'SULLIVAN 1990; WU et al. 1985).

Such IR retrieval techniques are appropriate for convective clouds, that can be easily identified in the infrared and/or water vapour channels (e.g. LEVIZZANI et al. 2001; LEVIZZANI 2003), but show considerable drawbacks concerning mid-latitudinal precipitation systems of extra-tropical cyclones (hereafter denoted as advective-stratiform precipitation areas) (e.g. EBERT et al. 2007; FRÜH et al. 2007; KÄSTNER et al. 2006; ADLER et al. 2001; AMORATI et al. 2000; EBERT et al. 1998; POMPEI et al. 1995; NEGRI & ADLER 1993; LEVIZZANI et al. 1990). Such advective-stratiform clouds are mainly formed by widespread lifting processes along frontal zones and are characterized by relatively warm and a more homogeneous spatial distribution of cloud top temperatures, that differ not significantly neither between regions of different rainfall intensities nor between raining and non-raining cloud areas. Therefore, retrieval techniques based solely on IR temperature measurements lead to an underestimation of the detected rain area and to uncertainties concerning the assigned rainfall rate. In this context EBERT et al. (1998) claimed improvements for satellite rainfall estimation including an enhanced delineation of raining and non-raining areas as well as possible classification of rain into convective and advective-stratiform types. Likewise DE GONCALVES et al. (2006) demanded for improvements in remotely sensed precipitation fields before they could be used as input for e.g. hydrological models.

To overcome the drawbacks of existing IR retrieval techniques, several authors suggested to use optical and microphysical cloud parameters derived from multispectral data of new generation satellite systems (e.g. KOBAYASHI 2007; LENSKY & ROSENFELD 2003a,b; BA & GRUBER 2001; ROSENFELD & GUTMAN 1994; ROSENFELD & LENSKY 1998; ROSENFELD et al. 2004). NAUSS & KOKHANOVSKY (2006) proposed a technique for the low earth orbit (LEO) system Terra-MODIS (BARNES et al. 1998) to delineate precipitating cloud areas in mid-latitudes by using an auto-adaptive threshold for the effective particle radius (a_{ef}) as a function of the cloud optical thickness (τ). The technique is based on the conceptual model that precipitating cloud areas are characterized by a combination of (i) droplets large enough to fall against the updraft wind field within the cloud and (ii) a large enough vertical cloud extension, that favours the growth of precipitation droplets and prevents them from evaporation below the cloud bottom (see also LENSKY & ROSENFELD 2003b). Since neither the droplet spectrum nor the geometrical thickness of a cloud can be computed

without additional theoretical assumptions, the effective particle radius (HANSEN & TRAVIS 1974) and the cloud optical thickness are used as a measure for the particle size and the cloud thickness. As a consequence, precipitating cloud areas can be characterized by a large enough combination of a_{ef} and τ, i.e. a large enough cloud water path (CWP), which is linearly related to the product of a_{ef} and τ.

1.2 Objective of the work

The new European meteorological GEO system MSG (Meteosat Second Generation) with its payload SEVIRI (Spinning Enhanced Visible and InfraRed Imager) provides the enhanced spectral resolution (AMINOU 2002; SCHMETZ et al. 2002) to infer information about cloud properties (a_{ef}, τ) and offers the potential of an improved precipitation detection (LEVIZZANI et al. 2001; LEVIZZANI 2003). At the same time it allows the application of existing sophisticated IR retrieval techniques suitable for convectively dominated rainfall areas. Apart from its enhanced spectral resolution MSG SEVIRI offers a high spatial (3 by 3 km at sub satellite point) and temporal (15 minutes, compared to 2 scenes per day for LEO systems as Terra-MODIS) resolution necessary for a quasi-continuous area-wide monitoring of the rainfall distribution, which is essential for the applications introduced above. As a consequence, MSG SEVIRI offers the great potential to answer the demand for area-wide precipitation data sets in a high spatio-temporal resolution.

Since, no operational rainfall retrieval technique appropriate for the mid-latitudes exists for MSG SEVIRI the objective of the present work is:

- The development of an operational day- and night-time rainfall retrieval for MSG SEVIRI.

Following the identified drawbacks of existing retrieval techniques, the focus lies on the detection of precipitation fields in connection with extra-tropical cyclones in the mid-latitudes (see chapter 2.3).

The new developed retrieval technique relies on the conceptual model for an improved rain area delineation introduced above. Furthermore, the conceptual design is significantly extended, concerning the dominant precipitation processes in connection with extra-tropical cyclones, that lead to different rainfall intensities (see chapter 2.3):

- Beside its use for the identification of the rain area the cloud water path (which presents the product of the a_{ef} and τ; see chapter 2.4) is further related to the rainfall intensity.

- Information about the cloud phase is additionally incorporated for an improved rain area identification and rainfall intensity differentiation, since effective precipitation processes in mid-latitude frontal systems are mainly coupled to ice particles in the upper part of the clouds and the so called Bergeron-Findeisen process (HOUZE 1993; see chapter 2.3).
- Information about the cloud top height is related to the vertical extension and the resulting rainfall intensity of convective precipitation clouds (see chapter 2.4).

Based on the underlying considerations and the introduced conceptual model, the central hypotheses of this work are:

- MSG SEVIRI allows the discrimination of the rain area based on information about the cloud water path and the cloud phase.
- MSG SEVIRI allows the separation of subareas of differing precipitation processes and rainfall intensities based on information about the cloud water path, the cloud phase and the cloud top height.
- The discrimination of the rain area and the separation into subareas of differing precipitation processes and rainfall intensities can be performed with comparable accuracy during day- and night-time.

Addressing the needs and requirements identified, the central aims of the present work are:

- To develop a coherent day- and night-time technique for the detection of rain areas suitable for precipitation fields in connection with extra-tropical cyclones based on MSG SEVIRI.
- To develop a coherent day- and night-time technique for the process-based segmentation of subareas of different rainfall intensities based on MSG SEVIRI.

In this context the significant innovations of the newly developed day- and night-time rainfall retrieval technique for MSG SEVIRI can be formulated as follows:

- The development of a new technique for the detection of the rain area during day-time for MSG SEVIRI. The technique relies on information about the cloud water path and is extended by incorporating information about the cloud phase in the upper cloud regions, which is essential concerning precipitation processes in the mid-latitudes.
- The development of a new methodology for rain area identification during night-time for MSG SEVIRI based on

information about the cloud water path and the cloud phase. Since no technique for the retrieval of the cloud water path during night-time exists for SEVIRI, this requires the conception and development of an entirely new technique.

- The development of a new technique for precipitation process and rainfall intensity separation for MSG SEVIRI based on information about the cloud water path, the cloud phase in the upper cloud regions and the cloud top height. As no such technique exists for SEVIRI, this requires the development and assembly of an entirely new methodology.

An operational retrieval technique for MSG SEVIRI allowing an improved identification of the rain area and a proper rainfall intensity differentiation in quasi-continuous manner at high spatial and temporal resolutions is of valuable benefit for the applications presented above ranging from now-casting to climatological purposes. As pointed out by BENNARTZ (2007), beside the identification of precipitating areas the assignment of instantaneous precipitation rates at the ground level is typically associated with large uncertainties. As a consequence, recent studies in support of now-casting attempt to separate different rainfall intensity classes instead of rain rates at the ground (e.g. WENG et al. 2003).

The area under investigation chosen for the development and validation of the new technique is Central Europe, which can be regarded as sufficiently representative for mid-latitudes precipitation formation processes (see also chapter 2.3). Furthermore, the dense ground-based radar network of the German Weather Service (DWD 2005) provides reliable data for the development and validation of the new technique.

1.3 Structure of the thesis

The structure of the work is presented in figure 1. After the introduction a review of existing rainfall retrieval techniques based on optical satellite data is given in **Chapter 2.1**. From this review the need for the development of a rain area detection and process separation technique evolves (**Chapter 2.2**). The dominant precipitation processes in extra-tropical cyclones are introduced in **Chapter 2.3**. This forms the theoretical background for more detailed hypotheses and objectives as well as for the conceptual design of the newly developed technique for rain area identification and process-oriented intensity separation presented in **Chapter 2.4**.

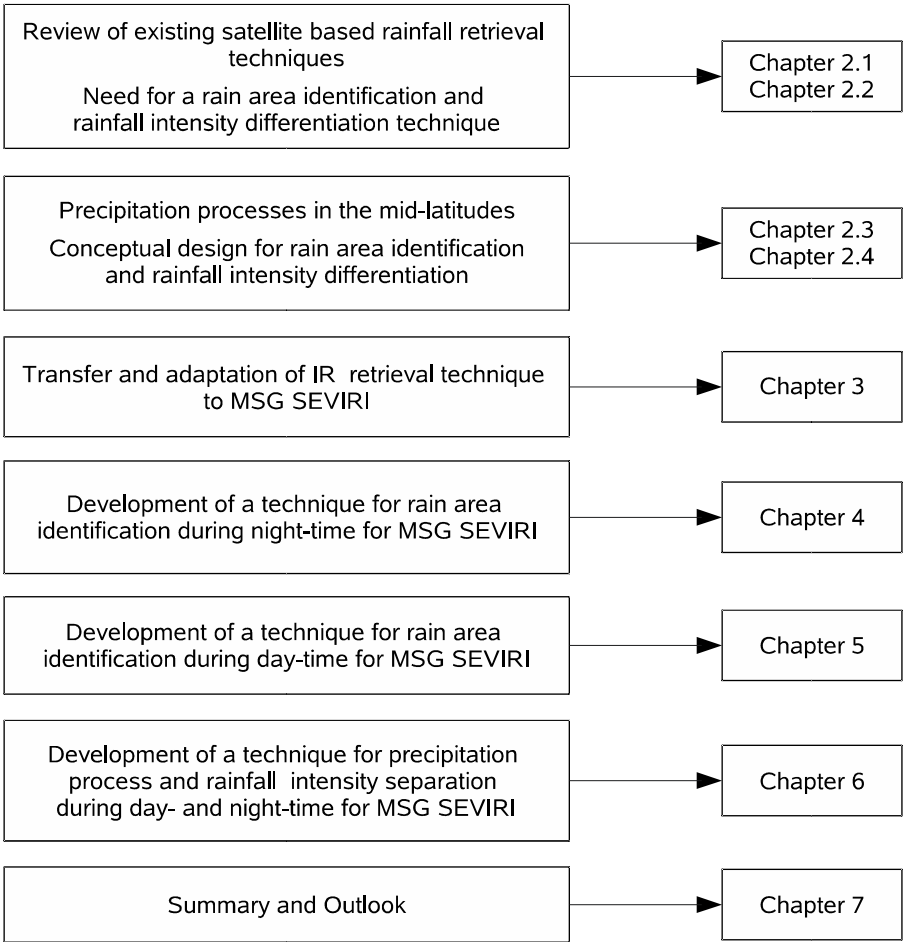

Figure 1.1: Structure of this work.

Chapter 3 presents the transformation of a first-generation IR retrieval technique appropriate for convective precipitation processes in the mid-latitudes to the second generation sensor. As pointed out in conjunction with the central aims of this work, the development of a coherent technique for the detection of raining cloud areas for MSG SEVIRI applicable during day- and night-time would be the first central objective. However, because the first-generation IR retrieval technique is also needed to assess the improvement attained by the new rain area discrimination technique, its transformation to MSG SEVIRI is tackled first.

In **Chapter 4** the newly developed technique for rain area detection using SEVIRI night-time data is introduced.

Chapter 5 describes the newly developed algorithm for the detection of raining cloud areas with SEVIRI during day-time.

In **Chapter 6** the novel technique for the separation of the rainfall area into subareas of differing precipitation processes and rainfall intensities during day- and night-time is presented.

Finally, in **Chapter 7** a summary of the previous chapters and an outlook are given.

The work was part of the GLOWA-Danube project with the aim to develop integrative and sustainable water management strategies to cope with regional effects of Global Change on the water cycle in the Upper Danube catchment (MAUSER et al. 2002). GLOWA-Danube is a subprogramme of the BMBF (Federal Ministry of Education and Research) programme GLOWA (Global Change in the Hydrological Cycle) as a major approach towards the realisation of integrative, interdisciplinary and application-oriented Global Change research.

Furthermore, the work of the SORT (SEVIRI Operational Rainfall Retrieval Technique) project founded by the German Research Council DFG (BE 1780/18-1).

It is also integrated into the Advanced Multi-Sensor Precipitation Estimate Project (AMPE) with the objective to develop a new integrative rainfall retrieval technique based on current MW sensors and MSG SEVIRI as well as into the wider framework of the MSG Principal Investigator Research Announcement of Opportunity (RAO) programme conducted by the European Space Agency (ESA) and the European Organisation for the Exploitation of Meteorological Satellites (EUMETSAT).

The work also concurs with the main objective of the International Precipitation Working Group (IPWG) a permanent Working Group of the Coordination Group for Meteorological Satellites (CGMS) and the World Meteorological Organisation (WMO) on operational and research satellite based quantitative precipitation measurement issues and challenges.

References

ADLER, R. F. & R. A. MACK (1984): Thunderstorm cloud height-rainfall rate relations for use with satellite rainfall estimation techniques. - *Journal of Climate and Applied Meteorology, 23*: 280 – 296.

ADLER, R. F. & A. J. NEGRI (1988): A satellite technique to estimate tropical convective and stratiform rainfall. - *Journal of Applied Meteorology, 27*: 30–51.

ADLER, R. F., C. KIDD, G. PETTY, M. MORISSEY & H. M. GOODMAN (2001): Intercomparison of global precipitation products: The third

precipitation intercomparison project (PIP-3). - *Bulletin of the American Meteorological Society, 82:* 1377-1396.

AMORATI, R., P. P. ALBERONI, V. LEVIZZANI & S. NANNI (2000): IR-based satellite and radar rainfall estimates of convective storms over Northern Italy. - *Meteorological Applications, 7*: 1-18.

AMINOU, D. M. A. (2002): MSG's SEVIRI instrument. - *ESA Bulletin, 111*: 15–17.

ARKIN, P. A. & B. N. MEISNER (1987): The relationship between large-scale convective rainfall and cold cloud over the western hemisphere during 1982-84. - *Monthly Weather Review, 115*: 51-74.

BA, M. B. & A. GRUBER (2001): GOES Multispectral Rainfall Algorithm (GMSRA). - *Journal of Applied Meteorology, 40*: 1500-1514.

BARNES, W. L., T. S. PAGANO & V. V. SALOMONSON (1998): Prelaunch characteristics of the Moderate Resolution Imaging Spectroradiometer (MODIS) on EOS-AM1. - *IEEE Transactions on Geoscience and Remote Sensing, 36:* 1088–1100.

BENNARTZ, R. (2007): Passive microwave precipitation measurements at mid- and high-latitudes. In: LEVIZZANI, V., P. BAUER, & F. J. TURK (Ed.): Measuring precipitation form space. - *Advances in global change research, 28*. Springer: Netherlands.

DE GONCALVES, L. G. G., W. J. SHUTTLEWORTH, B. NIJSSEN, E. J. BURKE, J. A. MARENGO, S. C. CHOU, P. HOUSER & D. L. TOLL (2006): Evaluation of model-derived and remotely sensed precipitation products for continental South America. - *Journal of Geophysical Research, 111:* D16113, doi:10.1029/2005JD006276.

DWD (2005): Weather radar network. - Available online at http://www.dwd.de/en/Technik/Datengewinnung/Radarverbund/Radarbroschuere_en.pdf, 10 November 2007.

EBERT, E. E. & M. J. MANTON (1998): Performance of Satellite Rainfall Estimation Algorithms during TOGA COARE. - *Journal of Atmospheric Sciences, 55*: 1538-1557.

EBERT, E. E., J. E. JANOWIAK & C. KIDD (2007): Comparison of near-real-time precipitation estimates from satellite observations and numerical models. - *Bulletin of the American Meteorological Society, 88*: 47–64.

EVANS, J. E. (2001): Tactical weather decision support to complement "strategic" traffic flow management for convective weather. 4th USA/ Europe Air Traffic Management R&D Seminar, Santa Fe, New Mexico.

FRÜH, B., J. BENDIX, T. NAUSS, M. PAULAT, A. PFEIFFER, J. W. SCHIPPER, B. THIES & H. WERNLI (2007): Verification of precipitation from regional climate simulations and remote-sensing observations with respect to ground-based observations in the upper Danube catchment. - *Meteorologische Zeitschrift, 16*: 275–293.

HANSEN, J. E. & L. D. TRAVIS (1974): Light scattering in planetary atmospheres. - *Space Science Reviews, 16*: 527–610.

HONG, Y., K.-L. HSU, S. SOROOSHIAN & X. GAO (2004): Precipitation Estimation from Remotely Sensed Imagery Using an Artificial Neural Network Cloud Classification System. - *Journal of Applied Meteorology, 43*: 1834-1852.

HOUZE, R. A. (1993): Cloud Dynamics, Vol. 53. of International Geophysics Series, Academic Press, San Diego.

HSU, K.-L., X. GAO & S. SOROOSHIAN (2002): Rainfall estimation using cloud texture classification mapping. *Proceedings of the 1st IPWG Workshop*.

KÄSTNER, M., F. TORRICELLA & S. DAVOLIO (2006): Intercomparison of satellite-based and model-based rainfall analyses. - *Meteorological Applications, 13*: 213-223.

KOBAYASHI, T. (2007): Significant differences in the cloud droplet effective radius bet nonprecipitating and precipitating clouds. - *Geophysical Research Letters, 34*: L15811, doi:10.1029/2007GL029606.

LENSKY, I. M. & D. ROSENFELD (2003a): A night-time delineation algorithm for infrared satellite data based on microphysical considerations. - *Journal of Applied Meteorology, 42*: 1218–1226.

LENSKY, I. M. & D. ROSENFELD (2003b): Satellite-based insights into precipitation formation processes in continental and maritime convective clouds at night-time. - *Journal of Applied Meteorology, 42*: 1227–1233.

LEVIZZANI, V., F. PORCÙ & F. PRODI (1990): Operational rainfall estimation using METEOSAT infrared imagery: An application in Italy's Arno river basin – Its potential and drawbacks. - *ESA Journal, 14*: 313-323.

LEVIZZANI, V., J. SCHMETZ, H. J. LUTZ, J. KERKMANN, P. P. ALBERONI & M. CERVINO (2001): Precipitation estimations from geostationary orbit and prospects for Meteosat Second Generation. - *Meteorological Applications, 8:* 23–41.

LEVIZZANI, V. (2003): Satellite rainfall estimations: new perspectives for meteorology and climate from the EURAINSAT project. - *Annales Geophysicae-Italy, 46*: 363–372.

MAURER, E. P., A. W. WOOD, J. C. ADAM, D. P. LETTENMAIER & B. NUSSEN (2002): A long-term hydrologically based dataset of land surface fluxes and states for the conterminous United States. - *Journal of Climate, 15*: 3237-3251.

MAUSER, W., R. STOLZ & A. COLGAN (2002): GLOWA-Danube: Integrative Techniques, Scenarios and Strategies regarding Global Change of the Water Cycle. GSF Forschungszentrum für Umwelt und Gesundheit (Hrsg.): GLOWA. German Program on Global Change in the Hydrological Cycle (Phase I, 2000-2003). Status Report 2002, München, 31-34.

MÜNCHNER RÜCK (2003): Topics. Annual review: natural catastrophes 2002. München, 49 pp.

NAUSS, T. & A. A. KOKHANOVSKY (2006): Discriminating raining from non-raining clouds at mid-latitudes using multispectral satellite data. - *Atmospheric Chemistry and Physics, 6*: 5031–5036.

NAUSS, T. & A. A. KOKHANOVSKY (2007): Assignment of rainfall confidence values using multispectral satellite data at mid-latitudes: first results. - *Advances in Geosciences, 10*: 99–102.

NEGRI, A. J. & R. F. ADLER (1993): An intercomparison of three satellite infrared rainfall techniques over Japan and surrounding waters. - *Journal of Applied Meteorology, 32*: 357-373.

NEW, M., M. TODD, M. HULME & P. JONES (2001): Precipitation measurements and trends in the twentieth century. - *International Journal of Climatology, 21*: 1899-1922.

O'SULLIVAN, F., C. H. WASH, M. STEWART & C. E. MOTELL (1990): Rain estimation from infrared and visible GOES satellite data. - *Journal of Applied Meteorology, 29*: 209-223.

POMPEI, A., M. MARROCU, P. BOI & G. DALU (1995): Validation of retrieval algorithms for the infrared remote sensing of precipitation with the Sardinian gauge network data. - *Il Nuovo Cimento, 18 C*: 483-496.

PORCÙ, F., F. PRODI, S. FRANCESCHETTI & S. PASETTI (1997): Short term climatology of cloud systems leading to flood events in Europe (1991-1996). *Proceedings of the 1997 Meteorological Satellite Data User's Conference, EUMETSAT:* 461-466.

PORCÙ, F., M. BORGA & F. PRODI (1999): Rainfall estimation by combining radar and infrared satellite data for nowcasting purposes. - *Meteorological Applications, 6*: 289-300.

REUDENBACH, C., G. HEINEMANN, E. HEUEL, J. BENDIX & M. WINIGER (2001): Investigation of summertime convective rainfall in Western Europe based on a synergy of remote sensing data and numerical

models. - *Meteorology and Atmospheric Physics, 76*: 23–41.Rodell et al., 2004

REUDENBACH, C. (2003): Konvektive Sommerniederschläge in Mitteleuropa. Eine Kombination aus Satellitenfernerkundung und numerischer Modellierung zur automatischen Erfassung mesoskaliger Niederschlagsfelder. - *Bonner Geographische Abhandlungen, 109*: 152 pp.

REUDENBACH, C., T. NAUSS, & J. BENDIX (2007): Retrieving precipitation with GOES, Meteosat and Terra/MSG at the tropics and mid-latitudes. In: LEVIZZANI, V., P. BAUER, & F. J. TURK (Ed.): Measuring precipitation form space. - *Advances in global change research, 28*. Springer: Netherlands.

ROSENFELD, D. & G. GUTMAN (1994): Retrieving microphysical properties near the tops of potential rain clouds by multispectral analysis of AVHRR data. - *Atmospheric Research, 34*: 259-283.

ROSENFELD, D. & I. LENSKY (1998): Satellite-based insights into precipitation formation processes in continental and maritime convective clouds. - *Bulletin of the American Meteorological Society, 79*: 2457-2476.

ROSENFELD, D., E. CATTANI, S. MELANI & V. LEVIZZANI (2004): Considerations on daylight operation of 1.6 µm vs. 3.7 µm channel on NOAA and METOP Satellites. - *Bulletin of the American Meteorological Society, 85*: 873– 881.

SCHMETZ, J., P. PILI, S. TJEMKES, D. JUST, J. KERKMANN, S. ROTA & A. RATIER (2002): An introduction to Meteosat Second Generation (MSG). - *Bulletin of the American Meteorological Society, 83*: 977–992.

TRENBERTH, K.E., A. DAI, R. M. RASMUSSEN & D. B. PARSONS (2003): The changing character of precipitation. - *Bulletin of the American Meteorological Society, 84:* 1205-1217.

TSONIS, A. A. (1987): Determining rainfall intensity and type from GOES imagery in the mid-latitudes. - *Remote Sensing of the Environment, 21*: 29-36.

VICENTE, G. A., R. A. SCOFIELD & W. P. MENZEL (1998): The operational GOES infrared rainfall estimation technique. - *Bulletin of the American Meteorological Society, 79*: 1883-1898.

WENG, F. Z., L. M. ZHAO & R. R. FERRARO (2003): Advanced microwave sounding unit cloud and precipitation algorithms. - *Radio Science, 38*: Art. No. 8068.

WU, R., J. A. WEINMAN & R. T. CHIN (1985): Determination of rainfall rates from GOES satellite images by a pattern recognition technique. - *Journal of Atmospheric and Oceanic Technology, 2:* 314-330.

CHAPTER 2

Conceptual Design

2 Conceptual Design

This chapter describes the conceptual design of the new operational technique for rain area discrimination and precipitation intensity separation operating day and night based on MSG SEVIRI for Central Europe. In the first chapter, the current status of already existing rainfall retrieval techniques is presented, which justifies the development of a new technique for rain area identification together with a precipitation process and rainfall intensity separation scheme in the mid-latitudes. Afterwards, dominant precipitation processes in the mid-latitudes, which are mostly connected to extra-tropical cyclones are introduced. In the following, the underlying conceptual design of the newly developed scheme is described.

2.1 Existing satellite based rain retrieval techniques

The variety of existing satellite based rain retrieval techniques can be separated by their complexity on the one hand, and by the sensor characteristics on the other hand. Furthermore, a differentiation in inclined orbits (TRMM (Tropical Rainfall Measurement Mission), KUMMEROW et al. 1998)), polar orbits (e.g. NOAA-AVHRR (National Oceanic and Atmospheric Administration – Advanced Very High Resolution Radiometer), HASTINGS et al. 1992)) and geostationary orbits (e.g. GOES-VISSR (Geostationary Operational Environmental Satellite – Visible and Infrared Spin Scan Radiometer)), MENZEL & PURDOM 1994; MSG SEVIRI, SCHMETZ et al. 2002) is possible.

While GEO systems only dispose of optical sensors, passive microwave sensors are only available on LEO systems (e.g. SSM/I (Special Sensor Microwave Imager), HOLLINGER et al. 1990)).

Because the identified demand for area-wide precipitation detection in a high spatio-temporal resolution necessary for a quasi-continuous rainfall monitoring in near-real-time can only be fulfilled by GEO systems, the following overview is restricted to optical sensors available on geostationary satellite systems.

A comprehensive overview on existing satellite based rainfall retrievals can be found in STEPHENS & KUMMEROW (2007), ANAGNOSTOU (2004), LEVIZZANI et al. (2001), LEVIZZANI (2003), SCOFIELD & KULIGOWSKI (2003), KIDD (2001), KIDDER & VONDER HAAR (1995). Regarding explanations about TRMM-PR (Precipitation Radar), the reader is referred to IGUCHI et al. (2000) and FERREIRA et al. (2001).

Generally, optical rainfall retrievals consists of two components. In a first step, the rain area is delineated by means of cloud top

characteristics. In the second step, a rain rate is assigned to the identified rain areas. This is realized by using empirically inferred or model based transfer functions between the cloud top characteristics (mostly the cloud top temperature) and the rain rate. Traditionally, sensor channels in the thermal infrared (IR, 10-13 µm) are used to characterize the cloud top properties, because this data is available day and night. If a channel in the water vapour absorption band (WV, 6.5-7.5 µm) is available, it is additionally used to improve the rainfall retrieval. Sometimes, channels in the visible (VIS, 0.4-0.9 µm) and in the near infrared spectrum (NIR, 1.2-3.9 µm) are also taken into account leading to significantly improved rainfall retrievals especially in recent times. However, these channels can principally only be used during day-time and have been restricted to one visible channel on GEO systems covering Africa and Europe until the launch of the MSG system, that is operational since early 2004. The following overview is arranged by the complexity of the algorithms according to BARRETT & MARTIN (1981).

2.1.1 Cloud index methods

Cloud index methods use empirically inferred thresholds for the cloud top temperature in the IR channel to detect the rain area, to which a fixed rain rate is assigned. Cloud index methods are mainly used in climatological studies with temporally and spatially aggregated precipitation data. The assigned rain rate is based on a statistical transfer function between the cloud top temperature in the IR channel and the rain rate measured with conventional gauges or ground-based radar. The most popular cloud index method is the GOES Precipitation Index (GPI, ARKIN & MEISNER 1987), which uses a cloud top temperature of 235 K as threshold to delineate precipitating clouds. For latitudes between 30° and 50° a temperature threshold of 220 K is defined as appropriate (ARKIN & MEISNER 1987). These thresholds are based on studies conducted by ARKIN (1979) during the Global Atmosphere Research Programme (GARP), Atlantic Tropical Experiment (GATE) concerning the relationship between spatially averaged rainfall rates and the frequency of clouds with cold tops. After the identification a constant rain rate of 3 mm/h is assigned to the raining pixels. The result is spatially aggregated to a 2.5° by 2.5° raster. The GPI is used operationally by the Working Group on Data Management (WGDM) of the Global Precipitation Climatology Project (GPCP) within the framework of the World Climate Research Programme (WCRP) to derive weekly and monthly precipitation data on a global scale (ARKIN & JANOWIAK 1991; ARKIN et al. 1994; XIE & ARKIN 1997; HUFFMAN et al. 1997). KERRACHE & SCHMETZ (1988)

transferred the GPI to Meteosat First Generation (MFG) Metesoat Visible and Infra-Red Imager radiometer (MVIRI). MENZ (1997) and BA & NICHOLSON (1998) used the GPI successfully over eastern Africa. TODD et al. (1999) developed an algorithm based on similar principles to the GPI technique and variants. In contrast it combines satellite and rain gauge data from north-east Africa to continuously calibrate key variables in an attempt to account for local and regional variability in cloud and rainfall relations. The auto-estimator technique proposed by VICENTE et al. (1998) uses the GOES 10.7 μm band to compute real-time precipitation amounts based on a power-law regression algorithm. This regression is derived from a statistical analysis between surface radar derived instantaneous rainfall estimates and satellite-derived IR cloud top temperatures collocated in time and space. COPPOLA et al. (2006) presented a neural network approach to daily rainfall estimation in Ethiopia and Zambia. The algorithm combines numerical weather model information with the IR satellite imagery to derive daily rainfall values. Another methodology for rainfall retrievals using IR brightness temperature and radar rainfall observations is illustrated by FALKOVICH et al. (2000) during the Tropical Ocean Global Atmosphere Coupled Ocean Atmosphere Response Experiment (TOGA-COARE). They proposed to convert the rain rate to a normally distributed set and than develop a relationship between IR brightness temperature and the rainfall rate.

2.1.2 Feature based methods

Feature based methods rely on the assumption that the relationship between the satellite cloud top brightness temperature and surface rainfall rate are non-unique for most pixel-based rainfall estimation algorithms. This is based on the observation that cold-topped cloud pixels with the same infrared brightness temperature may belong to different cloud types, thereby, indicating different rain rates at the ground surfaces.

WU et al. (1985) proposed a technique, that considers radiances from clouds observed in visible and infrared images from GOES satellites to estimate rainfall by means of a pattern recognition algorithm. The radiance features used were the radiance maxima, minima, and the means. The textural features included the edge strengths per unit area and the maxima and means of the mean, contrast, angular second moment, and entropy in four directions. HSU et al. (2002) developed a scheme, which relies on IR cloud top temperature. The algorithm first classifies cloud types based on the texture features of regional cloud images and then regresses the relationships of cloud brightness temperature and surface rain rate

respective to different cloud types using radar rainfall data. BELLERBY (2004) described a geostationary infrared satellite precipitation monitoring methodology, that draws on techniques from machine vision to develop a mathematical representation of cloud shapes and textures and the form of their embedding meteorological context. Quantitative feature descriptions derived from GOES infrared imagery were translated into 15 minute precipitation estimates through the use of an artificial neural network, that was trained using ground-based radar data from Florida. The Precipitation Estimation from Remotely Sensed Information using Artificial Neural Networks (PERSIANN) Cloud Classification System (CCS) is presented by HONG et al. (2004). Using 10.7 μm geostationary satellite imagery, the algorithm first separates cloud images into distinctive cloud patches and than extracts cloud features, including coldness, geometry, and texture. After that, the cloud patches are clustered into well-organized subgroups. The rainfall rate is assigned to the classified cloud groups by means of cloud top IR temperature and rainfall relationships using gauge-corrected radar rainfall data with an hourly resolution.

2.1.3 Bi-spectral methods

Bi-spectral methods are based on the observation that different cloud types show wavelength dependent radiation properties. In contrast to the cloud index methods they additionally consider a VIS channel and are based on the assumption that precipitating clouds have a high reflectivity in the VIS channel and a cold cloud top temperature in the IR channel. Such an assumption is ideally valid for deep convective clouds as tropical Cumulonimbus. Cold clouds with a low reflectance (thin Cirrus) and warm clouds with a high reflectance (Stratus) are classified as non-raining. The discriminant function to separate raining and non-raining clouds is inferred from comparisons between both channels and ground-based radar data. A prominent example is the RAINSAT algorithm developed by LOVEJOY & AUSTIN (1979) and BELLON ET al. (1980) developed for Canada. CHENG et al. (1993) and CHENG & BROWN (1995) transferred the algorithm from GOES-VISSR to MFG MVIRI for the area of Great Britain. TSONIS & ISAAC (1985) and TSONIS (1987) used a cluster analysis to identify potentially raining clouds from a two dimensional VIS/IR histogram. O'SULLIVAN et al. (1990) additionally incorporate the textural structure in a 10 by 10 environment around the respective pixel.

Bi-spectral methods show an improved performance than pure IR techniques, especially for precipitation from warm clouds (KING et al. 1995), which are not considered by the relatively cold threshold in the IR channel. However, as mentioned above, stratiform precipitation is

explicitly excluded from the precipitation detection, which restricts the use of bi-spectral methods for precipitation processes in the mid-latitudes.

LENSKY & ROSENFELD (1997) and ROSENFELD & LENSKY (1998) demonstrated the possibility to infer different microphysical precipitation processes and to estimate rain area and rain rates over Israel by using a combination of the 3.7 µm reflectance of the LEO system NOAA-AVHRR during day-time together with IR brightness temperature. For another study over Israel, LENSKY & ROSENFELD (2003a,b) used information about the microstructure and precipitation potential of cloud revealed by the brightness temperature difference between an IR channel (11 µm) and a NIR channel (3.7 µm) of NOAA-AVHRR at night-time to detect potentially precipitating clouds.

CAPACCI & CONWAY (2005) and NAUSS & KOKHANOVSKY (2006, 2007) documented the potential of the combined use of a visible channel together with a channel in the near infrared in order to retrieve microphysical and optical cloud properties and used this information for the rain area identification using data from the LEO system Terra-/ Aqua-MODIS. Notwithstanding the low temporal resolution of Terra-/ Aqua-MODIS and the restriction to day-time data, the authors emphasized the high potential regarding a potential application on SEVIRI data aboard the GEO system MSG. Recently, YAN & YANG (2007) proposed a dual spectral rain algorithm for MODIS. The reflectance of the MODIS of the 0.65 µm channel together with the water vapour absorption channel at 1.38 µm are applied to form multiregression curves used for day-time rainfall estimation.

2.1.4 Multispectral methods

Accordingly to bi-spectral techniques, multispectral methods are based on the observation that different cloud types show different radiation properties depending on wavelength. In contrast to the bi-spectral methods they consider radiation from more than two spectral channels.

For the area of Japan KURINO (1997) used the 11 µm brightness temperature, together with the brightness temperature difference between a 11 µm and a 12 µm channel and the brightness temperature difference between a 11 µm and a 6.7 µm channel to derive the probability of rain and the mean rain rate in comparison with ground-based radar data. In a case study over Taiwan WEI et al. (2006) demonstrated a multi-spectral spatial convolution approach for real-time rainfall forecasting using two infrared channels (11 µm and 12

µm) together with a water vapour channel (6.7 µm). The GOES multispectral rainfall algorithm from BA & GRUBER (2001) combines information from five GOES channels (0.65 µm, 3.9 µm, 6.7 µm, 11 µm, and 12 µm) for the detection of precipitating cloud areas. The rain rate is assigned by the product of rain probability and mean rain rate calculated as a function of the 11 µm brightness temperature.

2.1.5 Lifecycle methods

Lifecycle methods consider the temporal variability of convective systems and the involved precipitation processes. Therefore, they do not use a fixed rain rate as the former mentioned techniques. Lifecycle methods are often used for now-casting purposes (e.g. NOAA-NESDIS-Technique, SCOFIELD & OLIVER 1977) and for the monitoring of flood events (SCOFIELD 1987; SCOFIELD & NAIMENG 1994; VICENTE & SCOFIELD 1996). GRIFFITH et al. (1978; Griffith-Woodley-Technique) used the cloud top temperature difference between two consecutive scenes as a measure for the activity of convective clouds. Hence, this method relies explicitly on the high temporal resolution of GEO systems (better than 30 minutes). Because of the problematic automatic detection and tracking of single convective clouds in two consecutive scenes, NEGRI et al. (1984) classified different lifecyles of convective clouds based on a single scene and attained comparable results to GRIFFITH et al. (1978). AMORATI et al. (2000) showed that lifecycle methods perform well for events with extensive convective systems, but are inappropriate for the detection of stratiform and shallow convective precipitation systems in the mid-latitudes.

2.1.6 Cloud model techniques

Cloud model techniques try to explicitly consider cloud physical processes. The assigned rain rates are based on numerically simulated cloud top temperatures and the corresponding rain rate (GRUBER 1973; WYLIE 1979). Based on studies of ADLER & MACK (1984), ADLER & NEGRI (1988) developed the Convective Stratiform Technique (CST) for subtropical convective systems. Local temperature minima in the IR channel are used in a first step to identify convective cores. Potentially raining stratiform clouds in the adjacent vicinity of the convective cores (see chapter 2.3) are also detected by deduced temperature thresholds. Non-raining cirrus clouds are excluded by an empirically determined discriminant function based on ground-based radar data. The regression function between cloud top temperature and convective rain rate rests upon calculations conducted with a one dimensional cloud model. The detected stratiform areas obtain a fixed

rain rate of 2 mm/h. The CST has become a widely-used and intensively validated technique. While it can be applied successfully in the subtropics and tropics (BENDIX 1997, 2000), it shows deficiencies in outer-tropical regions (POMPEI et al. 1995; LEVIZZANI et al. 1990; NEGRI & ADLER 1993). For this reason REUDENBACH (2003) developed the Enhanced Convective Stratiform Technique (ECST) for convective systems in the mid-latitudes. By additionally considering the WV channel he achieved a more reliable differentiation between convective cores and non-raining cirrus clouds. The combination of the WV and the IR channel allows an auto-adaptive threshold determination for a flexible detection of convective systems and adjacent stratiform precipitating clouds. Recently REUDENBACH et al. (2007) introduced the Advective Convective Technique (ACT), a scheme for MFG MVIRI, that allows the differentiation of the convectively dominated precipitation areas into the subareas of rainfall from convective cores (Cumulonimbus, Cb), convective-stratiform precipitating Nimbostratus clouds (Nb in connection with Cb; see chapter 2.3), and enhanced advective-stratiform precipitating areas (shallow convective cells from aloft together with the "seeder-feeder" effect, see chapter 2.3). Because of the adaption to convective systems, the ECST as well as the ACT show still considerable deficiencies concerning the identification of widespread stratiform precipitation fields, which are not directly connected to convective cores and are characterized by relatively warm cloud tops.

2.2 The need for a satellite based technique for rain area identification and process classification

Most of the retrieval techniques introduced above are appropriate for convective clouds, that can be easily identified in the visible, infrared and/or water vapour channels (e.g. LEVIZZANI et al. 2001; LEVIZZANI 2003). These techniques are based on the assumption that clouds with a high reflectivity and a low temperature at the top posses a higher rainfall probability and rate than clouds with less reflective and lower tempered tops (e.g. ARKIN & MEISNER 1987; KING et al. 1995; RICHARDS & ARKIN 1981). However, while this conceptual model is valid for convective precipitating clouds and the associated precipitation processes (e.g. GRUBER 1973), several extensive evaluation studies revealed considerable drawbacks concerning mid-latitudinal precipitation processes in connection with extra-tropical cyclones (hereafter denoted as advective-stratiform precipitation areas; see chapter 2.3) (e.g. EBERT et al. 2007; FRÜH et al. 2007; KÄSTNER et al. 2006; ADLER et al. 2001; AMORATI et al. 2000; EBERT et al. 1998; POMPEI et al. 1995; NEGRI & ADLER 1993; LEVIZZANI et al. 1990). Such

precipitating cloud areas are mainly formed by widespread lifting processes along frontal zones and are characterized by relatively warm top temperatures and a more homogeneous spatial distribution of the cloud top temperature, that differs not significantly between raining and non-raining regions (BROWNING & MONK 1982; HERZEGH & HOBBS 1980; HOBBS ET AL. 1980; HOUZE ET AL. 1981; SAARIKIVI 1989). Therefore, retrieval techniques based solely on IR cloud top temperature lead to an underestimation of the detected rain area and to uncertainties concerning the assigned rainfall rate.

Recently, CAPACCI & CONWAY (2005) and NAUSS & KOKHANOVSKY (2006, 2007) proposed new techniques for rain area identification based on the combined use of a VIS and NIR channel of the LEO system Terra-/Aqua-MODIS. These techniques also consider advective-stratiform precipitating clouds and allow an improved rain area detection in the mid-latitudes during day-time. However, because of the LEO system MODIS this technique is restricted in its temporal resolution.

Bearing in mind the overview of existing satellite based rain retrieval techniques, this short summary reveals that their exists a great deficit regarding the detection of precipitation in the mid-latitudes especially in connection with extra-tropical cyclones in a operational quasi-continuous manner (day- and night-time) at high spatial and temporal resolutions. The existing IR techniques are appropriate for convectively dominated precipitation processes but reveal considerable shortcomings concerning advective-stratiform precipitating cloud areas. New techniques based on microphysical and optical cloud properties, that have been applied to LEO systems, which provide the necessary spectral resolution show enhancements in rain area identification. Anyhow, as the VIS and NIR channel needed to retrieve the cloud properties are only available during day-time, these techniques are restricted to day-time scenes. Apart from the fact that LEO systems offer only a low temporal resolution insufficient for the requirements identified in the introduction, it has to be further mentioned that these new techniques are only applicable for the discrimination of the rain area.

The new European geostationary satellite system MSG SEVIRI provides a high temporal (15 minutes) and spatial (3 by 3 km at SSP) resolution appropriate for a quasi-continuous precipitation detection in near-real-time. Furthermore, it offers an enhanced spectral resolution enabling the retrieval of cloud properties for an improved rainfall detection in the mid-latitudes.

Based on the enhanced spatial and temporal resolution and considering the demand for a quasi-continuous precipitation

monitoring, the main objective of the present work is the development of an operational technique for rain area discrimination together with precipitation process and rainfall intensity separation during day- and night-time based on MSG SEVIRI.

Such a technique offers a great potential for hydrological and climatological studies as well as for now-casting purposes. Beside the application in climatological studies where the spatio-temporal precipitation distribution is analysed, the new technique provides the basis for enhanced quantitative precipitation measurements in the mid-latitudes and offers new possibilities related to hybrid (i. e. combining optical and microwave imager data) rainfall retrievals.

The dominant precipitation processes in the mid-latitudes especially in connection with extra-tropical cyclones, that have to be considered by the newly developed scheme are introduced in the following chapter. These form the basis for the new extended conceptual model applicable for the proper detection of the rain area and its further differentiation into subareas of differing precipitation processes and rainfall intensities, which is presented afterwards.

2.3 Precipitation processes in the mid-latitudes

Following the conceptual model of rainbands dominated by different rainfall processes and leading to differing rainfall intensities within extra-tropical cyclones summarized by HOUZE (1993) and mainly based on the results of the CYCLES (CYCLonic Extra-tropical Storms) project the rainfall area can be separated into the following subareas (see figure 2.1):

- Advective-stratiform background precipitation areas (light precipitation intensities).
- Precipitation from clouds of intermediary character between convectively dominated and advective-stratiform background precipitation areas (light to moderate precipitation intensities).
- Enhanced advective-stratiform precipitation from Ns with ice particles from embedded shallow generating cells, that fall from above ("seeder-feeder" effect) in connection with wide cold-frontal rainbands and warm-frontal rainbands (moderate precipitation intensities).
- Convective-stratiform precipitation from Ns in connection with convective cores (Cb) within narrow cold-frontal rainbands (moderate to high precipitation intensities) (HOUZE 1997, 1993).

- Precipitation from convective cores in connection with narrow cold-frontal rainbands (very high precipitation intensities from Cb).

The overall precipitation pattern is mostly confined to the regions of vertical motion associated with the cyclone and the major zones of active frontogenesis (i.e. cold-frontal and warm-frontal zones). The general frontal precipitation field is formed by background advective-stratiform precipitation areas consisting of basic stratiform precipitation processes, that dominate the frontal system. They are the result of widespread rising processes and are characterized by light rain rates (HOUZE 1993). Within this advective-stratiform envelope elongated regions of enhanced precipitation intensities, so-called rainbands, are embedded. The wide cold-frontal and the warm-frontal rainbands are characterized by enhanced advective-stratiform precipitation intensities. The narrow cold-frontal rainbands represent lines of intense convection, which results in higher rainfall intensities. Warm-sector and post-frontal rainbands outside the envelope of the frontal precipitation system often consist of lines of convective showers or thunderstorms.

Figure 2.2 shows a schematic cross-section through an extra-tropical cyclone indicating the associated cloud structures and precipitation mechanisms. The intensification of the advective-stratiform background rainfall rates in the envelope of the frontal precipitation systems is caused by the approach of unstable and dry air masses in the upper levels of the advective-stratiform clouds and the accompanied locally confined strengthening of the buoyancy (HOUZE 1993; HEYMSFIELD 1977). The convection is located next to cloud areas of advective-stratiform background precipitation. The ice particles grown and carried up to upper levels by the convective updrafts fall out and are advected into in the neighbouring advective-stratiform region where they grow by condensed water vapour deposited onto the ice particles. This so-called "seeder-feeder" effect (see figure 2.3) leads to intensified rainfall rates. These areas of intermediary character between the advective-stratiform background and the convectively dominated precipitation areas are characterized by light to moderate rainfall rates.

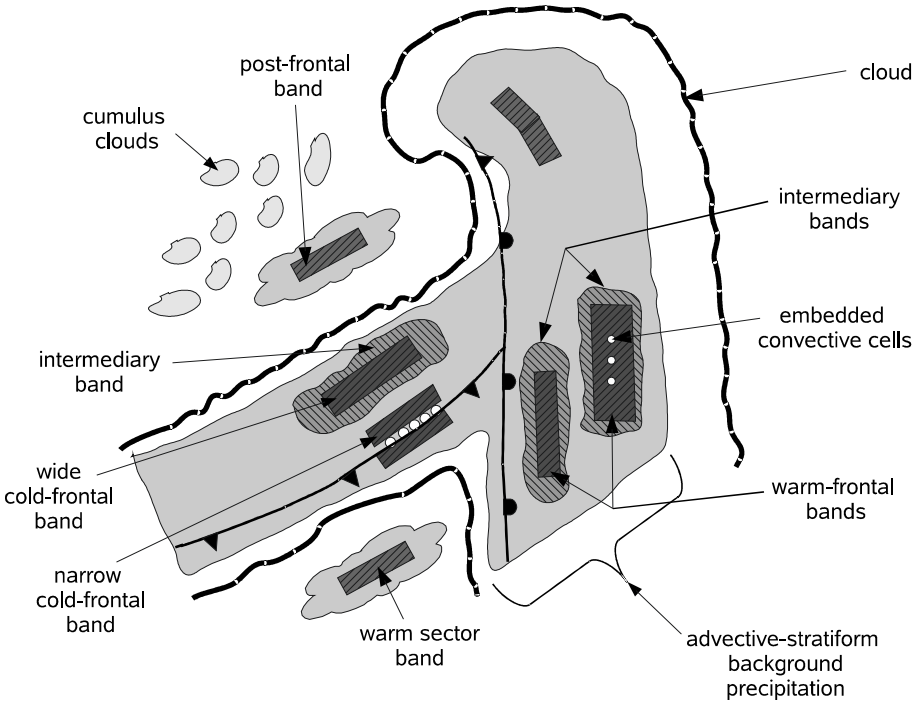

Figure 2.1: Idealization of the cloud and precipitation pattern associated with a mature extra-tropical cyclone (Adapted from Houze (1993) after Matejka et al. (1980) and Houze et al. (1981)).

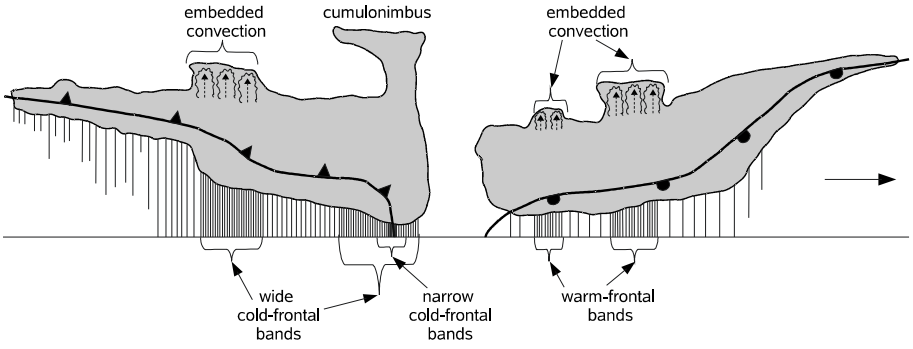

Figure 2.2: Cloud structure and precipitation mechanisms of an extra-tropical cyclone. Vertical hatching below cloud bases represents precipitation. The density of the hatching corresponds qualitatively to the precipitation rate (Adapted from Houze (1993) after Matejka et al. (1980)).

The wide cold-frontal rainbands emanate from a layer aloft, above the front, which is characterized by enhanced mean ascent. In addition to the enhanced mean ascent, these rainbands contain shallow convective generating cells. Within these cells precipitation particles are generated, that augment the general advective-stratiform background precipitation rate at lower levels by the "seeder-feeder" mechanism (see figure 2.3), as they fall through lower layers of the frontal cloud (RUTLEDGE & HOBBS 1983). The "seeder-feeder" effect, which is also named Bergeron-Findeisen process is depicted in figure 2.3. The increased buoyancy in the generating convective cells enables the development and the accelerated growth of ice particles in the upper parts of the cloud ("seeder-zone"), necessary for effective precipitation formation processes. As these ice particles fall through the cloud they grow by vapour deposition, aggregation and riming processes in the middle cloud parts ("feeder-zone"). Because the ice particles can become larger and heavier than rain droplets they lead to higher fall velocities and higher rainfall rates. These processes lead to increased rainfall intensities within the advective-stratiform background precipitation area (RUTLEDGE & HOBBS 1983). The enhanced mean ascent is associated with a local steepening of the frontal zone together with discontinuities within the rising air masses along the cold front. Although the frontal system provides a favourable environment for the formation of wide cold-frontal rainbands their dynamics are somewhat separable from the frontal dynamics. While multiple wide cold-frontal rainbands can occur within the space and time domain of a single cold-frontal system their essential dynamics are superimposed on the larger frontogenetical circulation. Wide cold-frontal rainbands move with the winds in the layer of enhanced vertical air motion and generating cells. They can move faster than the front itself, sometimes ending up ahead of the position of the front at the surface.

The warm-frontal rainbands are similar in dimension to the wide cold-frontal rainbands. They occur in the forward part of the cloud shield of the developing cyclone, where warm advection dominates. Generating cells, located above the rainbands move over the lower level rainbands and seed them with ice particles. The dynamic mechanisms leading to the enhanced vertical air motions in warm-frontal rainbands seem to be similar to wide cold-frontal rainbands although this has not been clearly identified (HOUZE 1993; HEYMSFIELD 1979; MATEJKA et al. 1980).

The narrow cold frontal rainbands are directly linked to the cold front at the ground and are the result of forced uplift of stable or just slightly unstable air masses. The rising air is part of the poleward

moving warm air current of the cyclone with high moisture. Colder and drier air subsiding on the cold side of the front forms the downward branch of the circulation. The warm moist air masses flow in an upward direction and predominantly parallel to the cold front with a slight bend to the cold air sector (BROWNING 1986). In connection with the sinking dry air masses of the cold air sector which, form the cold front, a zone of strong, concentrated convergence and abrupt upward motion arises. From the air lifted over this sharp surface front a narrow precipitating cloud band develops. Although the forced ascent can be strong, the precipitating clouds remain limited in vertical and horizontal extent to the zone of lifting forced by the sharp front (HOUZE 1993; HOBBS & PERSSON, 1982; MATEJKA et al. 1980).

The precondition for convective-stratiform precipitation from Ns in connection with convective cores (Cb) within narrow cold-frontal rainbands are ice particles in the upper parts of the cloud. Aggregation and riming processes in connection with such ice particles are necessary for the formation and growth of rain particles of sufficient size. The introduction of ice particles can occur in two ways. One possibility for the formation of the Ns is based on a decaying active convective core without any existing vertical wind shearing within the cloud. The decaying process alters the cloud characteristics as the ice particles begin to sink due to decreasing buoyancy in the upper cloud parts. At the same time, new convective cores are formed at the edge of the decaying system, which transport new ice particles in higher parts. With the decaying of this new system the area of the Ns further increases due to the mentioned processes. As a consequence, the Ns cloud is regenerated consistently by developing and decaying convective cores. Another possibility for the formation of the Ns implies consistently regenerating convective processes with vertical wind shearing within the cloud. The ice particles are generated within the updraft of the Cb and are subsequently advected horizontally into the Ns cloud where they settle until they reach the melting layer. Whether the convective-stratiform precipitating cloud areas associated with convective cores evolve without or with vertical shear of the horizontal wind field varies from one meteorological context to another. In reality both processes mainly occur in combination.

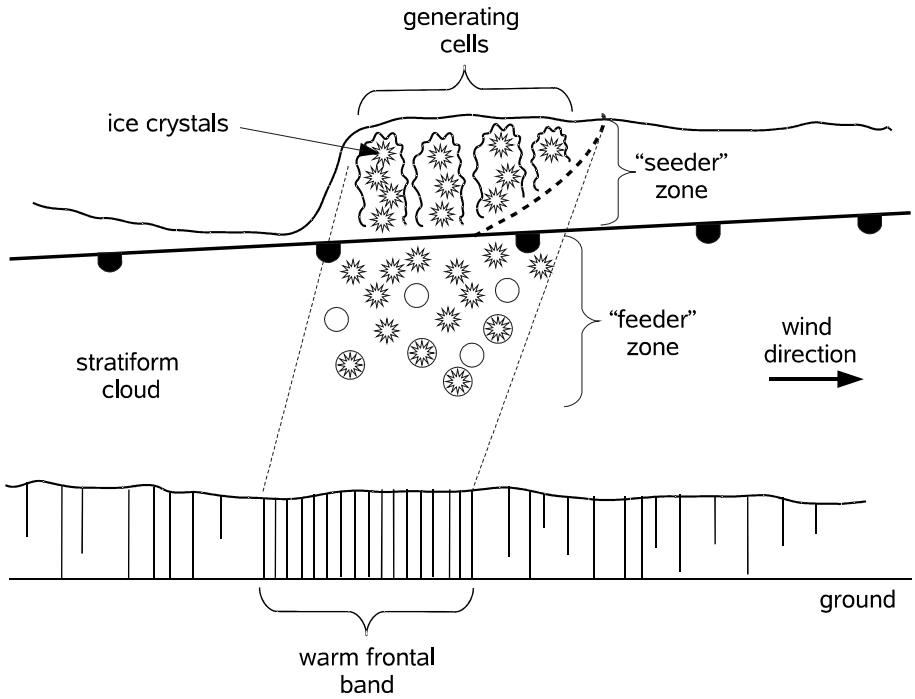

Figure 2.3: Schematic of the clouds and precipitation field of a warm-frontal rainband. The structure of the clouds and the predominant mechanisms of precipitation growth are indicated ("seeder-feeder" effect). Vertical hatching below cloud base represents precipitation; the density of the hatching corresponds qualitatively to the precipitation rate. The motion of the rainband in the figure is from left to right (Adapted from Houze (1993) after Matejka et al. (1980)).

Further detailed descriptions of the precipitation processes in connection with extra-tropical cyclones can be found in PRUPPACHER & KLETT (1997), HOUZE (1993) and ROGERS & YAU (1989). An overview on the different theories for the development of extra-tropical cyclones is given by KRAUS (1995).

Following the description of the precipitation processes and the resulting areas of differing rainfall intensities (i.e. rainbands) in connection with extra-tropical cyclones it can be stated that the narrow cold-frontal, the wide cold-frontal and the warm-frontal rainbands are dominated by convective precipitation processes. On the other hand the advective-stratiform background and the intermediary precipitation areas are of advective-stratiform character.

2.4 Conceptual Model for rain area identification and process classification in the mid-latitudes

As a result of the described precipitation processes in extra-tropical cyclones it can be stated that convectively dominated precipitating cloud areas are characterized by a large vertical extension and a cloud top rising high into the atmosphere. Therefore, the proposed relationship between cloud top temperature and rainfall probability and intensity as used in existing IR retrieval techniques can be retained for such cloud areas and their classification by means of IR temperature thresholds for cloud top temperature seems to be appropriate. At the same time it becomes obvious that a major part of the precipitating cloud areas in connection with extra-tropical cyclones are not necessarily connected to cold cloud top temperatures. For the detection and classification of these cloud areas a thresholds of cloud top temperature in a IR channel seems to be inappropriate. As mentioned in the introduction, this is the reason for an underestimation of the detected rain area and uncertainties concerning the assigned rainfall rate for precipitating cloud areas in extra-tropical cyclones.

With the advent of new generation satellite systems the retrieval of microphysical and optical cloud properties from multispectral satellite data became possible. In the following, several authors successfully used the information about cloud properties for the development of rainfall retrieval techniques showing an enhanced performance compared to existing IR retrieval techniques especially concerning precipitating advective-stratiform cloud areas (e.g. NAUSS & KOKHANOVSKY 2007, 2006; ROSENFELD et al. 2004; LENSKY & ROSENFELD 2003a,b). These techniques rely on the assumption that a combination of particles large enough to fall against the updraft wind field within the cloud and a large enough vertical cloud extension, that favours the growth of precipitation particles and prevents them from evaporation below the cloud bottom, is the precondition for a cloud to produce precipitation particles. The effective particle radius (a_{ef}) defined by the ratio between the third to the second power of the droplet spectrum is taken in place of the actual droplet spectrum. The cloud optical thickness (τ) defined by the integration of the extinction coefficient integrated over the cloud geometrical thickness is considered representatively for the cloud geometrical thickness. Multiplying both parameters according to

$$CWP = \frac{2}{3} \cdot \rho \cdot \tau \cdot a_{ef} \tag{2.1}$$

one gets the cloud water path (CWP) with ρ the density of water [g/m²]. The CWP, which represents the column amount of water in the cloud is related to the rainfall probability of a cloud and can therefore be used to detect precipitating cloud areas. This means, that cloud areas with a high CWP (large a_{ef} together with high τ) possess a high amount of cloud water and are characterized by a higher rainfall probability than cloud areas with a low CWP.

Furthermore, effective rain formation processes in connection with extra-tropical cyclones are mainly coupled to ice particles in the upper part of the clouds and the "seeder-feeder" effect (HOUZE 1993). For this reason, information about the cloud phase in the upper cloud parts must also be incorporated beside the cloud top height and the cloud water path when characterising precipitating cloud areas.

Considering the described dominant precipitation processes for advective-stratiform and convectively dominated precipitation areas within extra-tropical cyclones in connection with the objective to develop a new scheme for rain area identification together with precipitation process and intensity separation the following hypotheses are formulated:

- A sufficiently large cloud water path is the precondition for the development of precipitation particles falling from the cloud and reaching the surface level as rain.
- The existence of ice particles in the upper parts of the cloud is the precondition for the effective formation of precipitation particles.
- The rainfall intensity from convectively dominated clouds is linked to the cold top temperature, which can be used as a proxy for the vertical extension of high rising clouds.
- The rainfall intensity from advective-stratiform precipitating clouds is linked to the cloud water path, which can be used as a proxy for the water amount available within the cloud and to the particle phase in the upper cloud regions.

The principal of the newly introduced conceptual design is depicted in figure 2.4:

- Precipitating cloud areas are characterized by a sufficiently high cloud water path and ice particles in the upper part.
- Cloud areas with higher rainfall intensities are characterized by a higher cloud water path and to a higher amount of ice particles in the upper part.
- Convective clouds with very high rainfall intensities are characterized by a large vertical extension and a high rising cold cloud top.

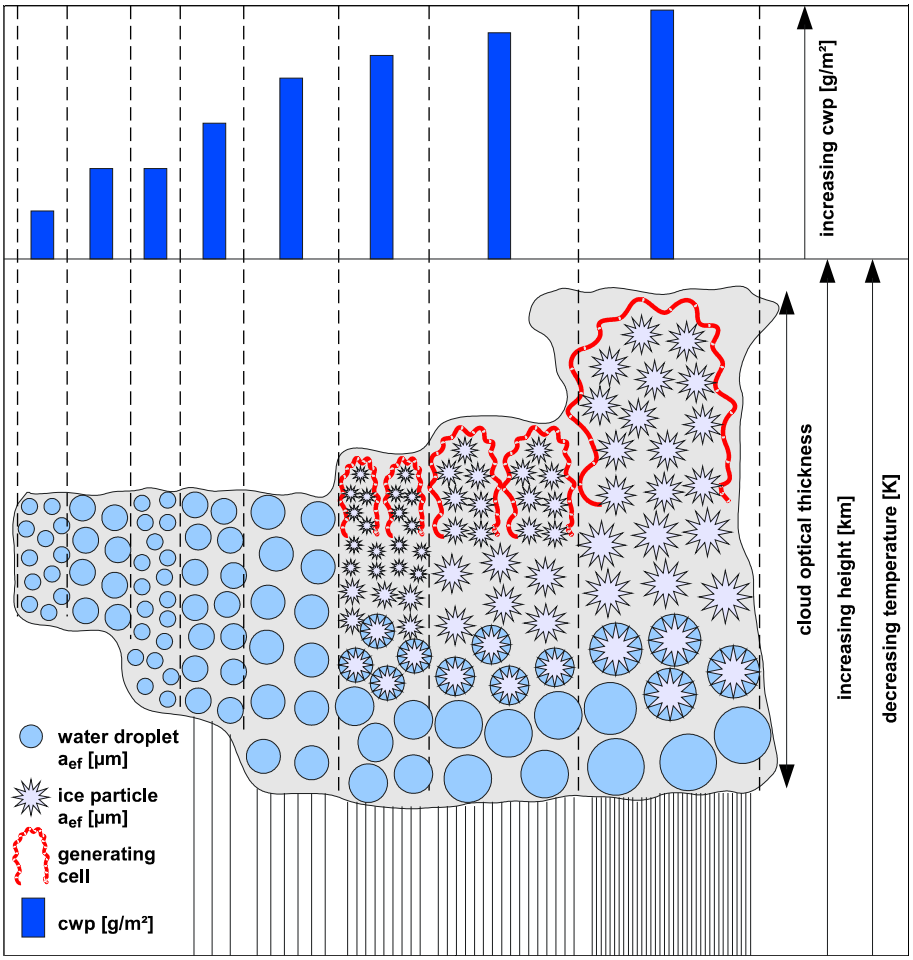

Figure 2.4: Conceptual model for rain area identification together with precipitation process and rainfall intensity separation based on information about the cloud water path, the cloud phase and the cloud top height (Adapted and extended after Lensky & Rosenfeld 2003a).

MSG SEVIRI provides an enhanced spectral resolution, which allows to infer information about the cloud water path, the cloud phase in the upper cloud parts and the cloud top height. Therefore, and based on the conceptual model introduced above, a new technique for the identification of rain areas together with their separation into areas of differing precipitation processes and rainfall intensities is developed for MSG SEVIRI in the context of the present work.

Since no operational precipitation retrieval technique appropriate for the mid-latitudes exists for MSG SEVIRI a distinct improvement concerning a quasi-continuous monitoring of the precipitation distribution in a high spatial and temporal resolution can be expected

by the newly developed scheme. The major innovations of the new technique are:

- The physically based detection and classification of the rain area on the basis of the novel consideration of information about the cloud water path, the cloud phase in the upper parts, and the cloud top height within the conceptual design.
- The consideration of different conceptual models depending on the dominating precipitation processes and their integration into the superior conceptual framework of rainbands within extra-tropical cyclones.

Thereby, an improved detection of the rain area as well as its further subdivision into areas of differing precipitation processes and rainfall intensities during day- and night-time is attained.

Based on the conceptual model presented above the following chapters describe the development of a technique for rain area identification and process-oriented intensity classification in the mid-latitudes using MSG SEVIRI day- and night-time data. An overview of the scheme's design is presented in figure 2.5. This figure shows the components of the scheme.

- **Chapter 3** presents the transfer and adaptation of an IR technique appropriate for convective precipitation processes in the mid-latitudes, that relies on information about the cloud top height to MSG SEVIRI.
- In **Chapter 4** and **Chapter 5** the developed techniques for rain area identification based on information about the cloud water path and the cloud phase in the upper cloud regions using SEVIRI day- and night-time data is introduced.
- **Chapter 6** presents the developed technique for the separation of the rainfall area into subareas of differing precipitation processes and rainfall intensities based on the combined information about the cloud water path, the cloud phase and the clout top height using MSG SEVIRI day- and night-time data.

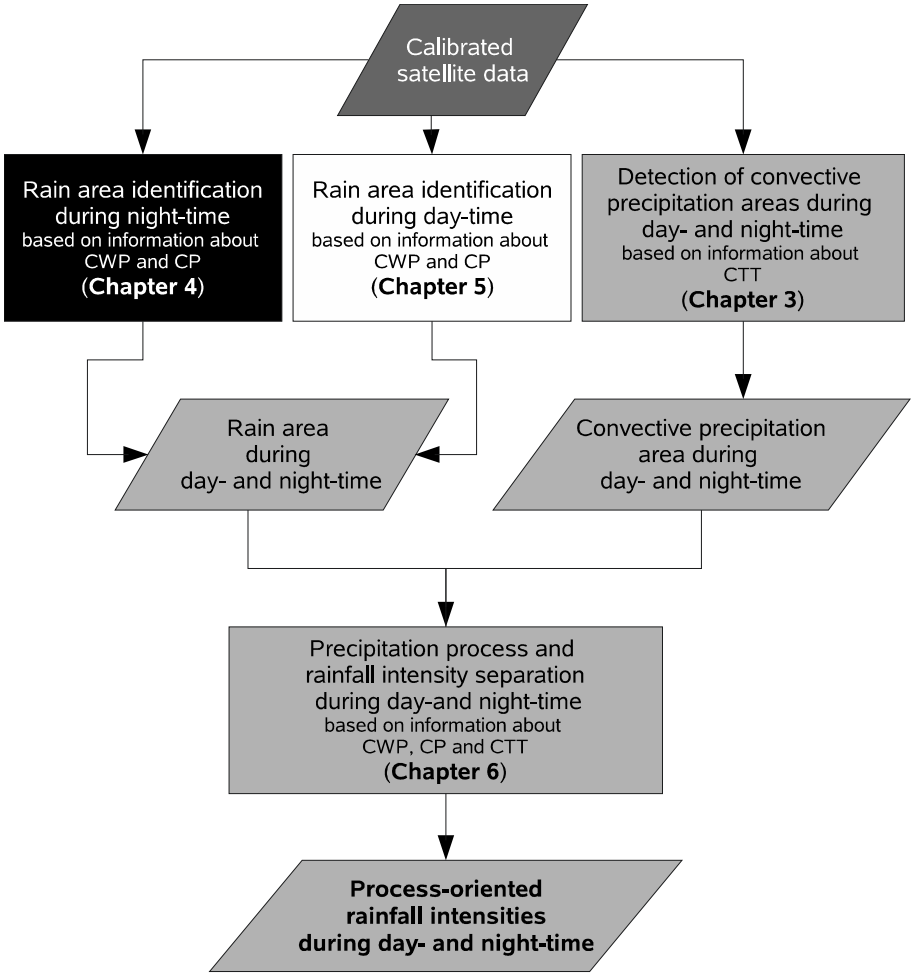

Figure 2.5: Overview of the new developed scheme for rain area identification and process-oriented rainfall intensity differentiation for MSG SEVIRI (CWP: cloud water path; CP: cloud phase; CTT: cloud top height).

References

ADLER, R. F. & R. A. MACK (1984): Thunderstorm cloud height-rainfall rate relations for use with satellite rainfall estimation techniques. - *Journal of Climate and Applied Meteorology, 23*: 280 – 296.

ADLER, R. F. & A. J. NEGRI (1988): A satellite technique to estimate tropical convective and stratiform rainfall. - *Journal of Applied Meteorology, 27*: 30–51.

ADLER, R. F., C. KIDD, G. PETTY, M. MORISSEY & H. M. GOODMAN (2001): Intercomparison of global precipitation products: The third precipitation intercomparison project (PIP-3). - *Bulletin of the American Meteorological Society, 82:* 1377-1396.

ANAGNOSTOU, E. N. (2004): Overview of overland satellite rainfall estimation for hydro-meteorological applications. - *Surveys in Geophysics, 25:* 511-537.

AMORATI, R., P. P. ALBERONI, V. LEVIZZANI, & S. NANNI (2000): IR-based satellite and radar rainfall estimates of convective storms over Northern Italy. - *Meteorological Applications, 7*: 1-18.

ARKIN, P. A. (1979): The relationship between the fractional coverage of high cloud and rainfall accumulations during GATE over the B-scale array. - *Monthly Weather Review, 107:* 1382-1387.

ARKIN, P. A. & B. N. MEISNER (1987): The relationship between large-scale convective rainfall and cold cloud over the western hemisphere during 1982-84. - *Monthly Weather Review, 115*: 51-74.

ARKIN, P. & J. E. JANOWIAK (1991): Analyses of the global distribution of precipitation. - *Dynamics of Atmospheres and Oceans, 16*: 5-16.

ARKIN, P. A., R. JOYCE & J. E. JANOWIAK (1994): The estimation of global monthly mean rainfall using infrared satellite data: The GOES Precipitation Index (GPI). - *Remote Sensing Reviews, 11:* 107-124.

BA, M. B. & A. GRUBER (2001): GOES Multispectral Rainfall Algorithm (GMSRA). - *Journal of Applied Meteorology, 40*: 1500-1514.

BA, M. B. & S. E. NICHOLSON (1998): Analysis of convective activity and its relationship to the rainfall over the Rift Valley lakes of East Africa during 1983-90 using the Meteosat infrared channel. - *Journal of Applied Meteorology, 37:* 1250-1264.

BARRET, E. C. & D. W. MARTIN (1981): The use of satellite data in rainfall monitoring. Academic Press, London, 340 pp.

BELLERBY, T. J. (2004): A Feature-Based Approach to Satellite Precipitation Monitoring Using Geostationary IR Imagery. - *Journal of Hydrometeorology, 5:* 910-921.

BELLON, A., S. LOVEJOY & G. L. AUSTIN (1980): Combining satellite and radar data for the short-range forecasting of precipitation. - *Monthly Weather Review, 108*: 1554–1556.

BENDIX, J. (1997): Adjustment of the Convective-Stratiform Technique (CST) to estimate 1991/93 El Niño rainfall distribution in Ecuador and Peru by means of Meteosat-3 data. - *International Journal of Remote Sensing, 18:* 1387-1394.

BENDIX, J. (2000): Precipitation dynamics in Ecuador and Northern Peru during the 1991/92 El Niño: a remote sensing perspective. - *International Journal of Remote Sensing, 21*: 533-548.

BROWNING, K. A. & G. A. MONK (1982): A simple model for the synoptic analysis of clod fronts. - *Quarterly Journal of the Royal Meteorological Society, 108:* 435-452.

BROWNING, K.A. (1986): Conceptual Models of Precipitation Systems. - *Weather and Forecasting, 6*: 23-41.

CAPACCI, D. & B. J. CONWAY (2005): Delineation of precipitation areas from MODIS visible and infrared imagery with artificial neural networks. - *Meteorological Applications, 12:* 291-305.

CHENG, M., R. BROWN & C. G. COLLIER (1993): Delineation of precipitation areas by correlation of METEOSAT visible and infrared data in the region of the United Kingdom. - *Journal of Applied Meteorology, 32*: 884–898.

CHENG, M. & R. BROWN (1995): Delineation of precipitation areas by correlation of Meteosat visible and infrared data with radar data. - *Monthly Weather Review, 123*: 2743-2757.

COPPOLA, E., D. I. F. GRIMES, M. VERDECCHIA & G. VISCONTI (2006): Validation of Improved TAMANN Neural Network for Operational Satellite-Derived Rainfall Estimation in Africa. - *Journal of Applied Meteorology and Climatology, 45*: 1557-1572.

EBERT, E. E. & M. J. MANTON (1998): Performance of Satellite Rainfall Estimation Algorithms during TOGA COARE. - *Journal of Atmospheric Sciences, 55*: 1538-1557.

EBERT, E. E., J. E. JANOWIAK & C. KIDD (2007): Comparison of near-real-time precipitation estimates from satellite observations and numerical models. - *Bulletin of the American Meteorological Society, 88*: 47–64.

FALKOVICH, A., S. LORD & R. TREADON (2000): A new methodology of rainfall retrievals from indirect measurements. - *Meteorological and Atmospheric Physics, 75*: 217-232.

FERREIRA, F., P. AMAYENC, S. OURY & J. TESTUD (2001): Study and test of improved rain estimates from the TRMM precipitation radar. - *Journal of Applied Meteorology, 40:* 1878-1899.

FRÜH, B., J. BENDIX, T. NAUSS, M. PAULAT, A. PFEIFFER, J. W. SCHIPPER, B. THIES & H. WERNLI (2007): Verification of precipitation from regional climate simulations and remote-sensing observations with respect to ground-based observations in the upper Danube catchment. - *Meteorologische Zeitschrift, 16*: 275–293.

GRIFFITH, C. G., W. L. WOODLEY, P. G. GRUBE, D. W. MARTIN, J. STOUT & D. N. SIKDAR (1978): Rain estimation from geosynchronous satellite imagery - visible and infrared studies. - *Monthly Weather Review, 106*: 1153-1171.

GRUBER, A. (1973): Estimating rainfall in regions of active convection. - *Journal of Applied Meteorology, 12:* 110-118.

HASTINGS, D. A., & J. E. WILLIAM (1992): The Advanced Very High Resolution Radiometer (AVHRR): A Brief Reference Guide. - *Photogrammetric Engineering and Remote Sensing, 58*: 1183-1188.

HERZEGH, P. H. & P. V. HOBBS (1980): The mesoscale and microscale structure and organisation of clouds and precipitation in midlatitude cyclones. II: Warm-frontal clouds. - *Journal of the Atmospheric Sciences, 37:* 597-611.

HEYMSFIELD, A. J. (1977): Precipitation development in stratiform ice clouds: a microphysical and dynamical study. - *Journal of the Atmospheric Sciences, 34*: 367-381.

HEYMSFIELD, G. M. (1979): Doppler radar study of a warm frontal region. - *Journal of the Atmospheric Sciences, 36:* 2093-2107.

HOBBS, P. V., T. J. MATEJKA, P. H. HERZEGH, J. D. LOCATELLI & R. A. HOUZE (1980): The mesoscale and microscale structure and organisation of clouds and precipitation in midlatitude cyclones. I: a case study of a cold front. - *Journal of the Atmospheric Sciences, 37:* 568-596.

HOBBS, P. V. & P. O. G. PERSSON (1982): The mesoscale and microscale structure and organisation of clouds and precipitation in midlatitude cyclones. Part V: The substructure of narrow cold-frontal rainbands. - *Journal of the Atmospheric Sciences, 39*: 280-295.

HOLLINGER, J. P., J. L. PEIRCE & G. A. POE (1990): SSM/I instrument evaluation. - *IEEE Transactions on Geoscience and Remote Sensing, 28*: 781-790.

HONG, Y., K.-L. HSU, S. SOROOSHIAN & X. GAO (2004): Precipitation Estimation from Remotely Sensed Imagery Using an Artificial Neural Network Cloud Classification System. - *Journal of Applied Meteorology, 43*: 1834-1852.

HOUZE, R. A., S. A. RUTLEDGE, T. J. MATEJKA & P. V. HOBBS (1981): The mesoscale and microscale structure and organisation of clouds and precipitation in midlatitude cyclones. III: Air motions and precipitation growth in a warm-frontal rainband. - *Journal of the Atmospheric Sciences, 38*: 639-649.

HOUZE R. A. (1993): Cloud Dynamics, Vol. 53. of International Geophysics Series, Academic Press, San Diego.

HOUZE R. A. (1997): Stratiform precipitation in regions of convection: A meteorological paradox? - *Bulletin of the American Meteorological Society, 78*: 2179-2196.

HSU, K.-L., X. GAO & S. SOROOSHIAN (2002): Rainfall estimation using cloud texture classification mapping. *Proceedings of the 1st IPWG Workshop*.

HUFFMAN, G. J., R. F. ADER, P. ARKIN, P., A. CHANG, R. FERRARO, A. GRUBER, J. JANOVIAK, A. MCNAB, B. RUDOLF & U. SCHNEIDER (1997): The global precipitation climatology project (GPCP) combined precipitation dataset. - *Bulletin of the American Meteorological Society, 78:* 5-20.

IGUCHI, T., T. KOZU, R. MENEGHINI, J. AWAKA & K. OKAMOTO (2000): Rain-profiling algorithm for the TRMM precipitation radar. - *Journal of Applied Meteorology, 39*: 2038-2052.

KÄSTNER, M., F. TORRICELLA & S. DAVOLIO (2006): Intercomparison of satellite-based and model-based rainfall analyses. - *Meteorological Applications, 13*: 213-223.

KERRACHE, M. & J. SCHMETZ (1988): A precipitation index from the ESOC climatological data set. - *ESA Journal, 12:* 379-383.

KIDD, C. (2001): Satellite rainfall climatology: a review. - *International Journal of Climatology, 21*: 1041-1066.

KIDDER, S. Q. & T. H. VONDER HAAR (1995): Satellite meteorology: an introduction. Academic Press, London , 466 pp.

KING, P. W. S., W. D. HOGG & P. A. ARKIN (1995): The role of visible data in improving satellite rain-rate estimates. - *Journal of Applied Meteorology, 34*: 1608-1621.

KRAUS, H. (1995): Das neue Bild von den atmosphärischen Fronten. - *Erdkunde, 49*. 81-105.

KUMMEROW, C. D. (1998): Beamfilling errors in passive microwave rainfall retrievals. - *Journal of Applied Meteorology*, 37: 356–370.

KURINO, T. (1997): A satellite infrared technique for estimating 'deep/shallow' precipitation. - *Advances in Space Research, 19*: 511–514.

LENSKY, I. M. & D. ROSENFELD (1997): Estimation of precipitation area and rain intensity based on the microphysical properties retrieved from NOAA AVHRR data. - *Journal of Applied Meteorology, 36*: 234-242.

LENSKY, I. M. & D. ROSENFELD (2003a): A night-time delineation algorithm for infrared satellite data based on microphysical considerations. - *Journal of Applied Meteorology, 42*: 1218–1226.

LENSKY, I. M. & D. ROSENFELD (2003b): Satellite-based insights into precipitation formation processes in continental and maritime convective clouds at night-time. - *Journal of Applied Meteorology, 42*: 1227–1233.

LEVIZZANI, V., F. PORCÙ & F. PRODI (1990): Operational rainfall estimation using METEOSAT infrared imagery: An application in Italy's Arno river basin – Its potential and drawbacks. - *ESA Journal, 14*: 313-323.

LEVIZZANI, V., J. SCHMETZ, H. J. LUTZ, J. KERKMANN, P. P. ALBERONI & M. CERVINO (2001): Precipitation estimations from geostationary orbit and prospects for Meteosat Second Generation. - *Meteorological Applications, 8:* 23–41.

LEVIZZANI, V. (2003): Satellite rainfall estimations: new perspectives for meteorology and climate from the EURAINSAT project. - *Annales Geophysicae-Italy, 46*: 363–372.

LOVEJOY, S. & G. L. AUSTIN (1979): The delineation of rain areas from visible and IR satellite data for GATE and mid-latitudes. - *Atmosphere-Ocean, 17:* 77-92.

MATEJKA, T. J., R. A. HOUZE & P. V. HOBBS (1980): Microphysics and dynamics of clouds associated with mesoscale rainbands in extratropical cyclones. - *Quarterly Journal of the Royal Meteorological Society, 106*: 29-56.

MENZ, G. & A. ZOCK (1997): Regionalisation of precipitation models in east Africa using Meteosat data. - *Journal of Climate, 17*: 1011-1027.

MENZEL, W. P. & J. F. PURDOM (1994): Introducing the GOES I: The first of a new generation of Geostationary Operational Environmental Satellites. - *Bulletin of the American Meteorological Society, 75:* 757-781.

NAUSS, T. & A. A. KOKHANOVSKY (2006): Discriminating raining from non-raining clouds at mid-latitudes using multispectral satellite data. - *Atmospheric Chemistry and Physics, 6*: 5031–5036.

NAUSS, T. & A. A. KOKHANOVSKY (2007): Assignment of rainfall confidence values using multispectral satellite data at mid-latitudes: first results. - *Advances in Geosciences, 10*: 99–102.

NEGRI, A. J., R. F. ADLER & J. P. WETZEL (1984): Rain estimation from satellites: An examination of the Griffith-Woodley Technique. - *Journal of Climate and Applied Meteorology, 23*: 102-116.

NEGRI, A. J. & R. F. ADLER (1993): An intercomparison of three satellite infrared rainfall techniques over Japan and surrounding waters. - *Journal of Applied Meteorology, 32*: 357-373.

O'SULLIVAN, F., C. H. WASH, M. STEWART & C. E. MOTELL (1990): Rain estimation from infrared and visible GOES satellite data. - *Journal of Applied Meteorology, 29*: 209-223.

POMPEI, A., M. MARROCU, P. BOI & G. DALU (1995): Validation of retrieval algorithms for the infrared remote sensing of precipitation with the Sardinian gauge network data. - *Il Nuovo Cimento, 18 C*: 483-496.

PRUPPACHER, H. R. & J. D. KLETT (1997): Microphysics of clouds and precipitation. Atmospheric and oceanographic sciences library 18, Kluwer, Dordrecht, 976 pp.

REUDENBACH, C., T. NAUSS, & J. BENDIX (2007): Retrieving precipitation with GOES, Meteosat and Terra/MSG at the tropics and mid-latitudes. In: LEVIZZANI, V., P. BAUER, & F. J. TURK (Ed.): Measuring precipitation form space. - *Advances in global change research, 28*. Springer: Netherlands.

REUDENBACH, C. (2003): Konvektive Sommerniederschläge in Mitteleuropa. Eine Kombination aus Satellitenfernerkundung und numerischer Modellierung zur automatischen Erfassung mesoskaliger Niederschlagsfelder. - *Bonner Geographische Abhandlungen, 109*: 152 pp.

ROGERS, R. R. & M. K. YAU (1989): A short course in cloud physics, 3rd edition, Pergamon Press, Oxford, 293 pp.

ROSENFELD, D. & I. LENSKY (1998): Satellite-based insights into precipitation formation processes in continental and maritime convective clouds. - *Bulletin of the American Meteorological Society, 79*: 2457-2476.

ROSENFELD, D., E. CATTANI, S. MELANI & V. LEVIZZANI (2004): Considerations on daylight operation of 1.6 µm vs. 3.7 µm channel on NOAA and METOP Satellites. - *Bulletin of the American Meteorological Society, 85*: 873– 881.

RUTLEDGE, S. A. & P. V. HOBBS (1983): The mesoscale and microscale structure and organisation of clouds and precipitation in midlatitude cyclones. VIII: a model for the "seeder-feeder" process in warm frontal rainbands. - *Journal of the Atmospheric Sciences, 40*:1185-1206.

SAARIKIVI, P. (1989): Characteristics of mesoscale precipitation bands in southern Finland. - *Monthly Weather Review, 117*: 2584-2593.

SCHMETZ, J., P. PILI, S. TJEMKES, D. JUST, J. KERKMANN, S. ROTA & A. RATIER (2002): An introduction to Meteosat Second Generation (MSG). - *Bulletin of the American Meteorological Society, 83*: 977–992.

SCOFIELD, R. A. & V. J. OLIVER (1977): A scheme for estimating convective rainfall from satellite imagery. NOAA Technical Memorandum NESS 86, Department of Commerce, Washington D.C., 47 pp.

SCOFIELD, R. A (1987): The NESDIS operational convective precipitation estimation technique. - *Monthly Weather Review, 115:* 1773-1793.

SCOFIELD, R. A. & L. NAIMENG (1994): The use of satellite imagery during the great floods of 1993. *Proceedings of the 7th Conference on Satellite Meteorology and Oceanography*: 345-350.

SCOFIELD, R. A. & R. J. KULIGOWSKI (2003): Status and Outlook of Operational Satellite Precipitation Algorithms for Extreme-Precipitation Events. - *Weather and Forecasting, 18:* 1037-1051.

STEPHENS, G. L. & C. D. KUMMEROW (2007): The Remote Sensing of Clouds and Precipitation from Space: A Review. - *Journal of the Atmospheric Sciences - Special Section, 64*: 3742-3765.

TODD, M. C., E. C. BARRETT, M. J. BEAUMONT & T. J. BELLERBY (1999): Estimation of daily rainfall over the upper Nile river basin using a continuously calibrated satellite infrared technique. - *Meteorological Applications, 6:* 201-210.

TSONIS, A. A. & G. A. ISAAC (1985): On a new approach for instantaneous rain area delineation in the midlatitudes using GOES data. - *Journal of Climate and Applied Meteorology, 24*: 1208-1218.

TSONIS, A. A. (1987): Determining rainfall intensity and type from GOES imagery in the midlatitudes. - *Remote Sensing of the Environment, 21*: 29-36.

VICENTE, G. A. & R. A. SCOFIELD (1996): Experimental GOES-8/9 derived rainfall estimates for flash flood and hydrological applications. *Proceedings of the 2000 Eumetsat Meteorological Satellite Data Users' Conference,* EUMETSAT: 89-96.

VICENTE, G. A., R. A. SCOFIELD & W. P. MENZEL (1998): The operational GOES infrared rainfall estimation technique. - *Bulletin of the American Meteorological Society, 79*: 1883-1898.

WEI, C., W.-C. HUNG & K.-S. CHENG (2006): A multi-spectral spatial convolution approach of rainfall forecasting using weather satellite imagery. - *Advances in Space Research, 37*: 747-753.

WU, R., J. A. WEINMAN & R. T. CHIN (1985): Determination of rainfall rates from GOES satellite images by a pattern recognition technique. - *Journal of Atmospheric and Oceanic Technology, 2:* 314-330.

WYLIE, D. P. (1979): An application of a geostationary satellite rain estimation technique to an extra-tropical area. - *Journal of Applied Meteorology, 18:* 1640-1648.

XIE, P. & P. A. ARKIN (1997): Global precipitation: a 17-year monthly analysis based on gauge observations, satellite estimates, and numerical model outputs. - *Bulletin of the American Meteorological Society, 78*: 2539-2558.

YAN, H. & S. YANG (2007): A MODIS Dual Spectral Rain Algorithm. - *Journal of Applied Meteorology and Climatology, 46*: 1305-1323.

CHAPTER 3

Detection of high Rain Clouds using Water Vapour Emission - Transition from Meteosat First (MVIRI) to Second Generation (SEVIRI)

Boris Thies, Thomas Nauß and Jörg Bendix

Submitted to Advances in Space Research

3 Detection of high rain clouds using water vapour emission - transition from Meteosat First (MVIRI) to Second Generation (SEVIRI)

Boris Thies, Thomas Nauß and Jörg Bendix

Philipps-University Marburg,
Department of Geography,
Laboratory for Climatology and Remote Sensing,
Deutschhausstraße 10, 35032 Marburg, Germany

Abstract

Positive brightness temperature differences between the water vapour (WV) and the infrared (IR) channels (ΔT_{WV-IR}) of the Meteosat First Generation (MFG) MVIRI instrument enable the detection and delineation of high rain clouds, which is a central element of the Enhanced Convective Stratiform Technique (ECST), a rainfall retrieval technique developed for MVIRI. In 2004, MFG MVIRI was replaced by Meteosat Second Generation (MSG) SEVIRI, which is characterized by a higher spectral, spatial and temporal resolution. The aim of the current paper is to test the transferability of the WV-IR difference technique developed for MVIRI to SEVIRI in order to guarantee the continuation of a long-term rainfall retrieval beyond the Meteosat system of the first generation. The presence and strength of positive ΔT_{WV-IR} for different SEVIRI WV-IR channel combinations is analyzed by means of radiative transfer calculations. The results reveal positive ΔT_{WV-IR} for all WV-IR combinations. However, in a comparison study of 80 temporally and spatially corresponding MVIRI- and SEVIRI-based ECST results, the difference between the $WV_{7.3}$ channel (6.85 – 7.85 μm) and the $IR_{12.1}$ channel (11.0 – 13.0 μm) has been identified as the most appropriate SEVIRI combination to properly reproduce the MVIRI-based ECST results. The successful application of positive ΔT_{WV-IR} to SEVIRI and the transfer of the adapted ECST from MVIRI to SEVIRI allows the continuation of satellite-derived precipitation time series applicable to e.g. climate change studies.

3.1 Introduction

Precipitation affects all aspects of life. Its coverage, frequency and amount is of great importance especially for agriculture, hydrology/water engineering, and ecology. However, the spatio-temporal characteristics of rainfall can hardly be reproduced by point observations or numerical models (TRENBERTH et al. 2003).

Especially in the absence of radar networks, data from geostationary weather satellites offer the opportunity to analyze precipitation characteristics in high spatial and temporal resolution. The operational geostationary satellite systems of the first generation launched in the 70ties now warrant long time series of data suitable for climate change studies.

Regarding the European and African continent, the Meteosat series of the European Meteorological Satellite Organisation (EUMETSAT) provides data since 1977, starting with Meteosat-1. Based on the Meteosat Visible and Infra-Red Imager radiometer (MVIRI), the precipitation retrieval scheme of the Enhanced Convective Stratiform Technique (ECST) has been developed (REUDENBACH et al. 2001, REUDENBACH 2003). The ECST is an improved version of the Convective-Stratiform Technique (CST, ADLER & NEGRI 1988, BENDIX 1997), which additionally uses the positive brightness temperature difference between the water vapour (WV) and the infrared (IR) channel ($\Delta T_{WV\text{-}IR}$) of MVIRI (see SCHMETZ et al. 1997, TJEMKES et al. 1997) for a more reliable detection of deep convective clouds and their separation from non-raining cirrus shields (KURINO 1997).

The phenomenon of positive $\Delta T_{WV\text{-}IR}$ is caused by the presence of water vapour in the lower stratosphere above the cloud (FRITZ & LASZLO 1993), which is transported there by deep convection with overshooting tops (e.g. PAGE 1982, KLEY et al. 1982). When the cloud top approaches the tropopause, it blocks lower tropospheric radiation from escaping into space and hence, the received signal at the satellite level originates from the cloud top and the atmosphere aloft. As the temperature in the stratosphere increases with height the water vapour above the cloud absorbs outgoing radiation from the high cloud top and emits radiation at higher temperatures. Because of the stronger water vapour absorption lines in the WV channel compared to the IR channel of MVIRI this results in higher brightness temperatures in the WV channel. As a result, the actual brightness temperature difference depends on the amount of stratospheric water vapour and the location of the cloud top with respect to the tropopause. Largest values for $\Delta T_{WV\text{-}IR}$ are calculated when the cloud top reaches the tropopause

inversion, where the brightness temperature in the IR channel is at a minimum (SCHMETZ et al. 1997, TJEMKES et al. 1997).

At the beginning of 2004, the Meteosat First Generation satellite program has been replaced by Meteosat Second Generation (MSG) with the Spinning Enhanced Visible and InfraRed Imager (SEVIRI) aboard. SEVIRI is characterised by an enhanced spectral, spatial and temporal resolution (SCHMETZ et al. 2002). Of special interest in the context of the detection of deep convective clouds by means of positive $\Delta T_{WV\text{-}IR}$ are the two water vapour ($WV_{6.2}$: 5.35 – 7.15 μm; $WV_{7.3}$: 6.85 – 7.85 μm) and the two infrared channels ($IR_{10.8}$: 9.8 – 11.8 μm; $IR_{12.1}$: 11.0 – 13.0 μm). Because of its differing spectral resolution with regard to MVIRI (WV: 5.7 – 7.1 μm; IR: 10.5 – 12.5 μm), it has to be examined if and how the brightness temperature difference between the water vapour and the infrared channels of SEVIRI can be used to delineate high rain clouds equal to MVIRI. A successful adaptation of this technique would guarantee the continuation beyond MVIRI in order to gain long time series of satellite-retrieved rainfall data applicable to climate change studies.

Therefore, the main objective of the present study is the investigation of positive $\Delta T_{WV\text{-}IR}$ for the different SEVIRI WV-IR combinations and the identification of the appropriate SEVIRI bands, which can be used to reproduce the results of the MVIRI-based ECST.

The paper is structured as follows. Section 3.2 gives a brief description of the utilized data and methods. Radiative transfer calculations concerning the SEVIRI WV and IR channels are presented in section 3.3.1. In section 3.3.2, a comparison of 80 simultaneous SEVIRI/MVIRI rain retrievals will illustrate the successful application of the appropriate SEVIRI channel combination. In section 3.3.3 the results of a case study are presented. The conclusion and a summary can be found in section 3.4.

3.2 Data and methods

For this study, simultaneous SEVIRI/MVIRI data are required. Between 2004 and 2006 MFG MVIRI was operated as a backup system for MSG SEVIRI. Therefore, temporally and spatially corresponding data from both systems are generally available for this time period. The current study is conducted for Central Europe and is based on 80 simultaneous MVIRI/SEVIRI scenes of July and August 2004 with sufficient precipitation intensities. MSG SEVIRI data is operationally received at the Marburg Satellite Station MSS (BENDIX et al. 2003), corresponding MFG MVIRI data are acquired from the EUMETSAT archive.

The availability of positive $\Delta T_{WV\text{-}IR}$ for the different SEVIRI WV-IR combinations was tested using the radiative transfer model Streamer (KEY & SCHWEIGER 1998, KEY 2001), which is based on the plane-parallel theory and uses the discrete ordinate solver DISORT (STAMNES et al. 1988). This medium spectral resolution model computes radiances and fluxes in the 0.28 – 500 µm wavelength range, using 129 bands with variable width. The spectral response functions (SRF) of the SEVIRI channels are realized by weighting coefficients for the spectral bands of the model (MELANI et al. 2003). Cloud optical and microphysical properties can be specified by the user and the effects of water vapour, carbon dioxide, oxygen and ozone are included using standard profiles or radiosonde data. A parameterized background tropospheric aerosol distribution with a 50 km visibility and background stratospheric amounts have been used for the calculations. Other relevant input parameters, as well as cloud optical and microphysical properties used for the simulations are mentioned in chapter 3.3.1.

The ECST rainfall retrieval algorithm will be used for the validation of the different SEVIRI WV-IR channel combinations by comparing the retrieved rain area of high-level rain clouds, which are expected to agree properly in simultaneous MVIRI and SEVIRI scenes. The ECST scheme, which was originally developed for MVIRI, has been adapted to SEVIRI. For a proper comparison of ECST results, MVIRI-based maps were projected to the SEVIRI viewing geometry. The use of the WV-IR-brightness temperature differences in the ECST for the delineation of high rain clouds is described in detail by REUDENBACH et al. (2001) and REUDENBACH (2003). Generally, positive brightness temperature differences between the MVIRI WV and the IR channel indicate high rain clouds. In the ECST, positive $\Delta T_{WV\text{-}IR}$ thresholds are statistically subdivided to distinguish between two classes of raining cloud areas: (i) active convective areas with high precipitation intensities and (ii) clouds with normal stratiform precipitation intensities in the adjacent environment of active convective areas. In the current study, these two classes will be derived for both, MVIRI and SEVIRI imagery and used separately during the validation (see section 3.3.2).

The indirect validation of the different SEVIRI WV-IR combinations with the corresponding MVIRI retrieval is conducted by applying standard validation scores for dichotomous data sets: (i) Bias, (ii) probability of detection (POD), (iii) false alarm ratio (FAR) and (iv) critical success index (CSI). The calculation of the verification scores is described e.g. by STANSKI et al. (1989). The

statistics were calculated separately for each rainfall class (convective, convective-stratiform) and for the entire rain area.

The four different SEVIRI WV-IR combinations are tested:

- $WV_{6.2}$–$IR_{10.8}$: difference between WV 5.35 – 7.15 μm and IR 9.8 – 11.8 μm
- $WV_{6.2}$–$IR_{12.1}$: difference between WV 5.35 – 7.15 μm and IR 11.0 – 13.0 μm
- $WV_{7.3}$–$IR_{10.8}$: difference between WV 6.85 – 7.85 μm and IR 9.8 – 11.8 μm
- $WV_{7.3}$–$IR_{12.1}$: difference between WV 6.85 – 7.85 μm and IR 11.0 – 13.0 μm

3.3 Results

3.3.1 Radiative Transfer Calculations

In order to check if positive $\Delta T_{WV\text{-}IR}$ for the four SEVIRI WV-IR combinations enable an appropriate detection of high-level rain clouds, a deep convective weather event, the Cologne-hail storm on 4 July 1994 was chosen for the radiative transfer calculations. This highly convective storm encompassing the two classes of high-raining clouds was associated with a squall line over Germany (for a detailed description of the weather situation refer to REUDENBACH et al. 2001). For the Streamer simulations, an optically thick Cumulonimbus cloud with a base height of 2 km was used together with the 12:00 LT radiosonde profile from Essen, Germany. To get an idea of the development of $\Delta T_{WV\text{-}IR}$ for a rising cumulus the vertical extension of the cloud was varied between 6 and 11 km. The parameterized optical and microphysical cloud properties are those of deep convective Cumulonimbus clouds, taken from the parameterization of ZHANG et al. (1995) and SCHEMENAUER & ISAAC (1984) who described the typical lifecycle of summertime cumulus clouds. Essential input parameters are the effective radius of water droplets (R_e), the mean effective diameter of ice crystals (D_e) ,the liquid water content (LWC) and the ice water content (IWC). Table 3.1 summarizes the relevant input parameters used in the calculations. The settings are applied to simulate the resulting cloud top temperatures in each SEVIRI WV and IR channel (see chapter 3.3.2).

Table 3.1: Input parameters for the radiative transfer calculations.

Solar zenith angle [°]	Satellite zenith angle [°]	Relative azimuth angle [°]	R_e [µm]	LWC [g/m³]	D_e [µm]	IWC [g/m³]
45	55	130	30	0.5	60	0.07

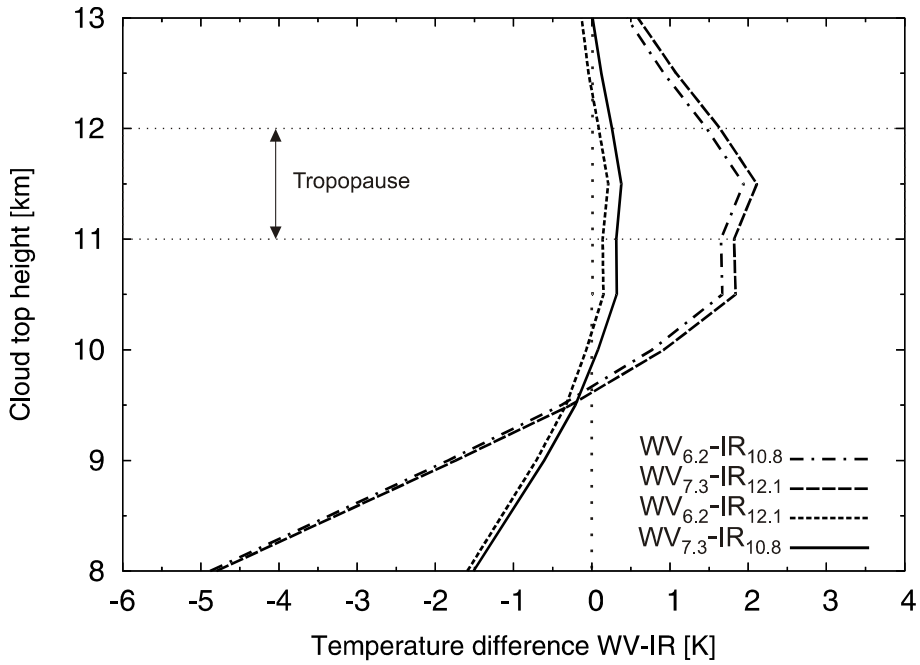

Figure 3.1: Simulated $\Delta T_{WV\text{-}IR}$ for each SEVIRI WV-IR channel combination as a function of cloud top height.

The calculated $\Delta T_{WV\text{-}IR}$ for different cloud top heights for each WV-IR combination are depicted in figure 3.1. As the cloud top rises, $\Delta T_{WV\text{-}IR}$ increases and the maximum temperature difference is observed when the cloud reaches the tropopause at about 11.5 km, which is indicated in the radiosonde profile by an isothermal layer between 11 and 12 km. Then $\Delta T_{WV\text{-}IR}$ decreases again because the water vapour amount above the cloud top decreases with further cloud top rises. The results of the radiative transfer calculations agree quite well with the findings of SCHMETZ et al. (1997) and TJEMKES et al. (1997) for MVIRI. Therefore, it is concluded that the approach to detect convective cores by means of positive temperature differences

between the WV and the IR channel can be generally transferred to SEVIRI.

The varying amount of the calculated $\Delta T_{WV\text{-}IR}$ for each WV-IR combination can be explained by the channels spectral range and spectral response function (SRF). To investigate this feature, calculations were performed for each channel for both a cloud free atmosphere and a cloud reaching the tropopause with a top height at 12 km channel. The results are displayed in figure 3.2. Note that the calculated temperatures in figure 3.2 are not weighted by the SRF of the respective channel. This was done to allow a detailed analysis of the calculated temperatures over the complete spectral range of each channel. The resulting brightness temperatures in each channel, obtained by the integration of the calculated temperatures over the spectral interval and the weighting by the SRF of the respective channel, are depicted in table 3.2.

In a cloud free atmosphere (figure 3.2 upper panel) the radiation in the infrared channels originates from the surface and the lower troposphere. Generally, the signal in the 11.0 – 13.0 μm interval ($IR_{12.1}$; figure 3.2 a) comes from slightly higher parts in the troposphere compared to the 9.8 – 11.8 μm interval ($IR_{10.8}$; figure 3.2 b, see also SCHMETZ et al. 2002). This is due to its higher sensitivity to water vapour absorption (KLEESPIES et al. 1990) resulting in an emission spectrum at higher altitudes and lower temperatures. Integrated and weighted with the exact SRF, the brightness temperature in the $IR_{12.1}$ channel is colder than in the $IR_{10.8}$ channel (see table 3.2).

Table 3.2: Simulated brightness temperature (BT) [K] in each infrared and water vapour channel of SEVIRI, obtained by the integration of the calculated spectra over the spectral interval and the weighting by the SRF of each channel.

	$BT_{IR12.1}$ [K]	$BT_{IR10.8}$ [K]	$BT_{WV7.3}$ [K]	$BT_{WV6.2}$ [K]
Cloud free atmosphere	287.2	290.1	252.4	234
Cloud top at 12km	216.8	217	217	218.4

The 5.35 – 7.15 µm interval ($WV_{6.2}$; figure 3.2 d) covers the centre of the water vapour absorption band, whereas the 6.85 – 7.85 µm interval ($WV_{7.3}$; figure 3.2 c) is positioned closer to its edge. Consequently, the main part of the radiation in the $WV_{6.2}$ channel originates from higher parts of the troposphere (~300 hPa level, see SCHMETZ et al. 2002) compared to the $WV_{7.3}$ channel where the radiation originates also from lower layers (~500 hPa level; see SCHMETZ et al. 2002). Integrated over the spectral interval and taking into account the exact SRF, the brightness temperature in the $WV_{6.2}$ channel is colder than in the $WV_{7.3}$ channel (see table 3.2).

When an opaque cloud is inserted in the profile at the level of the tropopause (figure 3.2 lower panel), radiation from the troposphere is blocked from escaping into space and the received radiation originates from cloud top and stratospheric emissions. As the temperature in the stratosphere increases with height, the emission in the $IR_{10.8}$ channel results in higher temperatures than in the $IR_{12.1}$ channel since the absorption at the edge of the $IR_{10.8}$ channel increases slightly (figure 3.2 f). Integrated over the spectral region and considering the SRF of the infrared channels, this leads to slightly higher temperatures in the $IR_{10.8}$ as compared to the $IR_{12.1}$ channel (see table 3.2). The absorption lines in the $WV_{6.2}$ channel (figure 3.2 h) are stronger throughout the entire spectral region compared to the $WV_{7.3}$ channel (figure 3.2 g) resulting in higher temperatures in the $WV_{6.2}$ channel for the cloudy case (see table 3.2).

In the light of the results depicted in figure 3.2 the differences concerning the calculated $\Delta T_{WV\text{-}IR}$ for each SEVIRI WV-IR combination (see figure 3.1) can be explained as follows. For cloud tops below the tropopause the temperature in the $WV_{6.2}$ channel is lower than in the $WV_{7.3}$ channel and the temperature in the $IR_{10.8}$ channel is higher than in the $IR_{12.1}$ channel. Thus, the minimum and maximum temperature differences are obtained by the $WV_{6.2}$–$IR_{10.8}$ and $WV_{7.3}$–$IR_{12.1}$ combinations respectively (see figure 3.1). When the cloud top reaches the tropopause and tropospheric radiation is blocked, the temperature in the $WV_{6.2}$ channel becomes higher than in the $WV_{7.3}$ channel, whereas the temperature in the $IR_{10.8}$ channel remains slightly higher than in the $IR_{12.1}$ channel. Therefore, minimum and maximum temperature differences are calculated for the $WV_{7.3}$–$IR_{10.8}$ and the $WV_{6.2}$–$IR_{12.1}$ combination respectively (see figure 3.1).

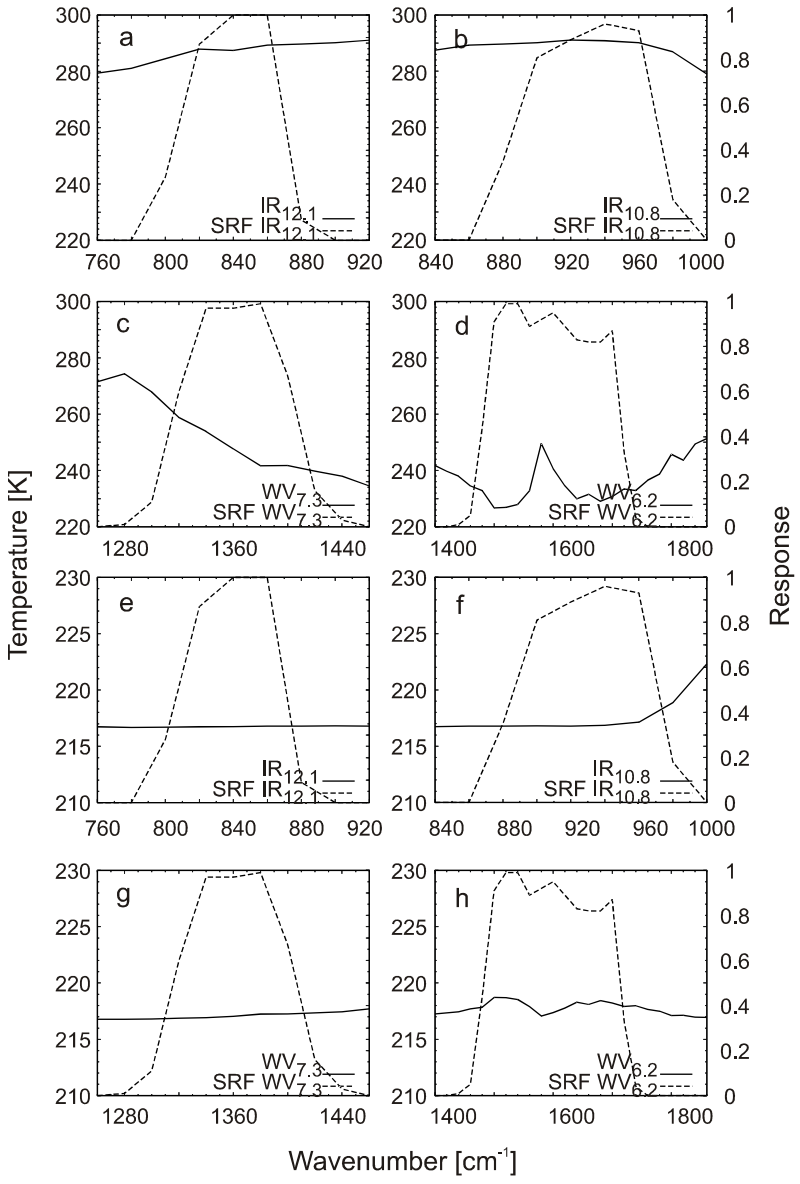

Figure 3.2: Results of the radiative transfer calculations for the spectral ranges of the SEVIRI WV-IR channel combinations (solid line) together with the SRF for each channel (dotted line). a) to d) results for a cloud free atmosphere: a) IR 11.0 – 13.0 µm ($IR_{12.1}$); b) IR 9.8 – 11.8 µm ($IR_{10.8}$); c) WV 6.85 – 7.85 µm ($WV_{7.3}$); d) WV 5.35 – 7.15 µm ($WV_{6.2}$). e) to h) results for a cloud top at 12 km: e) IR 11.0 – 13.0 µm ($IR_{12.1}$); f) IR 9.8 – 11.8 µm ($IR_{10.8}$); g) WV 6.85 – 7.85 µm ($WV_{7.3}$); h) WV 5.35 – 7.15 µm ($WV_{6.2}$).

Based on the results of the radiative transfer calculations, the method to detect deep convective precipitation clouds by means of positive $\Delta T_{WV\text{-}IR}$ can generally be applied to the SEVIRI WV-IR differences, which also implies the option to transfer the ECST to SEVIRI.

3.3.2 Statistical comparison of the ECST results based on MVIRI and on SEVIRI

For a successful transfer of the ECST algorithm, it has to be analyzed, which of the four possible WV-IR SEVIRI combinations yields the best results in reproducing the MVIRI retrievals. The calculated validation scores used for this analysis are summarized in table 3.3. They were computed separately for (i) the entire rainfall area and (ii) for each of the two individual classes (see chapter 3.2).

In general, the $WV_{7.3}$–$IR_{12.1}$ combination reveals the highest accordance with the MVIRI-based results regardless if the entire rainfall area or one of the two individual classes is used for the comparison. The calculated validation scores indicate good agreement between the two sensors with the highest quality for the entire rain area identified by the ECST and for the classified convective-stratiform precipitation area. On the other hand, the scores reflect a lower level of agreement for the detected active convective areas. This probably is caused by the higher spatial resolution of the SEVIRI data (3 by 3 km at nadir) leading to smaller and more fractional areas of the detected active convective pixels. Along with the projection of the MVIRI-based ECST results (5 by 5 km at nadir) to the SEVIRI viewing geometry (3 by 3 km at nadir) this can cause spatial misalignments between both data sets regarding the classified pixels. Because of the lower fraction of the classified rain area (see percentage rain area in table 3.3) these spatial misalignments have a strong influence on the quality of the calculated verification scores for the active convective areas. This interpretation is supported by the fact that despite the low quality of the validation results indicated by the POD, FAR, and CSI scores, the Bias and the fraction of the classified rain area is in good accordance between the MVIRI- and the SEVIRI-based results for the active convective areas.

Based on the results of this comparison study, the SEVIRI $WV_{7.3}$–$IR_{12.1}$ combination is identified as the appropriate channel combination to reproduce the results of the MVIRI-based ECST. The other SEVIRI WV-IR combinations are characterised by a stronger underestimation of the different detected rain areas. This is due to the higher amount of classified active convective cores by the $WV_{7.3}$–

$IR_{12.1}$ combination. As the convective-stratiform areas are classified in the adjacent environment of these active convective cores (see chapter 3.2), their higher amount results in a higher spatial extension of the convective-stratiform area. An explanation for the higher amount of classified active convective cores by the $WV_{7.3}$–$IR_{12.1}$ difference might be that cloud tops approaching the tropopause sooner result in positive $\Delta T_{WV\text{-}IR}$ for this channel combination. An evidence for this is the lower gradient for the simulated $\Delta T_{WV\text{-}IR}$ between cloud tops beneath and above the tropopause, that can be seen in figure 3.1.

The following case study will illustrate the effect of the different spatial resolution of the MVIRI and the SEVIRI data on the classified rain areas by the ECST.

Table 3.3: Calculated validation scores for 80 spatially and temporally corresponding MVIRI and SEVIRI based ECST results between July and August 2004.

	Rain Area SEVIRI [%]	Rain Area MVIRI [%]	Bias	POD	FAR	CSI
Whole area						
$WV_{6.2}$-$IR_{10.8}$	1.07	3.76	0.29	0.22	0.22	0.21
$WV_{6.2}$-$IR_{12.1}$	1.36	3.76	0.36	0.28	0.22	0.26
$WV_{7.3}$-$IR_{10.8}$	2.5	3.76	0.66	0.47	0.29	0.4
$WV_{7.3}$-$IR_{12.1}$	3.49	3.76	0.93	0.62	0.33	0.48
Convective- stratiform						
$WV_{6.2}$-$IR_{10.8}$	0.82	2.87	0.28	0.17	0.4	0.15
$WV_{6.2}$-$IR_{12.1}$	1.07	2.87	0.37	0.23	0.39	0.2
$WV_{7.3}$-$IR_{10.8}$	2.06	2.87	0.72	0.41	0.43	0.31
$WV_{7.3}$-$IR_{12.1}$	2.93	2.87	1.02	0.55	0.46	0.38
Active convective cores						
$WV_{6.2}$-$IR_{10.8}$	0.14	0.7	0.19	0.05	0.74	0.04
$WV_{6.2}$-$IR_{12.1}$	0.17	0.7	0.24	0.06	0.74	0.05
$WV_{7.3}$-$IR_{10.8}$	0.35	0.7	0.49	0.11	0.78	0.08
$WV_{7.3}$-$IR_{12.1}$	0.47	0.7	0.66	0.14	0.79	0.09

3.3.3 Case study

Figure 3.3 a-c illustrates a case study for the 18 July 2004 1:00 UTC. Figure 3.3 a shows the brightness temperature in the SEVIRI $IR_{10.8}$ channel. In Figure 3.3 b and 3.3 c the ECST results based on the WV and IR channels of MVIRI (3 b) and the ECST results based on the $WV_{7.3}$–$IR_{12.1}$ channel combination (3.3 c) are displayed.

The rain clouds over northern Germany, Denmark and southern Sweden were the result of a convergence line over western and southwestern Germany, which drafted rapidly to the northeast with a southwesterly upper air flow. This convergence line caused numerous and heavy thunderstorms, indicated by the cold cloud top temperatures in figure 3.3 a. The calculated indices for that scene are depicted in table 3.4.

Table 3.4: Calculated verification scores for ECST results based on MVIRI and on the $WV_{7.3}$–$IR_{12.1}$ channel combination of SEVIRI for the 18 July 2004 1:00 UTC.

	Bias	POD	FAR	CSI
Whole area	0.74	0.54	0.28	0.45
Convective-stratiform	0.85	0.46	0.46	0.33
Active convective cores	0.44	0.09	0.8	0.07

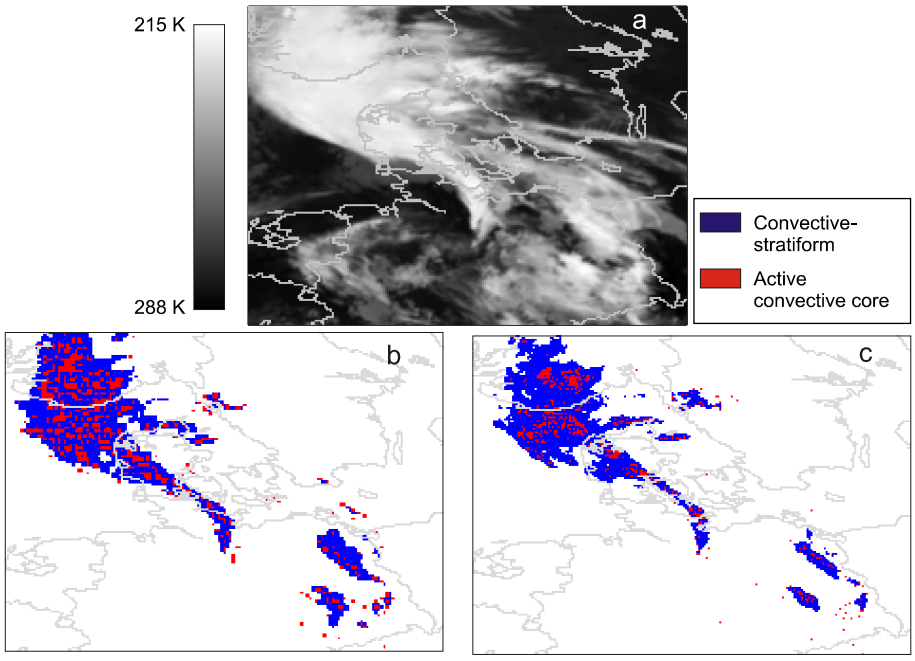

Figure 3.3: Brightness temperature [K] in the IR10.8 channel (a), MVIRI-based ECST results (b), ECST results based on the $WV_{7.3}$–$IR_{12.1}$ channel combination of SEVIRI (c) for the 18 July 2004 1:00 UTC.

A visual inspection of the ECST results in figure 3.3 b and c reveals that the spatial patterns of the identified precipitation areas correspond quite well between both data sets. Because of the higher spatial resolution of SEVIRI, the ECST result based on the $WV_{7.3}$–$IR_{12.1}$ combination is characterized by a more differentiated image especially concerning the detected active convective cores. Those form smaller and less contiguous areas compared to the MVIRI results. This causes the underestimation indicated by the Bias. Together with the above mentioned spatial misalignment caused by the projection of MVIRI to SEVIRI this also leads to a low CSI as well as to a low POD in connection with a high FAR. The Bias for the classified convective-stratiform precipitation area points also to an underestimation by the $WV_{7.3}$–$IR_{12.1}$ combination. This is a consequence of the smaller number of active convective cores since the convective-stratiform areas are classified in and with respect to the adjacent environment of those cores. The underestimation of the whole area identified by the ECST is a consequence of the underestimated area of the identified subclasses.

3.4 Summary and Conclusion

The phenomenon of positive brightness temperature differences between the WV and IR channels ($\Delta T_{WV\text{-}IR}$), which enables the detection of high rain clouds and forms the basis for the ECST rainfall retrieval, has been investigated for SEVIRI. Based on radiative transfer calculations, which revealed the existence of positive $\Delta T_{WV\text{-}IR}$ for all SEVIRI WV-IR combinations, the $\Delta T_{WV\text{-}IR}$ technique can be applied to SEVIRI. As a consequence, the ECST can be successfully transferred from MVIRI to SEVIRI.

In a comparison study with 80 temporally and spatially corresponding MVIRI- and SEVIRI-based ECST results, the difference between the $WV_{7.3}$ channel (6.85 – 7.85 μm) and the $IR_{12.1}$ channel (11.0 – 13.0 μm) has been identified as the most appropriate combination to reproduce the MVIRI-based ECST results. It should be stressed that the spatial resampling of the MVIRI data with a lower spatial resolution to the SEVIRI geometry leads to clear differences in the detection of active convective areas. However, this is not important for the question of transferability of the WV-IR method to SEVIRI. Apart from this main intention of the paper, the results clearly show the advantage of SEVIRI for a proper detection of active convective areas, which often disappear in the MVIRI retrieval due to the mixed-pixel effect. While the application of the $\Delta T_{WV\text{-}IR}$ technique to SEVIRI and the successful transfer of the ECST from MVIRI to SEVIRI generally guarantees the continuation of satellite

based precipitation time series applicable to climate change studies, the results underline that the SEVIRI data should be resampled to MVIRI geometry for consistency reasons when long time series of precipitation will be generated covering both, the first and the second generation of Meteosat satellites.

Acknowledgements

The current study is funded by the German Ministry of Research and Education (BMBF) in the framework of GLOWA-Danube project (G-D/2004/TP-10, precipitation/remote sensing). The authors would like to thank Dr. C. Reudenbach for providing the ECST source code and EUMETSAT for providing MFG MVIRI data.

References

ADLER, R. F. & A. J. NEGRI (1988): A satellite infrared technique to estimate tropical convective and stratiform rainfall. - *Journal of Applied Meteorology, 27:* 30-51.

BENDIX, J. (1997): Adjustment of the Convective-Stratiform Technique (CST) to estimate 1991/93 El Niño rainfall distribution in Ecuador and Peru by means of Meteosat-3 IR data. - *International Journal of Remote Sensing, 18:* 1387-1394 & 2707.

BENDIX, J., C. REUDENBACH & R. ROLLENBECK (2003): The Marburg Satellite Station. *Proceedings of the 2002 Meteorological Satellite Users' Conference. Dublin, 2–6 September 2002, EUMETSAT:* 139–146.

FRITZ, S. & I. LASZLO (1993): Detection of water vapour in the stratosphere over very high clouds in the tropics. - *Journal of Geophysical Research, 98*: D12: 22959-22967.

KEY, J. (2001): Streamer User's Guide, Cooperative Institute for Meteorological Satellite Studies, University of Wisconsin, 96 pp.

KEY, J. & A. J. SCHWEIGER (1998): Tools for atmospheric radiative transfer: Streamer and FluxNet. - *Computers & Geosciences, 24*: 443-451.

KLEESPIES, T. J. & L. M. MCMILLIN (1990): Retrieval of precipitable water from observations in the split window over varying surface temperatures. - *Journal of Applied Meteorology, 29:* 851-862.

KLEY, D., A. SCHMELTEKOPF, K. KELLY, R. WINKLER, T. THOMPSON & M. MCFARLAND (1982): Transport of water vapour through the tropical tropopause. - *Geophysical Research Letters, 9:* 617-624.

KURINO, T. (1997): A satellite infrared technique for estimating "deep/ shallow" convective and stratiform precipitation. - *Advances in Space Research, 19*: 511-514.

MELANI, S., E. CATTANI, V. LEVIZZANI, M. CERVINO, F. TORRICELLA & M. J. COSTA (2003): Radiative effects of simulated cirrus clouds on top of a deep convective storm in Meteosat Second Generation SEVIRI channels. - *Meteorology and Atmospheric Physics, 83*: 109-122.

PAGE, W. (1982): NASA experiment on tropospheric-stratospheric water vapour transport in the intertropical convergence zone. - *Geophysical Research Letters, 9*: 599-624.

REUDENBACH, C. (2003): Konvektive Sommerniederschläge in Mitteleuropa. Eine Kombination aus Satellitenfernerkundung und numerischer Modellierung zur automatischen Erfassung mesoskaliger Niederschlagsfelder. - *Bonner Geographische Abhandlungen, 109*: 152 pp.

REUDENBACH, C., G. HEINEMANN, E. HEUEL, J. BENDIX & M. WINIGER (2001): Investigation of summertime convective rainfall in Western-Europe based on a synergy of remote sensing data and numerical models. - *Meteorology and Atmospheric Physics, 76:* 23-41.

SCHEMENAUER, R. B. & G. A. ISAAC (1984): The importance of cloud top lifetime in the description of natural cloud characteristics. - *Journal of Climate and Applied Meteorology, 23*: 267-279.

SCHMETZ, J., P. PILI, S. TJEMKES, D. JUST, J. KERKMANN, S. ROTA & A. RATIER (2002): An introduction to Meteosat Second Generation (MSG). - *Bulletin of the American Meteorological Society, 83:* 977-992.

SCHMETZ, J., TJEMKES, S. A., GUBE, M. & VAN DE BERG, L. (1997): Monitoring deep convection and convective overshooting with Meteosat. - *Advances in Space Research, 19*: 433-441.

STANSKI, H. R., L. WILSON & W. BURROWS (1989): Survey of common verification methods in meteorology. - *World Weather Watch Technical Report No. 8, WMO, Geneva,* WMO/TD No. 358, 114 pp.

TJEMKES, S. A., L. VAN DE BERG & J. SCHMETZ (1997): Warm water vapour pixels over high clouds as observed by Meteosat. - *Contributions to Atmospheric Physics, 70:* 15-21.

TRENBERTH, K.E., A. DAI, R. M. RASMUSSEN & D. B. PARSONS (2003): The changing character of precipitation. - *Bulletin of the American Meteorological Society, 84:* 1205-1217.

CHAPTER 4

Discriminating raining from non-raining cloud areas at mid-latitudes using Meteosat Second Generation SEVIRI night time data

Boris Thies, Thomas Nauß and Jörg Bendix

METEOROLOGICAL APPLICATIONS
Meteorol. Appl. (2008)
Published online in Wiley InterScience
(www.interscience.wiley.com) DOI: 10.1002/met.56

Received 31 May 2007; Revised 21 December 2007; Accepted 3 January 2008

4 Discriminating raining from non-raining cloud areas at mid-latitudes using Meteosat Second Generation SEVIRI night time data

Boris Thies, Thomas Nauß and Jörg Bendix

Philipps-University Marburg,
Department of Geography,
Laboratory for Climatology and Remote Sensing,
Deutschhausstraße 10, 35032 Marburg, Germany

Abstract

A new method for the delineation of precipitation during night-time using multispectral satellite data is proposed. The approach is not only applicable to the detection of mainly convective precipitation by means of the commonly used relation between infrared cloud top temperature and rainfall probability but enables also the detection of stratiform precipitation (e.g. in connection with mid-latitude frontal systems).

The presented scheme is based on the conceptual model that precipitating clouds are characterized by a combination of particles large enough to fall, an adequate vertical extension (both represented by the cloud water path (CWP)), and the existence of ice particles in the upper part of the cloud. As no operational retrieval exists for Meteosat Second Generation (MSG) to compute the CWP during night-time, suitable combinations of brightness temperature differences (ΔT) between the thermal bands of Meteosat Second Generation-Spinning Enhanced Visible and InfraRed Imager (MSG SEVIRI, $\Delta T_{3.9\text{-}10.8}$, $\Delta T_{3.9\text{-}7.3}$, $\Delta T_{8.7–10.8}$, $\Delta T_{10.8–12.1}$) are used to infer implicit information about the CWP and to compute a rainfall confidence level. $\Delta T_{8.7–10.8}$ and $\Delta T_{10.8–12.1}$ are particularly considered to supply information about the cloud phase.

Rain area delineation is realized by using a minimum threshold of the rainfall confidence. To obtain a statistical transfer function between the rainfall confidence and the channel differences, the value combination of the channel differences is compared with ground-based radar data. The retrieval is validated against independent radar

data not used for deriving the transfer function and shows an encouraging performance as well as clear improvements compared to existing optical retrieval techniques using only IR thresholds for cloud top temperature.

4.1 Introduction

The estimation of rainfall by means of optical sensors aboard operational satellite systems has a long tradition as they provide information, from which may be inferred the spatio-temporal distribution of precipitation in a high spatial and temporal resolution.

Most of the retrievals developed so far for optical satellite data focus on precipitation generated by deep convective clouds since they can readily be identified by their cold cloud top temperature measured in the infrared (IR) channel (e.g. ADLER & NEGRI 1988; REUDENBACH 2003). However, these techniques have shown significant deficiencies concerning the detection of stratiform precipitating clouds, that are common for wide warm and cold frontal rain bands in connection with extra- tropical cyclones in the mid-latitudes (HOUZE 1993, hereafter denoted as advective-stratiform precipitation) (e.g. EBERT et al. 2007; FRÜH et al. 2007). These clouds are characterized by relatively warm top temperatures and a more homogeneous spatial distribution of cloud top temperature, that do not differ significantly between raining and non-raining regions. Therefore, a threshold value for cloud top temperature in the IR channel as used for deep convective clouds seems to be inappropriate for a reliable rain area delineation and leads to an underestimation of the detected precipitation area in such cases. Satellite systems of the new generation offer multispectral resolution, which can improve existing rain area delineation techniques. To overcome the shortcomings of the existing retrievals, NAUSS & KOKHANOVSKY (2006, 2007) proposed a new technique to delineate the rain area by means of the effective droplet radius and the optical thickness. It is based on the conceptual model that precipitating clouds are characterized by large particles, that can fall against updraft wind fields and a large vertical cloud extension, which favours the development and growth of large precipitation particles and prevents them from evaporating below the cloud base (LENSKY & ROSENFELD 2003a,b). Since neither the droplet spectrum nor the geometrical thickness of a cloud can be computed without additional theoretical assumptions, the effective droplet radius (a_{ef}) (HANSEN & TRAVIS, 1974) and the cloud optical thickness (τ) can be used as a measure for the particle size and the cloud thickness. Consequently, precipitating clouds can be characterized by a combination of the effective droplet radius and the optical thickness large enough to form precipitation

(NAUSS 2006). Multiplying both parameters according to equation (4.1)

$$LWP = \frac{2}{3} \cdot \tau \cdot a_{ef} \tag{4.1}$$

one gets the liquid water path (LWP), which in turn is directly related to the probability of a cloud producing rainfall and can therefore be used as a delineator between raining and non-raining clouds (NAUSS & KOKHANOVSKY 2006, 2007).

The proposed technique shows an improvement in rain area delineation especially for advective-stratiform rain clouds compared to existing techniques using only a threshold for cloud top infrared temperature. While the optical and microphysical cloud properties required for the rain area delineation can be retrieved during day-time using solar channels (e.g. NAKAJIMA & NAKAJIMA 1995; KAWAMOTO et al. 2001; KOKHANOVSKY et al. 2003; PLATNICK et al. 2003; KOKHANOVSKY & NAUSS 2005, 2006; NAUSS et al. 2005), no operational technique exists for Meteosat Second Generation (MSG) SEVIRI (Spinning Enhanced Visible and InfraRed Imager) to compute them during night-time. Nevertheless, several case studies have shown that implicit information about microphysical and optical cloud properties (a_{ef}, τ ,LWP) is available in the emissive channels during night-time. STONE et al. (1990), OU et al. (1993, 2002), GONZALEZ et al. (2002), and HUTCHISON et al. (2006) used a 3.7 µm channel and a 11 µm channel in combination to infer microphysical and optical cloud properties. The studies of WU (1984), INOUE (1985), and BAUM et al. (1994) have shown that both the brightness temperature differences (ΔT) between a 3.7 µm channel and an 11 µm channel ($\Delta T_{3.7-11}$) and between an 11 µm channel and a 12 µm channel (ΔT_{11-12}) are sensitive to the cloud's micro- physical and optical properties. BAUM et al. (1994) stated that brightness temperature differences used in combination provide more information regarding cloud properties than ΔT alone. ACKERMAN et al. (1998a) and HUANG et al. (2004) demonstrated the sensitivity of the ΔT between a 8.5 µm channel and an 11 µm channel ($\Delta T_{8.5-10.8}$) and of ΔT_{11-12} to effective particle radius. STRABALA et al. (1994) and ACKERMAN et al. (1998b) used $\Delta T_{8.5-10.8}$ and ΔT_{11-12} to discriminate between water and ice clouds. LENSKY & ROSENFELD (2003a) utilized $\Delta T_{3.7-11}$ to check passing criteria, that indicate that cloud geometrical depth and particle size are large enough to be considered as precipitating clouds. INOUE & AONASHI (2000) derived thresholds for $\Delta T_{3.7-11}$ and for ΔT_{11-12}, which they utilized for rain area delineation. Therefore, we propose a new rain area delineation scheme for night-time rain events in connection with extra-tropical

cyclones in the mid-latitudes based on optical multispectral satellite data.

The plan of this article is as follows. In section 4.2, the new developed Rain Area Delineation Scheme during Night-time (RADS-N) is presented. The new extended conceptual model is introduced followed by an analysis of the SEVIRI infrared channels concerning the required information to apply the conceptual model for rain area delineation. After the presentation of the new developed algorithm, its appraisal follows in section 4.3. The article closes with a short summary and some conclusions in section 4.4.

4.2 A new technique for rain area delineation during night-time

4.2.1 Basic considerations

The purpose of the present study is to propose a new rain area delineation scheme for night-time rain events in connection with extra-tropical cyclones in the mid-latitudes using MSG SEVIRI data (AMINOU 2002). The presented technique is based on the above-mentioned conceptual model that precipitation is favoured by a large cloud LWP or ice water path (IWP). Please note that for simplicity, LWP and IWP are hereafter both referred to as cloud water path (CWP). In addition to the day-time delineation scheme, the night-time approach is completed by incorporating information about the cloud phase, because effective rain formation processes in stratiform clouds, which are typical for wide warm or cold frontal rainbands of mid-latitude frontal systems, are mainly coupled to ice particles in the upper part of the clouds and the so called Bergeron–Findeisen process (HOUZE 1993). Consequently, the night-time rain delineation scheme is based on the extended conceptual model that precipitating clouds are characterized by a large enough CWP and the existence of ice particles in the upper part of the cloud.

As already mentioned, no operational technique exists to compute the CWP during night-time using the emissive channels of MSG SEVIRI. However, on the basis of findings mentioned in the introduction, the brightness temperature differences between the following SEVIRI channel differences are considered to provide implicit information on the CWP as well as on cloud phase to detect potentially precipitating cloud areas:

- $\Delta T_{3.9\text{-}10.8}$: ΔT between the 3.9 μm channel (3.48– 4.36 μm) and the 10.8 μm channel (9.8–11.8 μm)

- $\Delta T_{3.9\text{-}7.3}$: ΔT between the 3.9 µm channel and the 7.3 µm channel (6.85–7.85 µm)
- $\Delta T_{8.7\text{–}10.8}$: ΔT between the 8.7 µm channel (8.3– 9.1 µm) and the 10.8 µm channel
- $\Delta T_{10.8\text{–}12.1}$: ΔT between the 10.8 µm channel and the 12.1 µm channel (11–13 µm)

Regarding $\Delta T_{3.9\text{-}10.8}$, a large CWP is the product of a large effective particle radius and a high optical thickness. Large particles have a higher emission in the 3.9 µm channel compared to smaller particles. This is due to the increased scattering for smaller particles, which reduces the cloud emissivity. As a result, the brightness temperature in the 3.9 µm channel is higher for larger particles. This dependence on particle size is much less distinct in the 10.8 µm channel. Therefore, $\Delta T_{3.9\text{-}10.8}$ is higher for larger particles. For optically thin clouds the emission in the 3.9 µm channel is less than in the 10.8-µm channel. As a result, the 3.9 µm transmittance is larger than the 10.8 µm transmittance, which implies a larger transmissivity of below-cloud radiance of the former wavelength (Lensky & Rosenfeld 2003b). Thus, for optically thin clouds consisting of small or large particles (small or medium CWP), the brightness temperature of the 3.9 µm channel is larger than that of the 10.8 µm channel and $\Delta T_{3.9\text{-}10.8}$ reaches the highest values. Large particles together with a high optical thickness (large CWP) result in medium to high difference values, which are lower than for optically thin clouds. Thick clouds with small particles (medium CWP) lead to small $\Delta T_{3.9\text{-}10.8}$.

In general, $\Delta T_{3.9\text{-}7.3}$ should show similar characteristics as $\Delta T_{3.9\text{-}10.8}$. Because of the diminishing effect of the water vapour absorption and emission in mid- to low tropospheric levels on the brightness temperature (BT) in the 7.3 µm channel ($BT_{7.3}$) (Schmetz et al. 2002), $\Delta T_{3.9\text{-}7.3}$ should be generally higher than $\Delta T_{3.9\text{-}10.8}$. Therefore, $\Delta T_{3.9\text{-}7.3}$ is expected to provide additional information about the CWP. For thin clouds with small or large particles, respectively (small or medium CWP), $BT_{3.9}$ is larger than $BT_{7.3}$ and $\Delta T_{3.9\text{-}7.3}$ reaches the highest values. Large particles together with a high optical thickness (high CWP) result in medium to high difference values, which are lower than for optically thin clouds. Thick clouds with small particles (medium CWP) lead to small $\Delta T_{3.9\text{-}7.3}$.

Concerning $\Delta T_{8.7\text{–}10.8}$, cloud radiative properties in both channels are dependent upon the cloud particle size. Scattering processes and the dependence on particle size are stronger in the 8.7 µm channel relative to the 10.8 µm channel (Strabala et al. 1994). Therefore, for

larger particles the $\Delta T_{8.7-10.8}$ increases. The water vapour absorption in the 8.7 µm channel is higher relative to the 10.8 µm channel (SODEN & BRETHERTON 1996; SCHMETZ et al. 2002). This is why $\Delta T_{8.7-10.8}$ is lower for low optical thicknesses. For higher optical thicknesses, the $\Delta T_{8.7-10.8}$ increases. As a result, $\Delta T_{8.7-10.8}$ reaches high values for large effective particle radius and large optical thicknesses (large CWP). A low optical thickness in combination with small effective particle radius (small CWP) leads to minimum $\Delta T_{8.7-10.8}$. A low optical thickness with large particles (medium CWP) and a large optical thickness with small particles (medium CWP) result in medium values of $\Delta T_{8.7-10.8}$.

$\Delta T_{10.8-12.1}$ is positive at low optical thicknesses due to the increased water vapour absorption in the 12.1 µm channel relative to the 10.8 µm channel. For higher optical thicknesses, $\Delta T_{10.8-12.1}$ decreases as the transmittance and the influence of water vapour emission from beneath diminish (Inoue 1987; Baum et al. 1994). Particle absorption at 10.8 µm and 12.1 µm decreases with increasing effective radius. An increase in particle size acts to decrease $\Delta T_{10.8-12.1}$ (BAUM et al. 1994). As a result, $\Delta T_{10.8-12.1}$ reaches low values for large particles and large optical thicknesses (large CWP). High values for $\Delta T_{10.8-12.1}$ are characteristic of small optical thicknesses together with small effective particle radius (small CWP). Medium values for $\Delta T_{10.8-12.1}$ are produced from high optical thicknesses together with small effective particle radius (medium CWP) as well as for low optical thicknesses in combination with large effective particle radius (medium CWP).

Concerning information about the cloud phase, STRABALA et al. (1994) used $\Delta T_{8.5-11}$ and ΔT_{11-12} together to separate ice and water clouds. The differentiation is based on the observation that the increase of water particle absorption is greater between 11 and 12 µm than between 8 and 11 µm. The ice particle absorption increases more between 8 and 11 µm than between 11 and 12 µm (STRABALA et al. 1994). Therefore, $\Delta T_{10.8-12.1}$ of water clouds are greater than $\Delta T_{8.7-10.8}$. On the other hand, $\Delta T_{8.7-10.8}$ of ice clouds are greater than coincident $\Delta T_{10.8-12.1}$.

4.2.2 Radiative transfer calculations

To verify the theoretical considerations concerning the presented channel differences of MSG SEVIRI, introduced in the previous section, and their potential information content regarding the CWP and the cloud phase, radiative transfer simulations with the radiative transfer model Streamer (KEY & SCHWEIGER 1998; KEY 2001) were conducted for water and ice clouds. Streamer is based on the plane-

parallel theory and uses the discrete ordinate solver DISORT (STAMNES et al. 1988). The plane-parallel theory implies that the Earth, the atmosphere and clouds are assumed as plane-parallel horizontally homogeneous layers and that variations in the radiation and atmospheric parameters are permitted only in the vertical direction between the layers. Under this assumption, absorption and emission processes would be symmetrical with respect to the azimuthal angle. It follows that the radiation is a function of the vertical position and the zenith angle (LIOU 1992). The discrete ordinate approach involves the discretization of the basic radiative transfer equation and its reduction to a set of coupled linear first-order differential equations (LIOU 1973). The discrete ordinate solver proposed by STAMNES et al. (1988) solves the radiative transfer problem by dividing the atmosphere into homogeneous layers where the optical depth is used as the vertical coordinate. The homogeneous version of the radiative transfer equation is solved separately for each layer on the basis of an eigenvalue problem. The complete solution is derived by applying boundary and continuity conditions.

Streamer is a medium spectral resolution model and computes radiances and fluxes in the 0.28–500 μm wavelength range, using 129 bands with variable width. The spectral response functions (SRF) of the SEVIRI channels are realized by weighting coefficients for the spectral bands of the model (MELANI et al. 2003). Water cloud optical properties are based on data and the parameterization scheme from HU & STAMNES (1993). The parameterization of long-wave ice cloud optical properties follows the methodology of HU & STAMNES (1993) almost exactly and is based on Mie calculations using spherical particles (KEY 2001). Effects of water vapour, carbon dioxide, oxygen and ozone are included using a mid-latitude summer standard profile. A parameterized background tropospheric aerosol distribution with a 50 km visibility and background stratospheric amounts was used for the calculations. The cloud top height was kept constant at 7 km for water clouds and at 9 km for ice clouds, because stratiform raining clouds in connection with mid-latitude frontal systems mainly grow from the top downward and show a more homogeneous top structure. For other relevant input parameters refer to table 4.1. The input values for cloud properties are chosen to cover a wide range of characteristic qualities and are taken from the relevant literature (ZHANG et al. 1995; LENSKY & ROSENFELD 2003b; MELANI et al. 2003). The solar zenith angle is set to 100° to exclude solar radiation during night-time. Concerning the satellite zenith angle and the relative azimuth angle a representative mean value for Central Europe is used.

Table 4.1: Input parameters for the radiative transfer calculations (LWC/IWC: liquid/ice water content).

Solar zenith angle [°]	Satellite zenith angle [°]	Relative azimuth angle [°]	τ	a_{ef} (water) [µm]	a_{ef} (ice) [µm]	LWC [g/m³]	IWC [g/m³]
100	55	130	1 to 100	1 to 65	1 to 110	0.6	0.3

4.2.2.1 Information content regarding the cloud water path

Figure 4.1 shows the LWP (left column) and the IWP (right column) as a function of the calculated channel differences. The results for $\Delta T_{3.9\text{-}10.8}$ versus $\Delta T_{3.9\text{-}7.3}$, $\Delta T_{8.7\text{–}10.8}$, and versus $\Delta T_{10.8\text{–}12.1}$, respectively, are displayed in figure 4.1 (a)–(c). Figure 4.2 (a) and (b) shows the results for $\Delta T_{3.9\text{-}7.3}$ versus $\Delta T_{8.7\text{–}10.8}$,and versus $\Delta T_{10.8\text{–}12.1}$, respectively. The results for $\Delta T_{8.7\text{–}10.8}$ versus $\Delta T_{10.8\text{–}12.1}$ are depicted in figure 4.2 (c). For theoretical considerations concerning the relationship between the respective values of the CWP and the coincident ΔT values see section 4.2.1.

Regarding $\Delta T_{3.9\text{-}10.8}$ (figure 4.1 (a) and (c)), medium CWP (low τ with large a_{ef} and high τ with small a_{ef}) are represented by highest and small ΔT values. Medium ΔT values are indicative for large CWP (high τ with large a_{ef}). The results for $\Delta T_{3.9\text{-}7.3}$ (figures 4.1 (a), 4.2 (a) and (b)) show the same characteristics as for $\Delta T_{3.9\text{-}10.8}$ with generally higher $\Delta T_{3.9\text{-}7.3}$ values compared to $\Delta T_{3.9\text{-}10.8}$. This is due to the diminishing effect of the water vapour absorption and emission in mid- to low tropospheric levels on the brightness temperature (BT) in the 7.3 µm channel ($BT_{7.3}$) (SCHMETZ et al. 2002). $\Delta T_{8.7\text{–}10.8}$ values (figures 4.1 (b), 4.2 (a) and (c)) are high for large CWP (high τ with large a_{ef}). Medium values of $\Delta T_{8.7\text{–}10.8}$ are the result of medium CWP (high τ with small a_{ef} and low τ with large a_{ef}). The results for $\Delta T_{10.8\text{–}12.1}$ are depicted in figures 4.1 (c), 4.2 (b) and (c). Large CWP (high τ with large a_{ef}) are indicated by lowest values of $\Delta T_{10.8\text{–}12.1}$. Medium values of $\Delta T_{10.8\text{–}12.1}$ are characteristic for medium CWP (high with small a_{ef} and low τ with large a_{ef}).

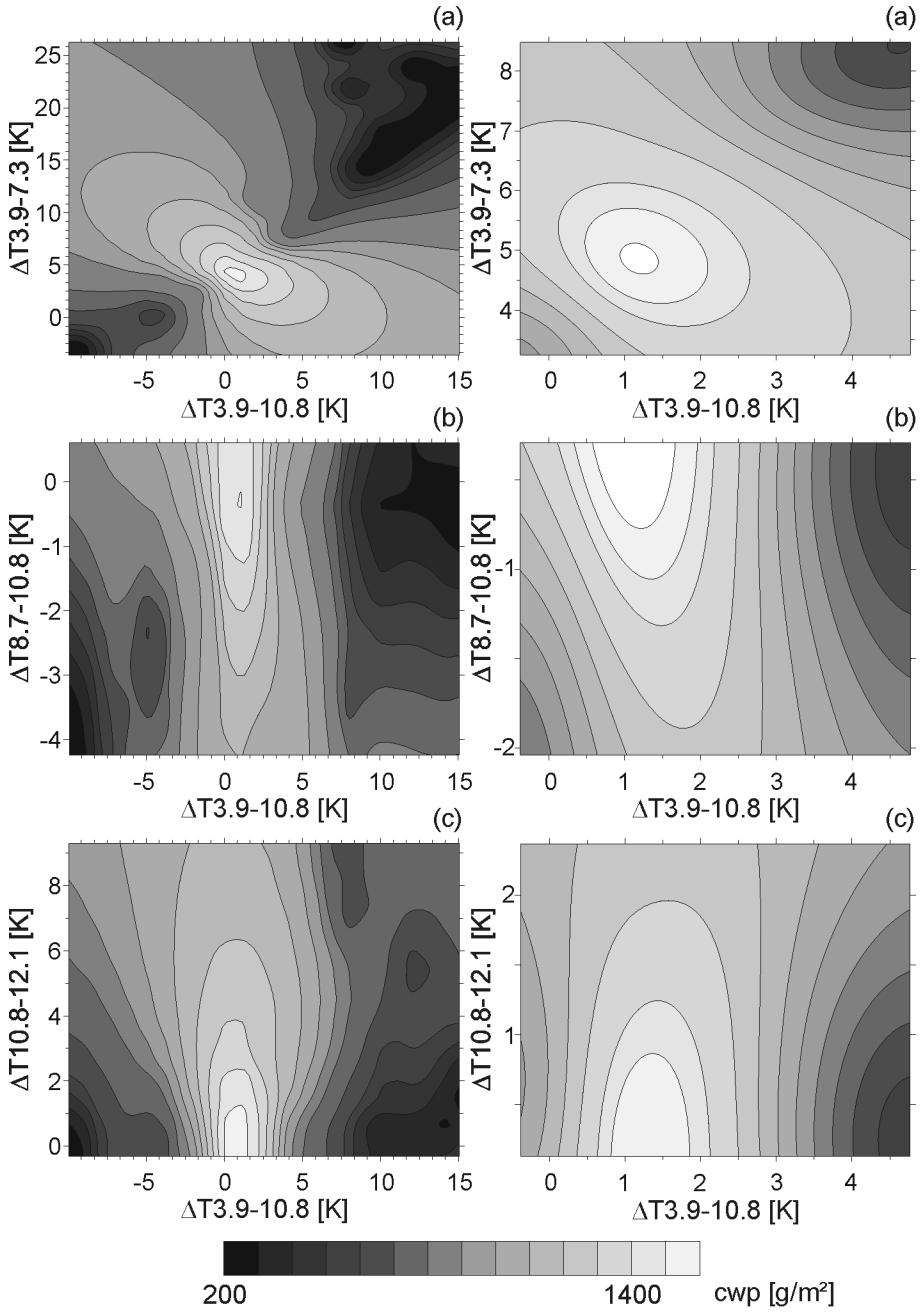

Figure 4.1: Cloud liquid water path (left column) and ice water path (right column) as a function of (a) $\Delta T_{3.9\text{-}10.8}$ versus $\Delta T_{3.9\text{-}7.3}$ (b), $\Delta T_{3.9\text{-}10.8}$ versus $\Delta T_{8.7\text{–}10.8}$, and (c) $\Delta T_{3.9\text{-}10.8}$ versus $\Delta T_{8.7\text{–}10.8}$.

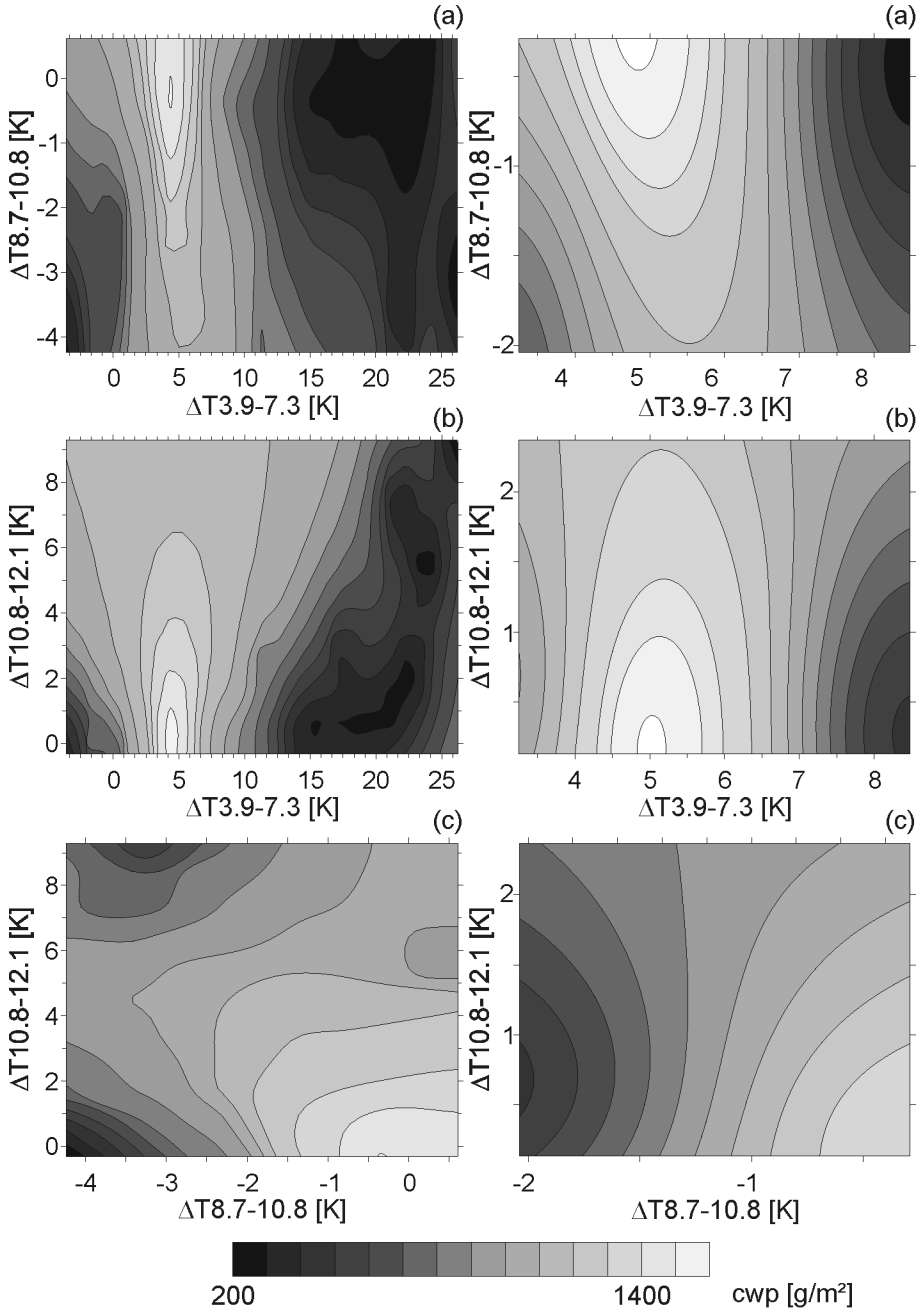

Figure 4.2. Cloud liquid water path (left column) and ice water path (right column) as a function of (a) $\Delta T_{3.9\text{-}7.3}$ versus $\Delta T_{8.7\text{–}10.8}$,(b) $\Delta T_{3.9\text{-}7.3}$ versus $\Delta T_{10.8\text{–}12.1}$, and (c) $\Delta T_{8.7\text{–}10.8}$ versus $\Delta T_{10.8\text{–}12.1}$.

The effect of the CWP on the respective channel differences presented in figures 4.1 and 4.2 is summarized in table 4.2. As can be seen in table 4.2 high $\Delta T_{3.9\text{-}10.8}$ together with high $\Delta T_{3.9\text{-}7.3}$ correspond to small CWP. Highest values for both ΔT correspond to medium CWP. Medium $\Delta T_{3.9\text{-}10.8}$ and $\Delta T_{3.9\text{-}7.3}$ are indicative for large CWP. Low $\Delta T_{3.9\text{-}10.8}$ and low $\Delta T_{3.9\text{-}7.3}$ are the result of a medium CWP (refer to figure 4.1 (a)). High (highest) $\Delta T_{3.9\text{-}10.8}$ together with low $\Delta T_{8.7\text{–}10.8}$ correspond to small (medium) CWP. Medium $\Delta T_{3.9\text{-}10.8}$ and high $\Delta T_{8.7\text{–}10.8}$ refer to large CWP. Low $\Delta T_{3.9\text{-}10.8}$ and medium $\Delta T_{8.7\text{–}10.8}$ are indicative for medium CWP (refer to figure 4.1 (b)). The same statements hold true for $\Delta T_{3.9\text{-}7.3}$ and $\Delta T_{8.7\text{–}10.8}$ in combination (refer to figure 4.2 (a)). High (highest) $\Delta T_{3.9\text{-}10.8}$ and high $\Delta T_{10.8\text{–}12.1}$ are the result of small (medium) CWP. Medium $\Delta T_{3.9\text{-}10.8}$ together with low to medium $\Delta T_{10.8\text{–}12.1}$ refer to large CWP. Low $\Delta T_{3.9\text{-}10.8}$ and medium $\Delta T_{10.8\text{–}12.1}$ correspond to a medium WP (refer to figure 4.1 (c)). The same features are characteristic for $\Delta T_{3.9\text{-}7.3}$ and $\Delta T_{10.8\text{–}12.1}$ in combination (refer to figure 4.2 (b)). Low $\Delta T_{8.7\text{–}10.8}$ together with high $\Delta T_{10.8\text{–}12.1}$ are indicative for small CWP. High $\Delta T_{8.7\text{–}10.8}$ and low $\Delta T_{10.8\text{–}12.1}$ correspond to large CWP. Medium $\Delta T_{8.7\text{–}10.8}$ and medium $\Delta T_{10.8\text{–}12.1}$ refer to medium CWP (refer to figure 4.2 (c)).

Table 4.2: The effect of the cloud water path (CWP) on the respective channel differences.

	$\Delta T_{3.9\text{-}10.8}$	$\Delta T_{3.9\text{-}7.3}$	$\Delta T_{8.7\text{-}10.8}$	$\Delta T_{10.8\text{-}12.1}$
small *cwp* (small τ with small a_{ef})	high	high	low	high
medium *cwp* (small τ with large a_{ef})	highest	highest	medium	medium
medium *cwp* (large τ with small a_{ef})	low	low	medium	medium
large *cwp* (large τ with large a_{ef})	medium	medium	high	low

4.2.2.2 Distinction of water and ice clouds

There is no clear separation between water and ice clouds, neither for $\Delta T_{3.9\text{-}10.8}$ (figure 4.1) nor for $\Delta T_{3.9\text{-}7.3}$ (figures 4.1 (a), 4.2 (a) and (b)). Following STRABALA et al. (1994) $\Delta T_{10.8–12.1}$ of water clouds should be greater than coincident $\Delta T_{8.7–10.8}$, while $\Delta T_{8.7–10.8}$ for ice clouds should be greater than coincident $\Delta T_{10.8–12.1}$. Such a distinct separation is not visible for $\Delta T_{8.7–10.8}$ and $\Delta T_{10.8–12.1}$ in figure 4.2 (c).

The marginal differences between water and ice clouds in the results of the radiative transfer calculations might be a consequence of the parameterization of long-wave ice cloud optical properties, which is based on Mie calculations using spherical particles, and which follows almost exactly the methodology used for water clouds (KEY 2001). It can be assumed that the similar shape of the water droplets and the spherical ice particles together with related parameterization schemes for water and ice clouds lead to comparable absorption and extinction behaviours and hence to similar results concerning the respective channel difference for both cloud types.

Generally, the value range of the respective ΔT is smaller for ice clouds than for water clouds. This might be due to the fact that spherical ice particles are more absorbing compared to water particles, resulting in similar absorption and extinction behaviours in the different wavelengths for ice clouds, and thus in a decreasing value range for the respective channel difference.

On the basis of radiative transfer results it has to be stated that a proper differentiation between ice and water clouds does not seem very effective. Nevertheless, in view of the good results obtained using $\Delta T_{8.7–10.8}$ together with $\Delta T_{10.8–12.1}$ for water and ice cloud differentiation with other sensors (e.g. MODIS, STRABALA et al. 1994; ACKERMAN et al. 1998), we use both temperature differences in the rain area delineation night-time scheme to include information about cloud phase.

The results of the radiative transfer simulations conform with the basic theoretical considerations concerning the relationship between the respective values of the CWP and the coincident channel differences (ΔT) introduced in section 4.2.1, which are based on the findings mentioned in the introduction. Consequently it can be concluded that implicit information about the CWP is available from the four channel differences. Together with the information about the cloud phase, an application of the new extended conceptual model for rain area delineation to MSG SEVIRI night-time data seems possible.

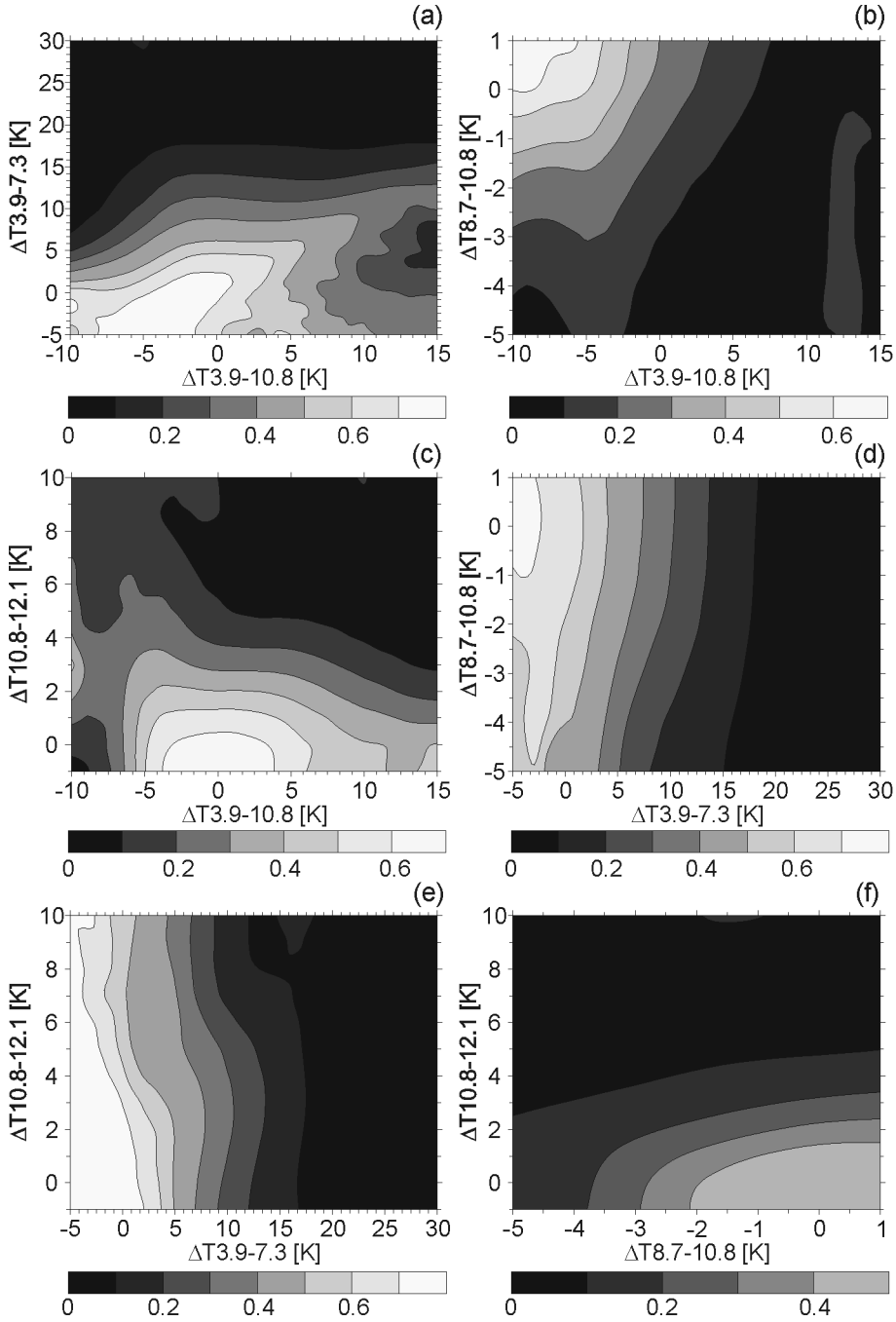

Figure 4.3: The rainfall confidence as a function of (a) $\Delta T_{3.9\text{-}10.8}$ versus $\Delta T_{3.9\text{-}7.3}$ (b), $\Delta T_{3.9\text{-}10.8}$ versus $\Delta T_{8.7\text{–}10.8}$ (c), $\Delta T_{3.9\text{-}10.8}$ versus $\Delta T_{10.8\text{–}12.1}$ (d), $\Delta T_{3.9\text{-}7.3}$ versus $\Delta T_{8.7\text{–}10.8}$ (e), $\Delta T_{3.9\text{-}7.3}$ versus $\Delta T_{10.8\text{–}12.1}$, and (f) $\Delta T_{8.7\text{–}10.8}$ versus $\Delta T_{10.8\text{–}12.1}$.

4.2.3 Transfer of the conceptual approach to MSG SEVIRI

To use the implicit information about the CWP and the cloud phase for a proper detection of potentially precipitating cloud areas (i.e. large enough CWP and ice particles in the upper part) the rainfall confidence is calculated as a function of the four channel differences (e.g. BELLON et al. 1980; CHENG et al. 1993; KURINO 1997; NAUSS & KOKHANOVSKY 2007). The computation of the pixel-based rainfall confidence is achieved by a comparison of the SEVIRI channel differences with ground-based radar data from the German weather service for night-time precipitation events from January to August 2004 (altogether 709 scenes). The ground-based radar data from the DWD C band-radar network consist of six classes representing different reflectivity intensities, which are all together considered as raining in comparison with collocated satellite pixels. A lower reflectivity threshold of 7.0 decibel for the first class is utilized to detect rain-bearing pixels (DWD 2005). The calculated rainfall confidence as a function of two different channel differences is depicted in figure 4.3. Equation (4.2) shows the calculation of the rainfall confidences as a function of two different channel differences:

$$RainConf\,(\Delta T_{1,}\Delta T_{2}) = \frac{N_{Rain}(\Delta T_{1,}\Delta T_{2})}{N_{Rain}(\Delta T_{1,}\Delta T_{2}) + N_{NoRain}(\Delta T_{1,}\Delta T_{2})} \quad (4.2)$$

where N_{Rain} and N_{NoRain} are the raining and the non-raining frequencies, respectively, and ΔT_1 and ΔT_2 denote the respective channel differences ($\Delta T_{3.9\text{-}10.8}$, $\Delta T_{3.9\text{-}7.3}$, $\Delta T_{8.7\text{–}10.8}$, $\Delta T_{10.8\text{–}12.1}$) combined for the calculation of the rainfall confidences.

For the combination of $\Delta T_{3.9\text{-}10.8}$ with $\Delta T_{3.9\text{-}7.3}$ (figure 4.3 (a)) high rainfall confidences can be found for small $\Delta T_{3.9\text{-}10.8}$ and small $\Delta T_{3.9\text{-}7.3}$ as well as for medium $\Delta T_{3.9\text{-}10.8}$ and medium $\Delta T_{3.9\text{-}7.3}$. These intervals coincide with those for medium to large CWP (refer to figure 4.1 (a)). Regarding the combination of $\Delta T_{3.9\text{-}10.8}$ with $\Delta T_{8.7\text{–}10.8}$ (figure 4.3 (b)) high rainfall confidences are indicated for small $\Delta T_{3.9\text{-}10.8}$ and medium $\Delta T_{8.7\text{–}10.8}$ as well as for medium $\Delta T_{3.9\text{-}10.8}$ and large $\Delta T_{8.7\text{–}10.8}$. Both value intervals correspond to medium and large CWP (refer to figure 4.1 (b)). The same characteristics are valid for the combination of $\Delta T_{3.9\text{-}7.3}$ and $\Delta T_{8.7\text{–}10.8}$ (figure 4.3 (d)) with the exception of high rainfall confidences for small $\Delta T_{3.9\text{-}7.3}$ and small $\Delta T_{8.7\text{–}10.8}$, which correspond to small and medium CWP (refer to figure 4.2 (a)). Concerning the combination of $\Delta T_{3.9\text{-}10.8}$ and $\Delta T_{10.8\text{–}12.1}$ (figure 4.3 (c)) high rainfall confidences are indicated for small $\Delta T_{3.9\text{-}10.8}$ and medium $\Delta T_{10.8\text{–}12.1}$ as well as for medium $\Delta T_{3.9\text{-}10.8}$ and small $\Delta T_{10.8\text{–}12.1}$, which coincide with medium to large

CWP (refer to figure 4.1 (c)). For the combination of $\Delta T_{3.9\text{-}7.3}$ and $\Delta T_{10.8\text{–}12.1}$ (figure 4.3 (e)) high rainfall confidences can be observed for small $\Delta T_{3.9\text{-}7.3}$ and medium $\Delta T_{10.8\text{–}12.1}$ as well as for medium $\Delta T_{3.9\text{-}7.3}$ and small $\Delta T_{10.8\text{–}12.1}$. These intervals correspond to medium and large CWP (refer to figure 4.2 (b)). For the combination of $\Delta T_{8.7\text{–}10.8}$ with $\Delta T_{10.8\text{–}12.1}$ (figure 4.3 (f)) high rainfall confidences are displayed for high $\Delta T_{8.7\text{–}10.8}$ and small $\Delta T_{10.8\text{–}12.1}$, which coincide with large CWP (refer to figure 4.2 (c)).

To summarize it can be stated that intervals of the channel differences representative of high rainfall confidences correspond with the intervals indicative for medium to large CWP. This corroborates the conceptual model that clouds with a large enough CWP together with ice particles in the upper parts possess a high probability of producing precipitation.

To make use of the combined information content in each channel difference for rain delineation, the rainfall confidence is computed as a function of the combined values of the four channel differences as shown in Equation (4.3) using the above mentioned 709 scenes:

$$RainConf(\Delta T_{1,}\Delta T_{2,}\Delta T_{3,}\Delta T_{4}) = \frac{N_{Rain}(\Delta T_{1,}\Delta T_{2,}\Delta T_{3,}\Delta T_{4})}{N_{Rain}(\Delta T_{1,}\Delta T_{2,}\Delta T_{3,}\Delta T_{4})+N_{NoRain}(\Delta T_{1,}\Delta T_{2,}\Delta T_{3,}\Delta T_{4})} \quad (4.3)$$

where N_{Rain} and N_{NoRain} are the raining and the non-raining frequencies, respectively. ΔT_1 stands for $\Delta T_{3.9\text{-}10.8}$, ΔT_2 for $\Delta T_{3.9\text{-}7.3}$, ΔT_3 for $\Delta T_{8.7\text{–}10.8}$,and ΔT_4 for $\Delta T_{10.8\text{–}12.1}$. These four channel differences are combined for the calculation of the rainfall confidences.

The threshold of the rainfall confidence appropriate for rain area delineation is determined by optimizing the equitable threat score (ETS), which is based on the number of pixels, that have been identified in the satellite (S) and radar (R) techniques as raining (S_Y, R_Y) or non-raining (S_N, R_N). It indicates how well the classified rain pixels correspond to the rain pixels observed by the radar, also accounting for pixels correctly classified by chance ($S_Y R_{YRandom}$). Its values range from -1/3 to 1 with the optimum value 1. The ETS is calculated as shown in Equation (4.4):

$$ETS = \frac{S_y R_y - S_y R_{yRandom}}{S_y R_y + S_n R_y + S_y R_n - S_y R_{yRandom}} \quad (4.4)$$

The calculation of $S_Y R_{YRandom}$ follows Equation (4.5):

$$S_y R_{yRandom} = \frac{(S_y R_y + S_n R_y)\cdot(S_y R_y + S_y R_n)}{T_{SR}} \quad (4.5)$$

where T_{SR} denotes the total number of pixels.

Additionally to the ETS, a visual inspection of the relative operation characteristic (ROC) plot (MASON 1982; JOLLIFFE & STEPHENSON 2003) (figure 4.4) was also considered to identify an appropriate rainfall confidence threshold. The probability of detection (POD) describes the ratio between pixels with S_YR_Y and R_Y, and gives the fraction of pixels, that have been correctly identified by the satellite technique, according to the radar product. The probability of false detection (POFD) describes the ratio between S_YR_N and R_N and indicates the fraction of the pixels incorrectly identified as rainfall events by the satellite algorithm. The optimum value for the POD is 1, while it is 0 for the POFD. The dotted diagonal line in the ROC plot represents the 'no skill' line (i.e. POD equals POFD). Value combinations above this line indicate that the approach has skill (i.e. POD larger than POFD).

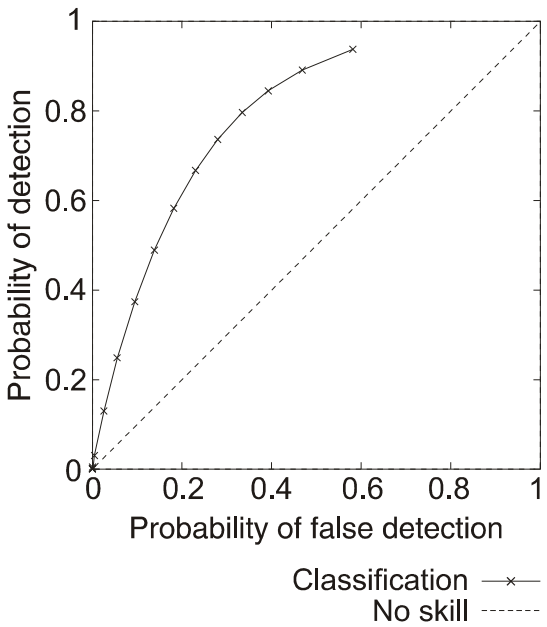

Figure 4.4: ROC curve based on the comparison between the combined values of the channel differences mentioned in the text from 709 MSG SEVIRI scenes and corresponding ground-based radar measurements over Germany. Different rainfall confidence threshold values starting with 0.1 at the upper right side of the graph and increasing to 0.7 at the lower left-side of the graph in steps of 0.05 (indicated by the crosses) were used to delineate the satellite-based rain area.

Different rainfall confidence threshold values between 0.1 and 0.7 were used to delineate the satellite-based rain area. The ETS, the POD and the POFD for the delineated rain areas based on the different rainfall confidence levels were calculated in comparison with ground-based radar data. As shown in figure 4.4, the 0.3 to 0.4 rainfall confidence threshold value seems to be most suitable for rain area delineation since corresponding POD – POFD combinations show the largest distance normal to the 'no skill' line. The delineated rain area using a rainfall confidence threshold of 0.35 yields the optimized ETS of 0.25. Therefore, the rainfall confidence of 0.35 is chosen as the minimum threshold for rain area delineation.

4.3 Appraisal of the new scheme

For the evaluation study, scenes from night-time precipitation events between January and August 2004 were classified by using the new developed RADS-N. The precipitation events chosen for the evaluation study are independent of the above-mentioned precipitation events used for algorithm development.

To evaluate the potential improvement by the new scheme, the 676 scenes were also classified by the enhanced convective stratiform technique (ECST) (REUDENBACH et al. 2001; REUDENBACH 2003), which is similar to the convective stratiform technique (CST) (ADLER & NEGRI 1988), but additionally includes the water vapour channel temperature for a more reliable deep convective/cirrus clouds discrimination (TJEMKES et al. 1997). The ECST, which was first transferred from Meteosat-7 MVIRI (Meteosat Visible and InfraRed Imager radiometer) to MSG SEVIRI (THIES et al. 2007), is used for the identification of convective rain areas since these regions approximately represent the performance of many present optical rainfall retrievals.

Table 4.3: Detected rain area by RADS-N, ECST, and ground-based radar network (radar).

	Rain Area [%] Mean	Rain Area [%] StDev	Rain Area [%] Min	Rain Area [%] Max
RADS-N	0.2	0.12	0	0.54
ECST	0.06	0.09	0	0.94
RADAR	0.15	0.07	0	0.36

Table 4.4: Results of the standard verification scores applied to the rain-area identified by RADS-N and ECST on a pixel basis. The scores are based on 676 precipitation scenes with 23 392 304 pixels, of which 4 746 069 have been identified as raining by RADS-N. POD (probability of detection); POFD (probability of false detection); FAR (false alarm ratio); CSI (critical success index) and ETS (equitable threat score).

Test	RADS-N				ECST			
	Mean	StDev	Min	Max	Mean	StDev	Min	Max
Bias	1.42	0.67	0.16	4.97	0.21	0.36	0	4.28
POD	0.62	0.18	0.12	0.97	0.09	0.14	0	0.95
POFD	0.24	0.13	0.01	0.84	0.04	0.08	0	0.94
FAR	0.52	0.14	0.11	0.88	0.57	0.32	0	1
CSI	0.37	0.13	0.1	0.74	0.07	0.1	0	0.53
ETS	0.22	0.12	-0.03	0.57	0.03	0.06	-0.06	0.35

Table 4.3 shows a comparison of the rain area detected by each technique. The verification scores calculated in comparison with the corresponding ground-based radar data are summarized in table 4.4. The bias describes the ratio between S_Y and R_Y and the false alarm ratio (FAR) gives the ratio between $S_Y R_N$ and S_Y. The critical success index (CSI), which encloses all pixels, that have been identified as raining by either the radar network or the satellite technique, describes the ratio between $S_Y R_Y$ and the sum of $S_Y R_Y$, $S_N R_Y$, $S_Y R_N$. All scores range from 0 to 1. The optimum value for the CSI is 1, while it is 0 for the FAR. Since the POD can be increased by just increasing the satellite rainfall area (i.e. by reducing the rainfall confidence threshold), it has to be analyzed in connection with corresponding values of the FAR and the POFD since both measure the fraction of the satellite pixels, that have been incorrectly identified as raining. The verification scores were calculated on a pixel basis of 676 single scenes without any spatio-temporal aggregation. For a detailed discussion of the verification scores see STANSKI et al. (1989) or the web site of the WWRP/WGNE (2007).

Compared to the strong underestimation of the rain area by the ECST, RADS-N slightly overestimates the rain area detected by the radar network (table 4.3). This is also indicated by the bias of 0.21 for the ECST and of 1.4 for RADS-N (table 4.4). The POD shows that 68% of the radar observed raining pixels are also identified by RADS-N, which points to a much better performance compared to 9% for the ECST, even if this coincides to a higher POFD of 0.24 for RADS-N in comparison to 0.04 for the ECST. However, the FAR shows that a lower fraction of the pixels was wrongly classified as rain by RADS-N (0.52) than by the ECST (0.57). The overall good performance of

RADS-N, indicated by the good range of the verification scores is further supported by the CSI (0.37) and the ETS (0.22), which outperform the results of the ECST (CSI: 0.07; ETS: 0.03).

The ROC plot in figure 4.5 gives an overview of the performance of RADS-N in comparison to the ECST. It underlines the good performance of the new developed scheme and the improvement in comparison to the ECST. For the main part of the classified scenes, the POD and POFD indicate a good skill with medium to high values for POD together with low to medium values for POFD. No skill is only valid for some scenes. In contrast, for scenes classified by the ECST, the POD and POFD indicate much lower or even no skills.

To gain a visual impression of the performance of the new developed RADS-N, the classified rain area for a scene from 31 May 2004, 0045 UTC is depicted in figure 4.6. Figure 4.6 (a) shows the BT in the 10.8 µm channel ($BT_{10.8}$); 4.6 (b) the rain area delineated by RADS-N as well as by ECST and 4.6 (c) the rain area detected by RADS-N in comparison to the radar data.

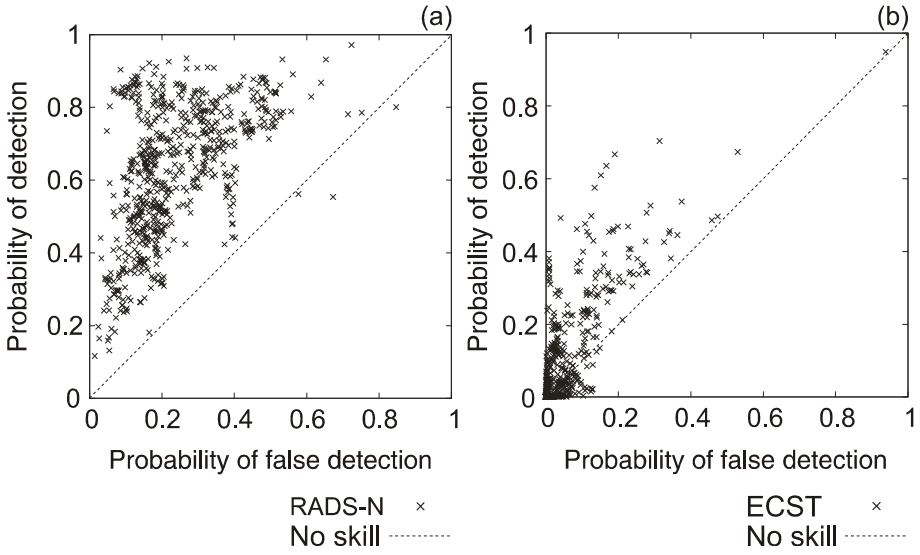

Figure 4.5: ROC curves for the comparison between RADS-N and ground-based radar (a), and ECST and ground-based radar (b). The calculated probability of detection (POD) and probability of false detection (POFD) are based on the 676 scenes mentioned in the text.

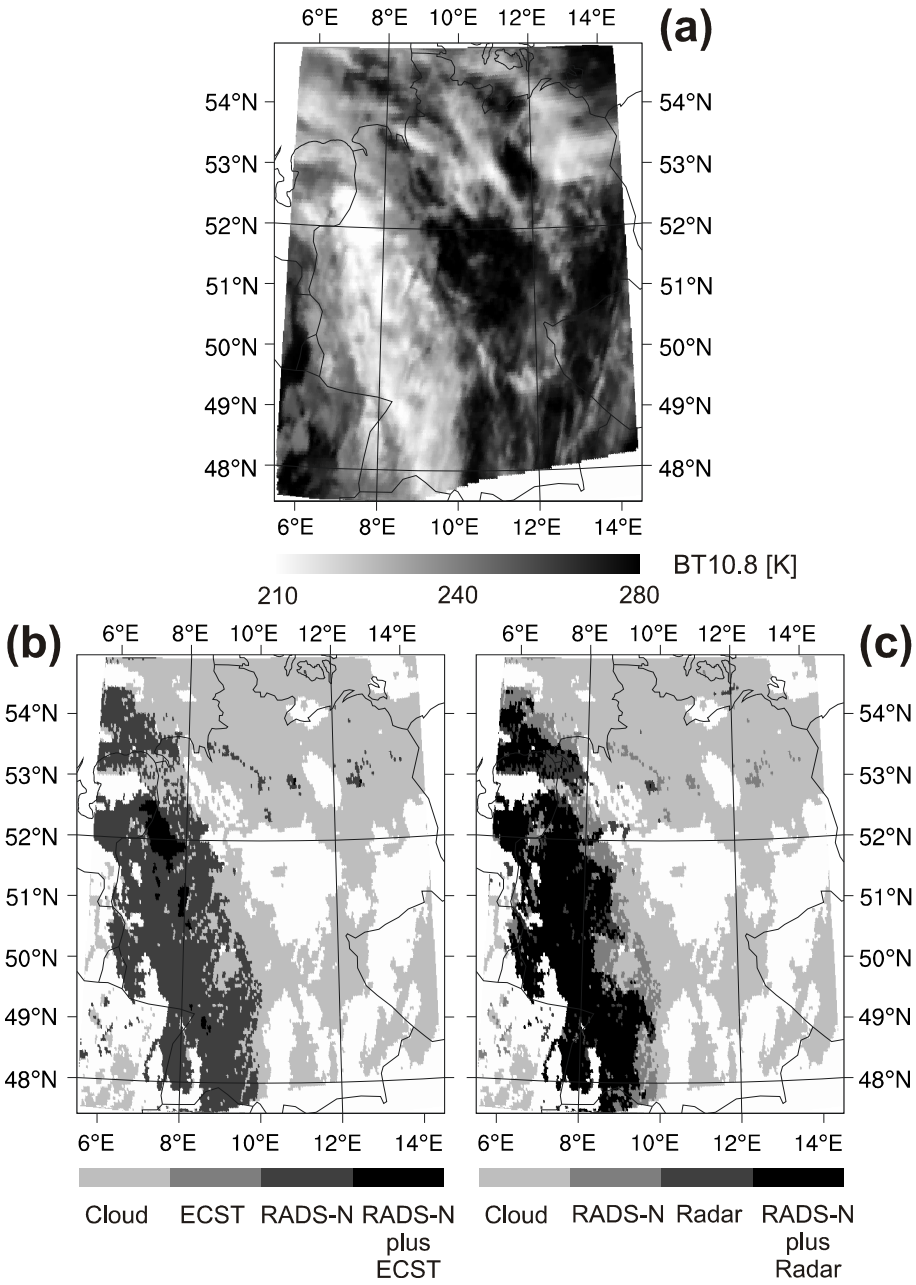

Figure 4.6: Delineated rain area for the scene from 31 May 2004, 00:45 UTC. Figure 4.6 (a) shows the $BT_{10.8}$ image; figure 4.6 (b) the rain area delineated by RADS-N as well as by ECST; and figure 4.6 (c) the rain area detected by RADS-N in comparison to the radar data.

4.4 Conclusions

A new algorithm for RADS-N using multispectral optical satellite data of MSG SEVIRI was proposed. The method allows not only a proper detection of mainly convective precipitation by means of the commonly used connection between infrared cloud top temperature and rainfall probability but also enables the detection of stratiform precipitation (e.g. in connection with mid-latitude frontal systems). It is based on the new extended conceptual model that precipitation is favoured by a large cloud liquid or ice water path and the presence of ice particles in the upper part of the cloud.

The technique considers information about both parameters inherent in the channel differences $\Delta T_{3.9\text{-}10.8}$, $\Delta T_{3.9\text{-}7.3}$, $\Delta T_{8.7–10.8}$,and $\Delta T_{10.8–12.1}$, to detect potentially precipitating cloud areas. All four channel differences are used to gain implicit knowledge about the CWP $\Delta T_{8.7–10.8}$ and $\Delta T_{10.8–12.1}$ are additionally considered to gain information about the cloud phase.

The information inherent in all four channel differences is merged and incorporated into the new developed rain delineation algorithm. Rain area delineation is realized by using the pixel-based rainfall confidence as a function of the respective value combination of the four channel differences. The calculation of the rainfall confidence is based on a comparison of the value combinations of the four channel differences with ground-based radar data. A minimum threshold of 0.35 for the rainfall confidence was determined as appropriate for rain area delineation.

The results of the algorithm were compared with the corresponding ground-based radar. The proposed technique performs better than existing optical retrieval techniques using only IR thresholds for cloud top temperature. The new developed algorithm shows encouraging performance concerning precipitation delineation during night-time in the mid-latitudes using MSG SEVIRI data. Together with the existing rain area delineation scheme for day-time scenes, which will be transferred from Terra- MODIS to MSG SEVIRI in the next step, the new algorithm offers the great potential for a 24 h technique for rain area delineation with a high spatial and temporal resolution.

Acknowledgements

The current study is funded by the German Ministry of Research and Education (BMBF) in the framework of GLOWA-Danube project (G-D/2004/TP-10, precipitation/remote sensing) as well as by the German Research Council DFG (BE 1780/18-1) within the SORT project.

The authors are grateful to the German weather service (DWD) for providing the radar data sets within the EUMETSAT/DWD Advanced Multisensor Precipitation Experiment (AMPE).

References

ACKERMAN, S. A., C. C. MOELLER, K. I. STRABALA, H. E. GERBER, L. E. GUMLEY, W. P. MENZEL & S. C. TSAY (1998a): Retrieval of effective microphysical properties of clouds: a wave cloud case study. - *Geophysical Research Letters, 25*: 1121–1124.

ACKERMAN, S. A., K. I. STRABALA, W. P. MENZEL, R. A. FREY, C. C. MOELLER & L. E. GUMLEY (1998b): Discriminating clear sky from clouds with MODIS. - *Journal of Geophysical Research-Atmospheres, 103*: 32141–32157.

ADLER, R. F. & A. J. NEGRI (1988): A satellite technique to estimate tropical convective and stratiform rainfall. - *Journal of Applied Meteorology, 27*: 30–51.

AMINOU, D. M. A. (2002): MSG's SEVIRI instrument. - *ESA Bulletin, 111*: 15–17.

BAUM, B. A., R. F. ARDUINI, B. A. WIELICKI, P. MINNIS & S. C. TSAY (1994): Multilevel cloud retrieval using multispectral HIRS and AVHRR data: night-time oceanic analysis. - *Journal of Geophysical Research – Atmospheres, 99*: 5499–5514.

BELLON, A., S. LOVEJOY & G. L. AUSTIN (1980): Combining satellite and radar data for the short-range forecasting of precipitation. - *Monthly Weather Review, 108*: 1554–1556.

CHENG, M., R. BROWN & C. G. COLLIER (1993): Delineation of precipitation areas by correlation of METEOSAT visible and infrared data in the region of the United Kingdom. - *Journal of Applied Meteorology, 32*: 884–898.

DWD (2005): Weather radar network. - Available online at http://www.dwd.de/en/Technik/Datengewinnung/Radarverbund/Radarbroschuere_en.pdf, 11 May 2007.

EBERT, E. E., J. E. JANOWIAK & C. KIDD (2007): Comparison of near-real-time precipitation estimates from satellite observations and numerical models. - *Bulletin of the American Meteorological Society, 88*: 47–64.

FRÜH, B., J. BENDIX, T. NAUSS, M. PAULAT, A. PFEIFFER, J. W. SCHIPPER, B. THIES & H. WERNLI (2007): Verification of precipitation from regional climate simulations and remote-sensing observations with

respect to ground-based observations in the upper Danube catchment. - *Meteorologische Zeitschrift, 16*: 275–293.

González, A., J. C. Pérez, F. Herrera, F. Rosa, M. A. Wetzel, R. D. Borys & D. H. Lowenthal (2002): Stratocumulus properties retrieval method from NOAA-AVHRR data based on the discretization of cloud properties. - *International Journal of Remote Sensing, 23*: 627–645.

Hansen, J. E. & L. D. Travis (1974): Light scattering in planetary atmospheres. - *Space Science Reviews, 16*: 527–610.

Houze, R. A. (1993): Cloud Dynamics, Vol. 53. of International Geophysics Series, Academic Press, San Diego.

Hu, Y. X. & K. Stamnes (1993): An accurate parameterization of the radiative properties of water clouds suitable for use in climate models. - *Journal of Climate. 6*: 728–742.

Huang, H.L., P. Yang, H. L. Wei, B. A. Baum, Y. X. Hu, P. Antonelli & S. A. Ackerman (2004): Inference of ice cloud properties from high spectral resolution infrared observations. - *IEEE Transactions on Geoscience and Remote Sensing, 42*: 842–853.

Hutchison, K., E. Wong & S. C. Ou (2006): Cloud base heights retrieved during night-time conditions with MODIS data. - *International Journal of Remote Sensing, 27*: 2847–2862.

Inoue, T. (1985): On the temperature and effective emissivity determination of semi-transparent cirrus clouds by bi-spectral measurements in the 10 μm window region. - *Journal of the Meteorological Society of Japan, 63*: 88–98.

Inoue, T. (1987): An instantaneous delineation of convective rainfall areas using split window data of NOAA-7 AVHRR. - *Journal of the Meteorological Society of Japan, 65*: 469–481.

Inoue, T. & K. Aonashi (2000): A comparison of cloud and rainfall information from instantaneous visible and infrared scanner and precipitation radar observations over a frontal zone in east Asia during June 1998. - *Journal of Applied Meteorology, 39*: 2292–2301.

Jolliffe, I. T. & D. B. Stephenson (2003): Forecast verification. A Practitioner's Guide in Atmospheric Science. John Wiley and Sons, Chichester.

Kawamoto, K., T. Nakajima & T. Y. Nakajima (2001): A global determination of cloud microphysics with AVHRR remote sensing. - *Journal of Climate, 14*: 2054–2068.

Key, J. (2001) Streamer user's guide. Cooperative Institute for Meteorological Satellite Studies. University of Wisconsin, Madison.

KEY, J. & A. J. SCHWEIGER (1998): Tools for atmospheric radiative transfer: Streamer and FluxNet. Computers & Geosciences 24: 443–451.

KOKHANOVSKY, A. A., V. V. ROZANOV, E. P. ZEGE, H. BOVENSMANN & J. P. BURROWS (2003): A semi-analytical cloud retrieval algorithm using backscattered radiation in 0.4–2.4 micrometers spectral range. - *Journal of Geophysical Research-Atmospheres, 108(D1)*: 4008, Doi:10.1029/2001JD001543.

KOKHANOVSKY, A. A. & T. NAUSS (2005): Satellite-based retrieval of ice cloud properties using a semi-analytical algorithm. - *Journal of Geophysical Research-Atmospheres, 110/D19*: D19206, Doi:10.1029/2004JD005744.

KOKHANOVSKY, A. A. & T. NAUSS (2006). Reflection and transmission of solar light by clouds: asymptotic theory. - *Atmospheric Chemistry and Physics, 6*: 5537–5545.

KURINO, T. (1997): A satellite infrared technique for estimating 'deep/shallow' precipitation. - *Advances in Space Research, 19*: 511–514.

LENSKY, I. M. & D. ROSENFELD (2003a): A night-time delineation algorithm for infrared satellite data based on microphysical considerations. - *Journal of Applied Meteorology, 42*: 1218–1226.

LENSKY, I. M. & D. ROSENFELD (2003b): Satellite-based insights into precipitation formation processes in continental and maritime convective clouds at night-time. - *Journal of Applied Meteorology, 42*: 1227–1233.

LIOU, K.-N. (1973): A numerical experiment on Chandrasekhar's discrete-ordinate method for radiative transfer: applications to cloudy and hazy atmospheres. - *Journal of the Atmospheric Sciences, 30*: 1303–1326.

LIOU, K.-N. (1992): Radiation & cloud processes in the atmosphere. Theory, Observation and Modelling. Oxford University Press. New York.

MASON, I. (1982): A model for assessment of weather forecasts. - *Australian Meteorological Magazine*, 30: 291–302.

MELANI, S., E. CATTANI, V. LEVIZZANI, M. CERVINO, F. TORRICELLA & M. J. COSTA (2003): Radiative effects of simulated cirrus clouds on top of a deep convective storm in Meteosat Second Generation SEVIRI channels. - *Meteorology and Atmospheric Physics, 83*: 109–122.

NAKAJIMA, T. Y. & T. NAKAJIMA (1995): Wide-area determination of cloud microphysical properties from NOAA AVHRR measurements

for FIRE and ASTEX regions. - *Journal of the Atmospheric Sciences, 52*: 4043–4059.

NAUSS, T., A. A. KOKHANOVSKY, T. Y. NAKAJIMA, C. REUDENBACH & J. BENDIX (2005): The intercomparison of selected cloud retrieval algorithms. - *Atmospheric Research, 78*: 46–78.

NAUSS, T. (2006): Das Rain Area Delineation Scheme RADS – ein neues Verfahren zur satellitengestützten Erfassung der Niederschlagsfläche über Mitteleuropa. - *Marburger Geographische Schriften, 143*: 160 pp.

NAUSS, T. & A. A. KOKHANOVSKY (2006): Discriminating raining from non-raining clouds at mid-latitudes using multispectral satellite data. - *Atmospheric Chemistry and Physics, 6*: 5031–5036.

NAUSS, T. & A. A. KOKHANOVSKY (2007): Assignment of rainfall confidence values using multispectral satellite data at mid-latitudes: first results. - *Advances in Geosciences, 10*: 99–102.

OU, S. C., K. N. LIOU, W. M. GOOCH & Y. TAKANO (1993): Remote sensing of cirrus cloud parameters using advanced very-high-resolution radiometer 3.7- and 10.9-µm channels. - *Applied Optics, 32*: 2171–2180.

OU, S. C., K. N. LIOU, Y. TAKANO, G. HIGGINS, N. LARSEN & R. SLONAKER (2002): Cloud effective particle size and cloud optical thickness. - Raytheon Systems Company, 195 pp. Available online at, http://140.90.86.6/IPOarchive/SCI/atbd/msoFEB56.pdf, 11 May 2007.

PLATNICK, S., M. D. KING, S. A. ACKERMAN, W. P. MENZEL, B. A. BAUM, J. C. RIÉDI & R. A. FREY (2003): The MODIS cloud products: algorithms and examples from Terra. - *IEEE Transactions on Geoscience and Remote Sensing, 41*: 459–473.

REUDENBACH, C., G. HEINEMANN, E. HEUEL, J. BENDIX & M. WINIGER (2001): Investigation of summertime convective rainfall in Western Europe based on a synergy of remote sensing data and numerical models. - *Meteorology and Atmospheric Physics, 76*: 23–41.

REUDENBACH, C. (2003): Konvektive Sommerniederschläge in Mitteleuropa. Eine Kombination aus Satellitenfernerkundung und numerischer Modellierung zur automatischen Erfassung mesoskaliger Niederschlagsfelder. - *Bonner Geographische Abhandlungen, 109*: 152 pp.

SCHMETZ, J., P. PILI, S. TJEMKES, D. JUST, J. KERKMANN, S. ROTA & A. RATIER (2002): An introduction to Meteosat Second Generation (MSG). - *Bulletin of the American Meteorological Society, 83*: 977–992.

SODEN, B. J. & F. P. BRETHERTON (1996): Interpretation of TOVS water vapour radiances in terms of layer-average relative humidities: Method and climatology for the upper, middle, and lower troposphere. - *Journal of Geophysical Research-Atmospheres, 101*: 9333–9343.

STAMNES, K., S. C. TSAY, W. WISCOMBE & K. JAYAWEERA (1988): Numerically stable algorithm for discrete-ordinate-method radiative transfer in multiple scattering and emitting layered media. - *Applied Optics, 27*: 2502–2509.

STANSKI, H. R., L. WILSON & W. BURROWS (1989): Survey of common verification methods in meteorology. - *World Weather Watch Technical Report No.8. WMO: Geneva*, WMO/TD No. 358, 114 pp.

STONE, R. S., G. L. STEPHENS, C. M. R. PLANT & S. BANKS (1990): The remote sensing of thin cirrus cloud using satellites, lidar and radiative transfer theory. - *Journal of Applied Meteorology, 29*: 353–366.

STRABALA, K. I., S. A. ACKERMAN & W. P. MENZEL (1994): Cloud properties inferred from 8-12-µm Data. - *Journal of Applied Meteorology, 33*: 212–229.

THIES, B., T. NAUSS & J. BENDIX (2007): Detection of high rain clouds using water vapour emission – transition from Meteosat First (MVIRI) to Second Generation (SEVIRI). - *Advances in Space Research,* submitted.

TJEMKES, S. A., L. VAN DE BERG & J. SCHMETZ (1997). Warm water vapour pixels over high clouds as observed by Meteosat. - *Contributions to Atmospheric Physics, 70*: 15–21.

WU, M. C. (1984): Radiation properties and emissivity parameterization of high level thin clouds. - *Journal of Climate and Applied Meteorology, 23*: 1138–1147.

WORLD WEATHER RESEARCH PROGRAM/WORKING GROUP ON NUMERICAL EXPERIMENTATION JOINT WORKING GROUP ON VERIFICATION (WWRP/WGNE): Forecast Verification – Issues, Methods and FAQ. - Available online at http://www.bom.gov.au/bmrc/wefor/staff/eee/verif/verif web page.html, 11 May 2007.

ZHANG, G., L. XU & C. HONGBIN (1995): A new parameterization scheme for shortwave radiative properties of water clouds. - *Journal of Applied Meteorology, 34*: 101–106.

CHAPTER 5

Discriminating raining from non-raining clouds at mid-latitudes using meteosat second generation day-time data

Boris Thies, Thomas Nauß and Jörg Bendix

Atmos. Chem. Phys., 8, 2341-2349, 2008
www.atmos-chem-phys.net/8/1/2008/

Received: 12 October 2007 – Published in Atmos. Chem. Phys. Discuss.: 13 November 2007
Revised: 25 March 2008 – Accepted: 21 April 2008 – Published:

5 Discriminating raining from non-raining clouds at mid-latitudes using meteosat second generation day-time data

Boris Thies, Thomas Nauß and Jörg Bendix

Philipps-University Marburg,
Department of Geography,
Laboratory for Climatology and Remote Sensing,
Deutschhausstraße 10, 35032 Marburg, Germany

Abstract

A new method for the delineation of precipitation during day-time using multispectral satellite data is proposed. The approach is not only applicable to the detection of mainly convective precipitation by means of the commonly used relation between infrared cloud top temperature and rainfall probability but enables also the detection of stratiform precipitation (e.g. in connection with mid-latitude frontal systems). The presented scheme is based on the conceptual model that precipitating clouds are characterized by a combination of particles large enough to fall, an adequate vertical extension (both represented by the cloud water path; CWP), and the existence of ice particles in the upper part of the cloud. The technique considers the $VIS_{0.6}$ and the $NIR_{1.6}$ channel to gain information about the cloud water path. Additionally, the brightness temperature differences $\Delta T_{8.7\text{-}10.8}$ and $\Delta T_{10.8\text{-}12.1}$ are considered to supply information about the cloud phase. Rain area delineation is realized by using a minimum threshold of the rainfall confidence. To obtain a statistical transfer function between the rainfall confidence and the four parameters $VIS_{0.6}$, $NIR_{1.6}$, $\Delta T_{8.7\text{-}10.8}$ and $\Delta T_{10.8\text{-}12.1}$, the value combinations of these four variables are compared to ground-based radar data. The retrieval is validated against independent radar data not used for deriving the transfer function and shows an encouraging performance as well as clear improvements compared to existing optical retrieval techniques using only IR thresholds for cloud top temperature.

5.1 Introduction

The detection of rainfall by means of optical sensors aboard geostationary (GEO) weather satellites has a long tradition as they provide information about the spatio-temporal distribution of this key parameter of the global water cycle in a high spatial and temporal resolution (e.g. ADLER & NEGRI 1988).

Most retrieval techniques developed so far for GEO systems are based on the relationship between cloud top temperature in the infrared channel and rainfall probability. Such retrievals, which are often referred to as IR retrievals, are appropriate for the tropics where precipitation is generally linked with deep convective clouds, that can be easily identified in the infrared and/or water vapour channels (e.g. LEVIZZANI et al. 2001; LEVIZZANI 2003), but show considerable drawbacks in the mid-latitudes (e.g. EBERT et al. 2007; FRÜH et al. 2007) where great parts of the precipitation originates from clouds formed by widespread frontal lifting processes in connection with extra-tropical cyclones (hereafter denoted as advective-stratiform precipitation).

These clouds are characterized by relatively warm top temperatures and a more homogeneous spatial distribution of cloud top temperature, that differ not significantly between raining and non-raining regions. Therefore, a threshold value for cloud top temperature in the IR channel as used for deep convective clouds seems to be improper for a reliable rain area delineation and leads to an underestimation of the detected precipitation area in such cases. To overcome this drawback, NAUSS & KOKHANOVSKY (2006, 2007) recently proposed a new scheme for the delineation of raining and non-raining cloud areas applicable to mid-latitudes using day-time multispectral satellite data from the LEO system Terra-MODIS (Moderate Resolution Imaging Spectroradiometer, see BARNES et al. 1998). It is based on the assumption that precipitating clouds must have a combination of large enough droplets, that can fall easily against updraft windfields and a large enough vertical extension, which favours the growth of precipitation droplets and prevents them from evaporation below the cloud bottom (see also LENSKY & ROSENFELD 2003). Since neither the droplet spectrum nor the geometrical thickness of a cloud can be computed without additional theoretical assumptions, the effective droplet radius (a_{ef}) (HANSEN & TRAVIS 1974) and the cloud optical thickness (τ) can be used as a measure for the particle size and the cloud thickness. Consequently, precipitating cloud areas can be characterized by a combination of the effective droplet radius and the optical thickness large enough to form precipitation (NAUSS 2006). Multiplying both parameters according to

$$LWP = \frac{2}{3} \cdot \tau \cdot a_{ef} \qquad (5.1)$$

one gets the liquid water path (LWP), which in turn is directly related to the rainfall probability of a cloud. As a result, precipitating cloud areas are characterized by a sufficiently large LWP, which can be used as a delineator between raining and non-raining clouds (NAUSS & KOKHANOVSKY 2006, 2007). The new proposed scheme shows an improvement in rain area delineation compared to existing techniques using only a threshold for cloud top infrared temperature especially for advective-stratiform precipitation clouds.

The LWP required for rain area delineation can be retrieved on a pixel basis during day-time using a combination of two solar channels (e.g. NAKAJIMA & NAKAJIMA 1995; KAWAMOTO et al. 2001; KOKHANOVSKY et al. 2003, 2005; PLATNICK et al. 2003; NAUSS et al. 2005). This is due to the fact that the reflection of solar light by a cloud in a non-absorbing wavelength (i.e. a visible channel between 0.4 and 0.8 μm) is strongly correlated to the optical thickness, while the reflection of solar light in a slightly absorbing wavelength (i.e. a near-infrared channel between 1.6 and 3.9 μm) is mainly a function of the cloud effective droplet radius.

To proof the conceptual model presented above within an initial test study, NAUSS & KOKHANOVSKY (2006, 2007) utilize the Semi-Analytical Cloud Retrieval Algorithm (SACURA, KOKHANOVSKY et al., 2003, 2005; NAUSS et al.,2005) to compute a_{ef}, τ , and finally LWP using Terra-MODIS data. SACURA is based on asymptotic solutions and exponential approximations of the radiative transfer theory valid for weakly absorbing media (KOKHANOVSKY & ROZANOV 2003, 2004), which are applicable for cloud retrievals up to a wavelength of around 2.2 μm. Compared to other lookup table techniques (e.g. NAKAJIMA & NAKAJIMA 1995; KAWAMOTO et al. 2001; PLATNICK et al. 2003) SACURA allows an instantaneous computation of the cloud properties, which is essential for an operational rain area delineation scheme for GEO systems, operating in near-real-time (NAUSS et al. 2005; NAUSS 2006).

SACURA has been validated over sea and land surfaces against the commonly used but computer-time expensive look-up table approaches of the Japanese Space Agency JAXA (NAKAJIMA & NAKAJIMA 1995; KAWAMOTO et al. 2001) and the NASA MODIS cloud property product MOD06 (PLATNICK et al. 2003) showing good agreement for optically thick (i.e. raining) cloud systems (NAUSS et al. 2005). However, as SACURA is only valid for water clouds it does not consider the ice phase, which leads to inaccuracies concerning precipitating clouds in the mid-latitudes, as efficient precipitation processes are mainly connected to the ice phase and the so called

Bergeron-Findeisen process (e.g. HOUZE 1993). Recently, KOKHANOVSKY & NAUSS (2005) and KOKHANOVSKY & NAUSS (2006) showed that a fast and accurate calculation of the effective cloud particle radius and the cloud optical thickness is possible for water and ice clouds, by using a non-absorbing visible and an absorbing near infrared channel (e.g. 0.8 µm and 1.6 µm). Differentiation between water and ice clouds can be realized by considering the brightness temperature difference between an 8 µm and an 11 µm channel together with the brightness temperature difference between an 11 µm and an 12 µm channel (STRABALA et al. 1994).

The new European meteorological GEO system MSG (Meteosat Second Generation) with its payload SEVIRI (Spinning Enhanced Visible and InfraRed Imager) provides the enhanced spectral resolution (AMINOU 2002; SCHMETZ et al. 2002; LEVIZZANI et al. 2001) to infer information about the liquid water path and the ice water path (hereafter both referred to as cloud water path; CWP) as well as about the cloud phase. Furthermore it offers a high temporal (15 min) and spatial (3×3 km at sub-satellite point) resolution necessary for a continuous area-wide monitoring of the rainfall distribution, which is essential for now-casting purposes.

Therefore, the objective of the present paper is to propose a new operational technique for rain area delineation in the mid-latitudes on a 15 min basis for MSG SEVIRI day-time data. It is based on the new conceptual model that precipitating clouds are characterized by a sufficiently large CWP and the existence of ice particles in the upper cloud parts.

The plan of the paper is as follows. The new developed Rain Area Delineation Scheme during day-time (RADS-D) is introduced in section 5.2 followed by an appraisal of the new technique in section 5.3. The paper is closed with a short summary and some conclusions.

5.2 A new technique for rain area delineation using MSG SEVIRI day-time data

As stated in the introduction SACURA is only applicable to water clouds. Concerning rain area delineation in the mid-latitudes this represents a shortcoming as effective precipitation processes in these regions are mainly connected to the ice phase and the so called Bergeron-Findeisen process. As a consequence, KOKHANOVSKY & NAUSS (2006) have already presented the fast and accurate forward radiative transfer scheme CLOUD, which enables the computation of the cloud properties for water and ice clouds, using one non-absorbing and one absorbing band available on MSG SEVIRI. However, a fast

inverse radiative transfer scheme is required for the operational retrieval of cloud properties, which is currently under final evaluation. Because no operational retrieval technique is currently available for MSG SEVIRI, that is applicable to water and ice clouds and that is fast enough concerning the 15 min scan cycle, the authors decided to use the original reflectance of the 0.56–0.71 µm ($VIS_{0.6}$) and 1.5–1.78 µm ($NIR_{1.6}$) SEVIRI channels for this study, instead of computed values of a_{ef} and τ. As soon as an adequate retrieval technique is available the proposed algorithm can be readily applied to the retrieved cloud properties. Information about the cloud phase are incorporated by means of the brightness temperature difference between the 8.7 µm channel (8.3–9.1 µm) and the 10.8 µm channel (9.8–10.8 µm) ($\Delta T_{8.7\text{-}10.8}$) together with the brightness temperature difference between the 10.8 µm channel and the 12.1 µm channel (11–13 µm) ($\Delta T_{10.8\text{-}12.1}$) (refer to STRABALA et al. 1994; ACKERMAN et al. 1998). The differentiation is based on the observation that the increase of water particle absorption is greater between 11 and 12 µm than between 8 and 11 µm. The ice particle absorption increases more between 8 and 11 µm than between 11 and 12 µm (STRABALA et al. 1994). Therefore, $\Delta T_{10.8\text{-}12.1}$ of water clouds are greater than $\Delta T_{8.7\text{-}10.8}$. On the other hand, $\Delta T_{8.7\text{-}10.8}$ of ice clouds are greater than coincident $\Delta T_{10.8\text{-}12.1}$.

To use the information about the CWP and the cloud phase for a proper detection of potentially precipitating cloud areas (i.e. a large enough CWP and ice particles in the upper part) the rainfall confidence is calculated as a function of the value combinations of the four variables $VIS_{0.6}$, $NIR_{1.6}$, $\Delta T_{8.7\text{-}10.8}$, and $\Delta T_{10.8\text{-}12.1}$ (e.g. BELLON et al. 1980; CHENG et al. 1993; KURINO 1997; NAUSS & KOKHANOVSKY 2007). The computation of the pixel based rainfall confidence is done by a comparison of these value combinations with ground-based radar data from the German Weather Service for day-time precipitation events from January to August 2004 (altogether 850 scenes). The ground-based radar data from the DWD C band radar network consist of six classes representing different reflectivity intensities, which are all together considered as raining in the comparison with collocated satellite pixels. A lower reflectivity threshold of 7.0 decibel for the first class is utilized to detect rain bearing pixels (DWD). Figure 5.1 shows the calculated rainfall confidence as a function of $VIS_{0.6}$ and $NIR_{1.6}$ (a), as well as a function of $\Delta T_{8.7\text{-}10.8}$ and $\Delta T_{10.8\text{-}12.1}$ (b). Equation (5.2) shows the calculation of the rainfall confidences as a function of two different variables.

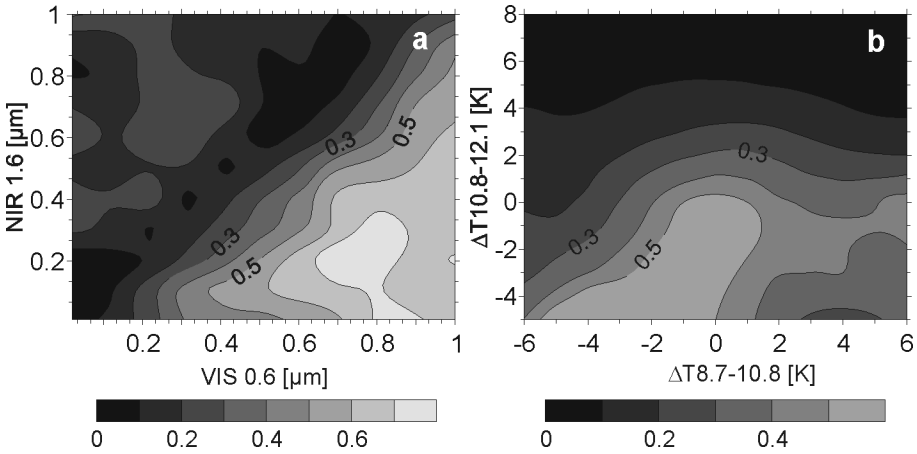

Figure 5.1: The rainfall confidence as a function of $VIS_{0.6}$ and $NIR_{1.6}$ (a), as well as a function of $\Delta T_{8.7\text{-}10.8}$ and $\Delta T_{10.8\text{-}12.1}$ (b) calculated with equation (5.2).

$$RainConf(x_1, x_2) = \frac{N_{Rain}(x_1, x_2)}{N_{Rain}(x_1, x_2) + N_{NoRain}(x_1, x_2)} \qquad (5.2)$$

where N_{Rain} and N_{NoRain} are the raining and the non-raining frequencies, respectively, and x_1 and x_2 denote the reflectance or brightness temperature difference ($VIS_{0.6}$, $NIR_{1.6}$, $\Delta T_{8.7\text{-}10.8}$, $\Delta T_{10.8\text{-}12.1}$) combined for the calculation of the rainfall confidence.

As can be seen in figure 5.1 a high values of the rainfall confidence coincide with high values of $VIS_{0.6}$ and low values of $NIR_{1.6}$, indicating a large CWP. High values of $VIS_{0.6}$ indicate a high optical thickness and low values of $NIR_{1.6}$ indicate large cloud particles as the absorption increases with increasing particle size. Figure 5.1 b shows that ice clouds, where $\Delta T_{8.7\text{-}10.8}$ are greater than coincident $\Delta T_{10.8\text{-}12.1}$, possess high rainfall confidences. On the other hand, for water clouds $\Delta T_{10.8\text{-}12.1}$ are greater than $\Delta T_{8.7\text{-}10.8}$. These areas are characterized by lower rainfall confidences. However, high $\Delta T_{10.8\text{-}12.1}$ values may also be connected with non precipitating Ci clouds. For example, INOUE (1987) classified clouds with $\Delta T_{10.8\text{-}12.1} \geq 2.5$ K as Ci clouds. Such values of $\Delta T_{10.8\text{-}12.1}$ are characterized by low rainfall confidences in figure 5.1 b. Following the results of STRABALA et al. (1994) the corresponding $\Delta T_{8.7\text{-}10.8}$ values should be as high as or greater than the $\Delta T_{10.8\text{-}12.1}$ values. To make use of the combined information content provided by the four parameters $VIS_{0.6}$, $NIR_{1.6}$, $\Delta T_{8.7\text{-}10.8}$ and $\Delta T_{10.8\text{-}12.1}$ for rain delineation, the rainfall confidence is computed as a function of the combined values of these four

variables as shown in equation (5.3) using the above mentioned 850 scenes:

$$RainConf(x_{1,}x_{2,}x_{3,}x_4)=\frac{N_{Rain}(x_{1,}x_{2,}x_{3,}x_4)}{N_{Rain}(x_{1,}x_{2,}x_{3,}x_4)+N_{NoRain}(x_{1,}x_{2,}x_{3,}x_4)} \quad (5.3)$$

where N_{Rain} and N_{NoRain} are the raining and the non-raining frequencies, respectively, and x_1, x_2, x_3, x_4 denote the reflectance or brightness temperature difference ($VIS_{0.6}$, $NIR_{1.6}$, $\Delta T_{8.7\text{-}10.8}$, $\Delta T_{10.8\text{-}12.1}$) combined for the calculation of the rainfall confidence.

The threshold of the calculated rainfall confidence appropriate for rain area delineation is determined by optimizing the Equitable Threat Score (ETS), which is based on the number of pixels, that have been identified in the satellite (S) and radar (R) techniques as raining (S_Y, R_Y) or non-raining (S_N, R_N). It indicates how well the classified rain pixels correspond to the rain pixels observed by the radar, also accounting for pixels correctly classified by chance ($S_YR_{YRandom}$). Its value can range from -1/3 to 1 with the optimum value 1. The ETS is calculated according to

$$ETS=\frac{S_yR_y-S_yR_{yRandom}}{S_yR_y+S_nR_y+S_yR_n-S_yR_{yRandom}} \quad (5.4)$$

with

$$S_yR_{yRandom}=\frac{(S_yR_y+S_nR_y)\cdot(S_yR_y+S_yR_n)}{T_{SR}} \quad (5.5)$$

where T_{SR} denotes the total number of pixels. Additionally to the ETS, a visual inspection of the Relative Operation Characteristic (ROC) plot (Mason 1982; Jolliffe & Stephenson 2003) was also considered to identify an appropriate rainfall confidence threshold (see figure 5.2). The Probability Of Detection (POD) describes the ratio between pixels with S_YR_Y and R_Y, and gives the fraction of pixels, that have been correctly identified by the satellite technique, according to the radar product. The Probability Of False Detection (POFD) describes the ratio between S_YR_N and R_N and indicates the fraction of the pixels incorrectly identified as rainfall events by the satellite algorithm. The optimum value for the POD is 1, while it is 0 for the POFD. The dotted diagonal line in the ROC plot represents the "no skill" line (i.e. POD equals POFD). Value combinations above this line indicate, that the approach has skill (i.e. POD larger than POFD).

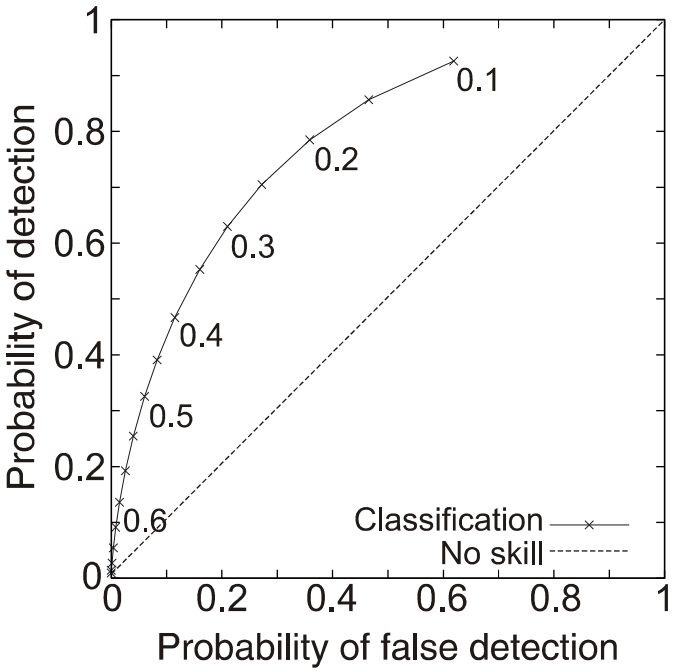

Figure 5.2: ROC plot based on the comparison between the combined values of the reflectances and brightness temperature differences mentioned in the text from 850 MSG SEVIRI scenes and corresponding ground-based radar measurements over Germany. Different rainfall confidence threshold values between 0.1 and 0.7 (step 0.05) indicated by the crosses were used to delineate the satellite-based rain area.

Different rainfall confidence threshold values between 0.1 and 0.7 were used to delineate the satellite-based rain area. The ETS, the POD and the POFD for the delineated rain areas based on the different rainfall confidence levels were calculated in comparison with ground-based radar data. As shown in figure 5.2, the rainfall confidence threshold value around 0.3 seems to be most suitable for rain area delineation since corresponding POD-POFD combinations show the largest distance normal to the "no skill" line. The delineated rain area using a rainfall confidence threshold of 0.34 yields the optimized ETS of 0.24. Therefore, the rainfall confidence of 0.34 is chosen as the minimum threshold for precipitating clouds during day-time.

5.3 Appraisal of the new scheme

For the evaluation study, scenes from day-time precipitation events between January and August 2004 were classified by using the new developed Rain Area Delineation Scheme during day-time (RADS-D). The precipitation events chosen for the evaluation study are

independent from the above mentioned precipitation events used for algorithm development. Altogether 720 day-time scenes were chosen.

To evaluate the potential improvement by the new scheme the validation scenes were also classified by the Enhanced Convective Stratiform Technique (ECST) (REUDENBACH et al. 2001; REUDENBACH 2003), which is similar to the Convective Stratiform Technique (CST) (ADLER & NEGRI 1988), but additionally includes the water vapour channel temperature for a more reliable deep convective/cirrus clouds discrimination (TJEMKES et al. 1997). The ECST, which was first transferred from Meteosat-7 MVIRI (Meteosat Visible and InfraRed Imager radiometer) to MSG SEVIRI (THIES et al. 2007), is used for the identification of convective rain areas since these regions approximately represent the performance of many present optical rainfall retrievals.

Standard verification scores following the suggestions of the International Precipitation Working Group (IPWG, TURK & BAUER 2006) were calculated on a pixel basis for each scene in comparison with corresponding ground-based radar data from the German Weather Service. The bias describes the ratio between S_Y and R_Y and the False Alarm Ratio (FAR) gives the ratio between $S_Y R_N$ and S_Y. The Critical Success Index (CSI), which encloses all pixels, that have been identified as raining by either the radar network or the satellite technique, describes the ratio between $S_Y R_Y$ and the sum of $S_Y R_Y$, $S_N R_Y$, $S_Y R_N$. All scores range from 0 to 1. The optimum value for the CSI is 1, while it is 0 for the FAR. Since the POD can be increased by just increasing the satellite rainfall area (i.e. by reducing the rainfall confidence threshold), it has to be analysed in connection with corresponding values of the FAR and the POFD since both measure the fraction of the satellite pixels, that have been incorrectly identified as raining. The verification scores were calculated on a pixel basis for each single scene without any spatio-temporal aggregation. For a detailed discussion of the verification scores see STANSKI et al. (1989) or the web site of the WWRP/WGNE.

The verification scores calculated for the 720 day-time validation scenes are summarized in table 5.1. RADS-D slightly overestimates the rain area detected by the radar network, which is indicated by the bias of 1.15. In contrast to this, the rain area is strongly underestimated by the ECST (bias of 0.22). 61% of the radar observed raining pixels are also identified by RADS-D. This indicates a much better performance compared to the POD of 9% for the ECST, even if this coincide with a higher POFD of 0.18 for RADS-D in comparison to 0.04 for the ECST. Anyhow, the FAR indicates that a lower fraction of the pixels where wrongly classified as rain by RADS-D

(0.46) than by the ECST (0.51). Altogether, the good performance of the new RADS-D is further supported by the CSI (0.39) and the ETS (0.25). Compared to ECST (CSI: 0.1; ETS: 0.06) this signifies a distinct improvement concerning the delineated rain area.

Table 5.1: Results of the standard verification scores applied to the rain-area identified by RADS-D and ECST on a pixel basis. The scores are based on 720 precipitation scenes with 24 914 160 pixels, of which 5 872 220 have been identified as raining by RADS-D. POD (Probability Of Detection); POFD (Probability Of False Detection), FAR (False Alarm Ratio); CSI (Critical Success Index); ETS (Equitable Threat Score).

Test	RADS-D				ECST			
	Mean	StDev	Min	Max	Mean	StDev	Min	Max
Bias	1.15	0.38	0.16	2.17	0.22	0.27	0	2.82
POD	0.61	0.21	0.12	0.98	0.12	0.17	0	0.97
POFD	0.18	0.09	0.02	0.54	0.04	0.05	0	0.78
FAR	0.46	0.12	0.03	0.84	0.51	0.27	0	1
CSI	0.39	0.14	0.1	0.77	0.1	0.14	0	0.64
ETS	0.25	0.11	-0.04	0.53	0.06	0.09	-0.05	0.39

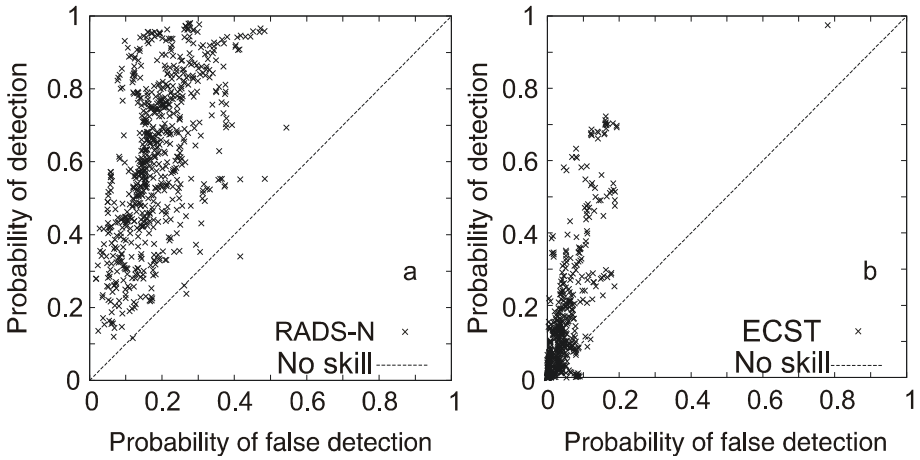

Figure 5.3: ROC plots for the comparison between RADS-D and ground-based radar (a), and ECST and ground-based radar (b). The calculated probability of detection (POD) and probability of false detection (POFD) are based on the 720 scenes mentioned in the text.

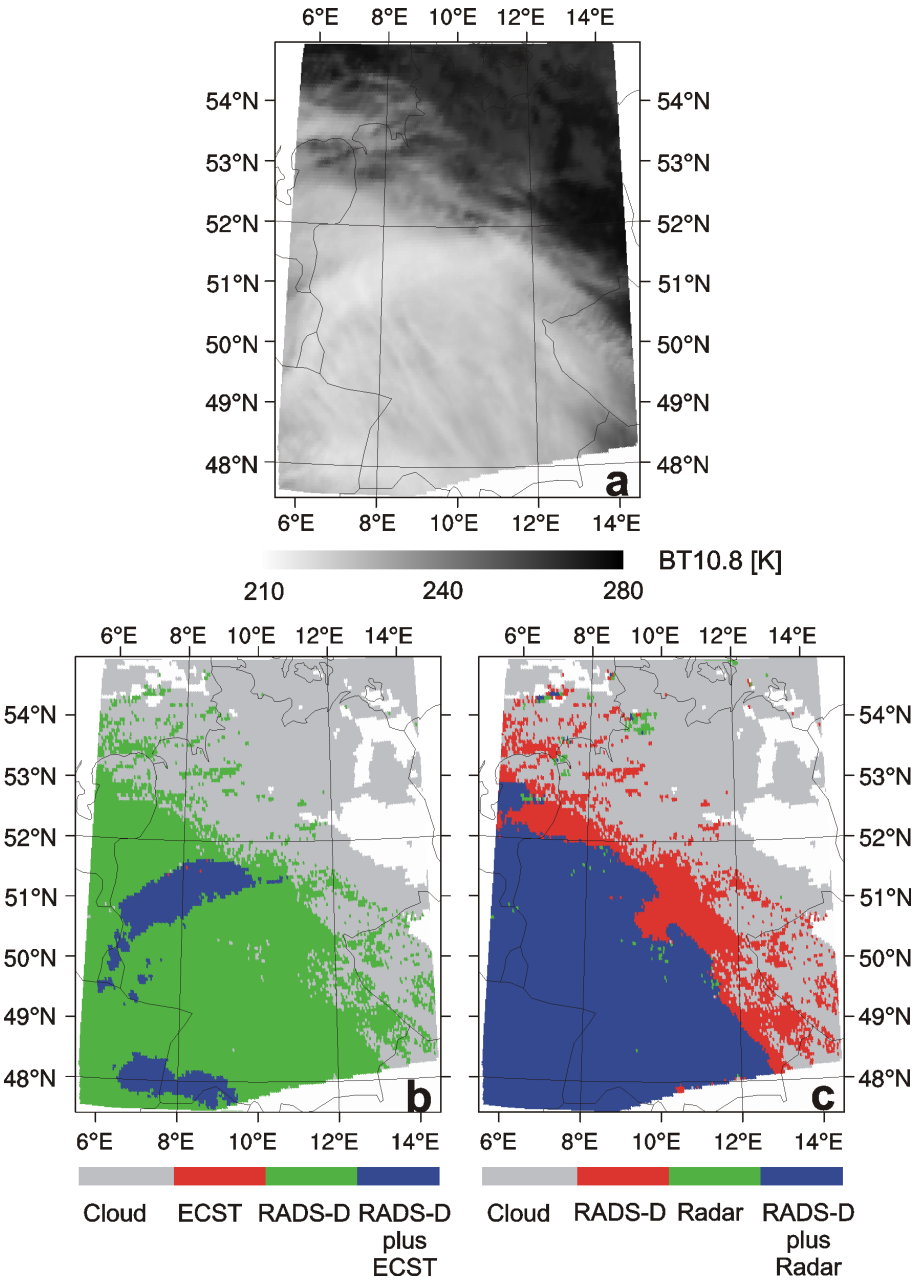

Figure 5.4: Delineated rain area for the scene from 12 January 2004 12:45 UTC. (a) $BT_{10.8}$ image; (b) rain area delineated by RADS-D as well as by ECST; (c) rain area detected by RADS-D in comparison to the radar data.

An overview of the performance of RADS-D in comparison to the ECST is given by the Relative Operation Characteristic (ROC) plot in figure 5.3. The visual impression additionally supports the good and

improved performance of the new developed scheme. The combination of medium to high values for POD together with low to medium values for POFD, which is valid for the main part of the classified scenes, underlines the overall good skill of the new scheme. In contrast, for scenes classified by the ECST the POD and POFD indicate much lower or even no skills.

To gain a visual impression of the performance of the new developed rain area delineation scheme, the classified rain area for a scene from 12 January 2004 12:45 UTC is depicted in figure 5.4. Figure 5.4 a shows the brightness temperature in the 10.8 µm channel ($BT_{10.8}$), figure 5.4 b the rain area delineated by RADS-D as well as by ECST, and figure 5.4 c the rain area detected by RADS-D in comparison to the radar data.

5.4 Conclusions

A new algorithm for rain area delineation during day-time using multispectral optical satellite data of MSG SEVIRI was proposed. The method allows not only a proper detection of mainly convective precipitation by means of the commonly used connection between infrared cloud top temperature and rainfall probability but also enables the detection of advective-stratiform precipitation (e.g. in connection with mid-latitude frontal systems). It is based on the conceptual model that precipitation is favoured by a large cloud water path and the presence of ice particles in the upper part of the cloud. The technique considers the $VIS_{0.6}$ and the $NIR_{1.6}$ channel to gain information about the cloud water path. Additionally, the channel differences $\Delta T_{8.7\text{-}10.8}$ and $\Delta T_{10.8\text{-}12.1}$ are considered to gain information about the cloud phase.

The information about the cloud water path and the cloud phase of the four variables is merged and incorporated into the new developed rain delineation algorithm. Rain area delineation is realized by using the pixel based rainfall confidence as a function of the respective value combination of the four variables. The calculation of the rainfall confidence is based on a comparison of the value combinations of the four variables with ground-based radar data. A minimum threshold for the rainfall confidence of 0.34 was determined as appropriate for rain area delineation.

The results of the algorithm were compared with corresponding ground-based radar. The proposed technique performs better than existing optical retrieval techniques using only IR thresholds for cloud top temperature. The new developed algorithm shows encouraging

performance concerning precipitation delineation during day-time in the mid-latitudes using MSG SEVIRI data.

In a next step the solar signal within the 3.9 µm channel will be additionally incorporated for an enhanced rain area delineation. Such an improvement can be expected because of the differing penetration depth of the radiation in the spectral range of the 1.6 µm and the 3.9 µm channels (CHANG & LI 2002). While the radiation in the 3.9 µm channel originates from the upper parts of the cloud and the cloud top, the radiation in the 1.6 µm channel penetrates about two times deeper into the cloud (PLATNICK 2000). As ROSENFELD et al. (2004) pointed out the combined and simultaneous use of the 1.6 µm and the 3.9 µm channel would be the best choice. Such a combination is possible with MSG SEVIRI. In this context it has to be mentioned that the information about the effective radius, retrieved from reflectance in the 1.6 µm and 3.9 µm channels, is only representative for the upper parts of the cloud. Nevertheless it is assumed that cloud areas with large liquid droplets and ice particles and a large cloud water path within the upper parts could be seen as a precondition for the formation of droplets large enough to fall as raindrops in the middle and lower portions of the cloud.

Together with the existing rain area delineation scheme during night-time (THIES et al. 2008) the new algorithm offers the great potential for a 24 h technique for rain area delineation with a high spatial and temporal resolution.

The night-time technique is based on the same conceptual model as the presented day-time scheme. However, since no operational retrieval exists for MSG to compute the cloud water path during night-time, suitable combinations of brightness temperature differences (1T) between the thermal bands of MSG SEVIRI ($\Delta T_{3.9\text{-}10.8}$, $\Delta T_{3.9\text{-}7.3}$, $\Delta T_{8.7\text{-}10.8}$, $\Delta T_{10.8\text{-}12.1}$) are used to infer implicit information about the cloud water path. $\Delta T_{8.7\text{-}10.8}$ and $\Delta T_{10.8\text{-}12.1}$ are particularly considered to supply information about the cloud phase. Similar to the day-time approach rain area delineation is realized by means of the pixel based rainfall confidence as a function of the respective value combination of the four brightness temperature differences.

A potential application of a new rainfall retrieval technique based on multispectral satellite data of the next generation GEO systems is the improved rainfall detection in a high spatial and temporal resolution. This is of valuable benefit for now-casting purposes in regions where ground-based radar networks are not available as well as for approaches, that attempt to merge passive microwave rainfall information with data from GEO systems in a higher temporal and spatial resolution. Up to now such hybrid techniques consider only IR

cloud top temperature and suffer from the inherent drawbacks especially regarding precipitation processes in connection with extra-tropical cyclones. Therefore, rainfall retrievals based on multispectral satellite data of the new generation GEO systems play an important role for quasi-continuous precipitation monitoring. In this context the study demonstrated the high potential offered by the enhanced spectral resolution of new generation multispectral optical satellite systems as MSG SEVIRI. The good validation results, that are obtained on a 15 minute basis without any spatial and temporal aggregation suggest, that the achieved accuracies are sufficient for the proposed applications. This is especially true, as for similar comparison studies the data are generally temporally aggregated over 3 h or 24 h, (e.g. validation web page of the international precipitation working group; IPWG; http://www.bom.gov.au/bmrc/SatRainVal/validation-intercomparison.html). Based on the improved rain area delineation, the next step an enhanced assignment of the associated rainfall rate can be tackled. Concerning this topic, comprehensive research efforts have just been started in order to develop a new method for the assignment of rainfall rates based on information about the cloud water path and the cloud phase since the commonly used relationship between rainfall rate and cloud top temperature in the IR channel seems to be insufficient especially for precipitating advective-stratiform cloud areas. For a comprehensive appraisal of the final retrieval scheme (rain area delineation with associated rainfall rate assignment) detailed validation studies are necessary. In this context a cooperation with the Italian National Research Council Institute of Atmospheric Sciences and Climate is intended with the objective of an extensive evaluation of the final algorithm in comparison with other retrieval techniques (e.g. the CMORPH technique of JOYCE et al. 2004).

Acknowledgements

The current study is funded by the German Ministry of Research and Education (BMBF) in the framework of the GLOWA-Danube project (G-D/2004/TP-10, precipitation/remote sensing) as well as by the German Research Council (DFG) (BE 1780/18-1) within the SORT project. The authors are grateful to the German Weather Service (DWD) for providing the radar data sets within the EUMETSAT/DWD Advanced Multisensor Precipitation Experiment (AMPE).

References

ACKERMAN, S. A., K. I. STRABALA, W. P. MENZEL, R. A. FREY, C. C. MOELLER & L. E. GUMLEY (1998B): Discriminating clear sky from clouds with MODIS. - *Journal of Geophysical Research-Atmospheres, 103*: 32141–32157.

ADLER, R. F. & A. J. NEGRI (1988): A satellite technique to estimate tropical convective and stratiform rainfall. - *Journal of Applied Meteorology, 27*: 30–51.

AMINOU, D. M. A. (2002): MSG's SEVIRI instrument. - *ESA Bulletin, 111*: 15–17.

BARNES, W. L., T. S. PAGANO & V. V. SALOMONSON (1998): Prelaunch characteristics of the Moderate Resolution Imaging Spectroradiometer (MODIS) on EOS-AM1. - *IEEE Transactions on Geoscience and Remote Sensing, 36:* 1088–1100.

BELLON, A., S. LOVEJOY & G. L. AUSTIN (1980): Combining satellite and radar data for the short-range forecasting of precipitation. - *Monthly Weather Review, 108*: 1554–1556.

CHANG, F.-L. & Z. LI (2002): Estimating the vertical variation of cloud droplet effective radius using multispectral near- infrared satellite measurements. - *Journal of Geophysical research – Atmosphere, 107(D15)*, doi:10.1029/2001JD000766.

CHENG, M., R. BROWN & C. G. COLLIER (1993): Delineation of precipitation areas by correlation of METEOSAT visible and infrared data in the region of the United Kingdom. - *Journal of Applied Meteorology, 32*: 884–898.

DWD (2005): Weather radar network. - Available online at http://www.dwd.de/en/Technik/Datengewinnung/Radarverbund/Radarbroschuere_en.pdf, 10 November 2007.

EBERT, E. E., J. E. JANOWIAK & C. KIDD (2007): Comparison of near-real-time precipitation estimates from satellite observations and numerical models. - *Bulletin of the American Meteorological Society, 88*: 47–64.

FRÜH, B., J. BENDIX, T. NAUSS, M. PAULAT, A. PFEIFFER, J. W. SCHIPPER, B. THIES & H. WERNLI (2007): Verification of precipitation from regional climate simulations and remote-sensing observations with respect to ground-based observations in the upper Danube catchment. - *Meteorologische Zeitschrift, 16*: 275–293.

HANSEN, J. E. & L. D. TRAVIS (1974): Light scattering in planetary atmospheres. - *Space Science Reviews, 16*: 527–610.

HOUZE, R. A. (1993): Cloud Dynamics, Vol. 53. of International Geophysics Series, Academic Press, San Diego.

INOUE, T. (1987): A cloud type classification with NOAA 7 split-window measurements. - *Journal of Geophysical Research – Atmosphere, 92:* 3991–4000.

JOLLIFFE, I. T. & D. B. STEPHENSON (2003): Forecast verification. A Practitioner's Guide in Atmospheric Science. John Wiley and Sons, Chichester.

JOYCE, R. J., J. E. JANOWIAK, P. A. ARKIN & P. XIE (2004): CMORPH: A method that produces global precipitation estimates from passive microwave and infrared data at high spatial and temporal resolution. - *Journal of Hydrometeorology, 5:* 487–503.

KAWAMOTO, K., T. NAKAJIMA & T. Y. NAKAJIMA (2001): A global determination of cloud microphysics with AVHRR remote sensing. - *Journal of Climate, 14*: 2054–2068.

KOKHANOVSKY, A. A., V. V. ROZANOV, E. P. ZEGE, H. BOVENSMANN & J. P. BURROWS (2003): A semi-analytical cloud retrieval algorithm using backscattered radiation in 0.4–2.4 micrometers spectral range. - *Journal of Geophysical Research-Atmospheres, 108(D1)*: 4008, Doi:10.1029/2001JD001543.

KOKHANOVSKY, A. A. & V. V. ROZANOV (2003): The reflection function of optically thick weakly absorbing turbid layers: a simple approximation. - *Journal of Quantitative Spectroscopy and Radiative Transfer, 77*: 165–175, 2003.

KOKHANOVSKY, A. A. & V. V. ROZANOV (2004): The physical parameterization of the top-of-atmosphere reflection function for a cloudy atmosphere -underlying surface system: the oxygen A-band case study. - *Journal of Quantitative Spectroscopy and Radiative Transfer, 85:* 35–55.

KOKHANOVSKY, A. A., V. V. ROZANOV, T. NAUSS, C. REUDENBACH, J. S. DANIEL, H. L. MILLER & J. P. BURROWS (2005): The semianalytical cloud retrieval algorithm for SCIAMACHY. I: The validation. - *Atmospheric Chemistry and Physics, 6*: 1905–1911.

KOKHANOVSKY, A. A. & T. NAUSS (2005): Satellite-based retrieval of ice cloud properties using a semi-analytical algorithm. - *Journal of Geophysical Research-Atmospheres, 110/D19*: D19206, Doi:10.1029/2004JD005744.

KOKHANOVSKY, A. A. & T. NAUSS (2006). Reflection and transmission of solar light by clouds: asymptotic theory. - *Atmospheric Chemistry and Physics, 6*: 5537–5545.

KURINO, T. (1997): A satellite infrared technique for estimating 'deep/shallow' precipitation. - *Advances in Space Research, 19*: 511–514.

LENSKY, I. M. & D. ROSENFELD (2003): A night-time delineation algorithm for infrared satellite data based on microphysical considerations. - *Journal of Applied Meteorology, 42*: 1218–1226.

LEVIZZANI, V., J. SCHMETZ, H. J. LUTZ, J. KERKMANN, P. P. ALBERONI & M. CERVINO (2001): Precipitation estimations from geostationary orbit and prospects for Meteosat Second Generation. - *Meteorological Applications, 8:* 23–41.

LEVIZZANI, V. (2003): Satellite rainfall estimations: new perspectives for meteorology and climate from the EURAINSAT project. - *Annales Geophysicae-Italy, 46:* 363–372.

MASON, I. (1982): A model for assessment of weather forecasts. - *Australian Meteorological Magazine*, 30: 291–302.

NAKAJIMA, T. Y. & T. NAKAJIMA (1995): Wide-area determination of cloud microphysical properties from NOAA AVHRR measurements for FIRE and ASTEX regions. - *Journal of the Atmospheric Sciences, 52*: 4043–4059.

NAUSS, T., A. A. KOKHANOVSKY, T. Y. NAKAJIMA, C. REUDENBACH & J. BENDIX (2005): The intercomparison of selected cloud retrieval algorithms. - *Atmospheric Research, 78*: 46–78.

NAUSS, T. (2006): Das Rain Area Delineation Scheme RADS – ein neues Verfahren zur satellitengestützten Erfassung der Niederschlagsfläche über Mitteleuropa. - *Marburger Geographische Schriften, 143*: 160 pp.

NAUSS, T. & A. A. KOKHANOVSKY (2006): Discriminating raining from non-raining clouds at mid-latitudes using multispectral satellite data. - *Atmospheric Chemistry and Physics, 6*: 5031–5036.

NAUSS, T. & A. A. KOKHANOVSKY (2007): Assignment of rainfall confidence values using multispectral satellite data at mid-latitudes: first results. - *Advances in Geosciences, 10*: 99–102.

PLATNICK, S. (2000): Vertical photon transport in cloud remote sensing problems. - *Journal of Geophysical Research - Atmosphere, 105:* 22919–22935.

PLATNICK, S., M. D. KING, S. A. ACKERMAN, W. P. MENZEL, B. A. BAUM, J. C. RIÉDI & R. A. FREY (2003): The MODIS cloud products: algorithms and examples from Terra. - *IEEE Transactions on Geoscience and Remote Sensing, 41*: 459–473.

REUDENBACH, C., G. HEINEMANN, E. HEUEL, J. BENDIX & M. WINIGER (2001): Investigation of summertime convective rainfall in Western Europe based on a synergy of remote sensing data and numerical models. - *Meteorology and Atmospheric Physics, 76*: 23–41.

REUDENBACH, C. (2003): Konvektive Sommerniederschläge in Mitteleuropa. Eine Kombination aus Satellitenfernerkundung und numerischer Modellierung zur automatischen Erfassung mesoskaliger Niederschlagsfelder. - *Bonner Geographische Abhandlungen, 109*: 152 pp.

ROSENFELD, D., E. CATTANI, S. MELANI & V. LEVIZZANI (2004): Considerations on daylight operation of 1.6 µm vs. 3.7 µm channel on NOAA and METOP Satellites. - *Bulletin of the American Meteorological Society, 85*: 873– 881.

SCHMETZ, J., P. PILI, S. TJEMKES, D. JUST, J. KERKMANN, S. ROTA & A. RATIER (2002): An introduction to Meteosat Second Generation (MSG). - *Bulletin of the American Meteorological Society, 83*: 977–992.

STANSKI, H. R., L. WILSON & W. BURROWS (1989): Survey of common verification methods in meteorology. - *World Weather Watch Technical Report No.8. WMO: Geneva*, WMO/TD No. 358, 114 pp.

STRABALA, K. I., S. A. ACKERMAN & W. P. MENZEL (1994): Cloud properties inferred from 8-12-µm Data. - *Journal of Applied Meteorology, 33*: 212–229.

THIES, B., T. NAUSS & J. BENDIX (2007): Detection of high rain clouds using water vapour emission – transition from Meteosat First (MVIRI) to Second Generation (SEVIRI). - *Advances in Space Research,* submitted.

THIES, B., T. NAUSS & J. BENDIX (2008): Discriminating raining from non-raining cloud areas at mid-latitudes using Meteosat Second Generation SEVIRI night-time data. - *Meteorological Applications*, DOI: 10.1002/met.56.

TJEMKES, S. A., L. VAN DE BERG & J. SCHMETZ (1997). Warm water vapour pixels over high clouds as observed by Meteosat. - *Contributions to Atmospheric Physics, 70*: 15–21.

TURK, J. & P. BAUER (2006): The International Precipitation Working Group and Its Role in the Improvement of Quantitative Precipitation Measurements. - *Bulletin of the American Meteorological Society*, 87: 643–647.

WORLD WEATHER RESEARCH PROGRAM/WORKING GROUP ON NUMERICAL EXPERIMENTATION JOINT WORKING GROUP ON VERIFICATION (WWRP/WGNE): Forecast Verification – Issues, Methods and FAQ. -

Available online at http://www.bom.gov.au/bmrc/wefor/staff/eee/verif/verif web page.html, 11 May 2007.

CHAPTER 6

Precipitation process and rainfall intensity separation using Meteosat Second Generation SEVIRI data

Boris Thies, Thomas Nauß and Jörg Bendix

Submitted to Journal of Geophysical Research – Atmosphere

6 Precipitation process and rainfall intensity differentiation using Meteosat Second Generation SEVIRI data

Boris Thies, Thomas Nauß and Jörg Bendix

Philipps-University Marburg,
Department of Geography,
Laboratory for Climatology and Remote Sensing,
Deutschhausstraße 10, 35032 Marburg, Germany

Abstract

A new consistent day and night technique for precipitation process separation and rainfall intensity differentiation using MSG SEVIRI data is proposed. It relies on information about the cloud water path (CWP), the cloud phase (CP) in the upper regions, and the cloud top height (CTH).

In a first step the rain area is separated into the subareas of convective and advective-stratiform precipitation processes. In the following both areas are divided into subareas of differing rainfall intensities. The process detection and subdivision of the convective precipitation area relies on information about the CTH gained from WV-IR differences and the IR cloud top temperature. The subdivision of the advective-stratiform precipitation area is based on information about the CWP and the CP in the upper cloud parts. Information about the CP is gained by considering the temperature differences $\Delta T_{8.7\text{-}10.8}$ and $\Delta T_{10.8\text{-}12.1}$. Information about the CWP is incorporated by considering the $VIS_{0.6}$ and $NIR_{1.6}$ channel during day-time and the temperature differences $\Delta T_{3.9\text{-}10.8}$, $\Delta T_{3.9\text{-}7.3}$, $\Delta T_{8.7\text{-}10.8}$, and $\Delta T_{10.8\text{-}12.1}$ during night-time.

The precipitation process areas and the rainfall intensity subareas classified by the proposed technique are validated against ground-based radar data. The results indicate an encouraging performance of the new algorithm concerning process separation and intensity differentiation and support the possibility of process-oriented rain area classification using MSG SEVIRI.

6.1 Introduction

Precipitation as a major part of the global water cycle affects all aspects of human life. However, the high spatial and temporal variability of this parameter still hampers its correct spatio-temporal detection and quantification. In this context geostationary (GEO) weather satellite systems with their high spatial and temporal resolution offer the potential for area-wide rainfall retrievals. This is of valuable benefit in areas without a dense ground-based weather radar network as well as in the context of techniques intending to merge passive microwave (PMW) based retrieval techniques with data from GEO satellite systems in order to overcome the low spatial and especially the low temporal resolution of the PMW sensors aboard low earth orbit (LEO) systems (e.g. JOYCE et al. 2004; KIDD et al. 2003 MILLER et al. 2001).

Most of the rainfall retrieval techniques based on optical satellite data of GEO systems developed so far rely on a relationship between cloud top temperature (CTT) measured in an infrared (IR) channel and the rainfall probability and intensity (e.g. ADLER & MACK 1984; ADLER & NEGRI 1988)). These so-called IR retrievals are based on the assumption that highly convective clouds with high rainfall intensities are characterized by a large vertical extension with a cold cloud top rising high into the troposphere.

Such IR retrieval techniques are appropriate for convective clouds, that can be easily identified in the infrared and/or water vapour channels (e.g. LEVIZZANI et al. 2001; LEVIZZANI 2003), but show considerable drawbacks concerning mid-latitudinal precipitation processes in connection with extra-tropical cyclones (hereafter denoted as advective-stratiform precipitation areas) (e.g. EBERT et al. 2007; FRÜH et al. 2007; KÄSTNER et al. 2006). Such precipitating clouds are mainly formed by widespread lifting processes along frontal zones and are characterized by relatively warm and spatially homogeneous CTT, that differ not significantly between raining and non-raining regions. Therefore, retrieval techniques based solely on the IR CTT lead to an underestimation of the detected rain area and to uncertainties concerning the assigned rainfall rate.

To overcome this drawbacks, several authors suggest to use optical and microphysical cloud parameters derived from multispectral data of new generation satellite systems to improve rainfall retrievals (e.g. LENSKY & ROSENFELD 2003a,b; LENSKY & ROSENFELD 2006; BA & GRUBER 2001; ROSENFELD & LENSKY 1998). NAUSS & KOKHANOVSKY (2006, 2007) proposed a technique for the LEO system Terra-MODIS (BARNES et al. 1998) to delineate precipitating cloud areas in mid-

latitudes by using an auto-adaptive threshold for the effective particle radius (a_{ef}) as a function of the cloud optical thickness (τ). According to this technique, precipitating cloud areas can be characterized by a combination of a_{ef} and τ large enough to form precipitation.

Based on the results of NAUSS & KOKHANOVSKY (2006, 2007) THIES et al. (2008a,b) introduced a new technique for the detection of precipitating cloud areas in the mid-latitudes applicable to the new generation GEO system Meteosat Second Generation (MSG) with its payload, the Spinning Enhanced Visible and InfraRed Instrument (SEVIRI) (AMINOU 2002, SCHMETZ et al. 2002). This technique relies on information about the cloud water path (CWP) and the cloud phase (CP) in the upper cloud parts. The basic assumption is that precipitating cloud areas are characterized by a sufficiently large CWP (which represents the product of a_{ef} and τ) and the existence of ice particles in the upper parts of the cloud (Bergeron-Findeisen process). The new technique shows a clearly improved performance in rain area detection compared to traditional IR techniques and points to the high potential offered by multispectral data from optical sensors aboard new generation GEO systems regarding a more accurate rainfall detection in a high spatial and temporal resolution.

Based on the good quality of existing IR retrieval techniques concerning convectively dominated precipitation areas and the improvements with respect to the advective-stratiform precipitation areas, that became possible by the enhanced spectral resolution of the new generation GEO satellites, a combination of an IR technique appropriate for convective precipitation processes in the mid-latitudes with information about cloud properties should enable a separation of the into subareas of different precipitation processes and rainfall intensities. Concerning the advective-stratiform precipitation area it is expected that the information about the CWP and the CP in the upper parts that allows a proper delineation of the rain area, further enables a subdivision into areas of differing rainfall intensities.

A proper process and intensity differentiation is of valuable benefit for now-casting purposes. As pointed out by BENNARTZ (2007), beside the identification of precipitating areas, the assignment of instantaneous precipitation rates at the ground is typically associated with large uncertainties. As a consequence recent studies in support of now-casting attempt to separate different rainfall intensity classes instead of rain rates (WENG et al. 2003). In this context, a proper classification into areas of different rainfall intensities offers the potential for an improved rainfall rate assignment in a next step. The application of distinct regression functions to each subarea can improve the representativeness of the retrieved regression function.

In this context, the enhanced spectral resolution provided by MSG SEVIRI enables the application of existing IR retrieval techniques on the one hand, but also the retrieval of cloud properties (i.e. CWP and CP) on the other hand. Moreover, its high spatial (3 by 3 km at sub satellite point) and temporal (15 minutes) resolution permit a quasi-continuous observation of the rainfall distribution.

The objective of the present study is therefore to investigate the potential of MSG SEVIRI concerning precipitation process separation and the division into subareas of differing rainfall intensities. For this purpose an existing IR retrieval technique appropriate to the detection and classification of convective precipitation processes in the mid-latitudes is adapted to MSG SEVIRI. Regarding the advective-stratiform rainfall area the information content about the CWP and the CP is investigated in terms of a rainfall intensity differentiation.

The structure of the paper is a follows. In section 6.2 the data and methods used in the presented study are introduced. The theoretical background and the conceptual design of the newly proposed retrieval scheme are presented in section 6.3. In section 6.4, the proposed technique for process separation and intensity differentiation is introduced. The appraisal of the new developed scheme follows in section 6.5. Finally, section 6.6 gives a short summary and some conclusions.

6.2 Data and methods

For this study, MSG SEVIRI data together with corresponding ground-based radar data are required. The SEVIRI data has been received at the Marburg Satellite Station (MSS) (Reudenbach et al. 2004; Bendix et al. 2003). The raw data has been processed by the FMet tool (Cermak et al. 2007). The radar data are provided by the ground-based C band radar network of the German Weather Service (DWD 2005; Seltmann 1997). The scan interval for both data sets is 15 minutes. For the spatial comparison the radar data with an original spatial resolution of 4 by 4 km were projected to the viewing geometry of SEVIRI with a spatial resolution of 3 by 3 km.

The data are divided into a training and a validation data set. The training data set is used for the development of the technique and consists of 1559 scenes of precipitation events from January to August 2004. The validation data set is considered for the appraisal of the proposed technique and consists of 1396 scenes of precipitation events from January to August 2004. The precipitation events in both data sets are independent from each other. Because of the differing information content about the CWP between day-time and night-time

scenes (refer to section 6.3.3) both data sets are divided into day- and night-time scenes. The training data set consists of 850 day-time and 709 night-time scenes. The validation data set comprises 720 day-time and 676 night-time scenes.

For the development and the appraisal of the proposed retrieval technique standard verification scores for dichotomous data sets are applied. The selection of the appropriate scores follows the suggestions of the International Precipitation Working Group (IPWG; TURK & BAUER 2006) and are shortly introduced in the following paragraphs. The respective subarea mentioned in the description represents each of the five rainfall intensity areas classified by the new developed technique (see section 6.3 and 6.4).

The bias describes the ratio between the number of pixels, that have been detected in the satellite (S) and radar (R) techniques as the respective subarea (S_Y, R_Y). The probability of detection (POD) describes the ratio between pixels with S_YR_Y and R_Y, and gives the fraction of pixels, that have been correctly identified by the satellite technique, according to the radar product. The probability of false detection (POFD) describes the ratio between S_YR_N and R_N and indicates the fraction of the pixels incorrectly identified by the satellite algorithm. The False Alarm Ratio (FAR) gives the ratio between S_YR_N and S_Y. The Critical Success Index (CSI), which encloses all pixels, that have been detected as the respective subarea by either the radar network or the satellite technique, describes the ratio between S_YR_Y and the sum of S_YR_Y, S_NR_Y, S_YR_N. All scores range from 0 to 1. The optimum value for the CSI is 1, while it is 0 for the FAR. Since the POD can be increased by just increasing the respective subarea (i.e. by reducing the minimum confidence threshold), it has to be analyzed in connection with corresponding values of the FAR and the POFD since both measure the fraction of the satellite pixels, that have been incorrectly identified as the respective subarea. The Equitable Threat Score (ETS) is based on the number of pixels, that have been identified in the satellite (S) and radar (R) technique as the respective subarea (S_Y, R_Y) or other subareas (S_N, R_N). It indicates how well the classified pixels of the respective subarea correspond to the pixels of the respective subarea observed by the radar, also accounting for pixels correctly classified by chance ($S_YR_{YRandom}$). Its values range from -1/3 to 1 with the optimum value 1. The Heidke Skill Score (HSS) also considers the probability of correctly classified pixels by chance. In contrast to the ETS the pixels correctly classified as not belonging to the respective subarea are also incorporated for the calculation of the HSS. It ranges from negative infinite to 1. The optimum value is 1. The Hansen

Kuipers discriminant (HKD) is a measure how well the satellite based technique can distinguish between pixels of the respective subarea and pixels of differing subareas. It ranges from -1 to 1 with an optimum value of 1. For a detailed discussion of the verification scores see STANSKI (1989) or the web site of the WWRP/WGNE.

6.3 Theoretical background and conceptual design

As stated above, a combination of an IR technique appropriate to convective precipitation processes in the mid-latitudes with information about cloud properties should enable a precipitation process and rainfall intensity differentiation of the rain area. The following sections present the theoretical background (section 6.3.1) together with the conceptual design (section 6.3.2) and the theoretical approach (section 6.3.3) of the proposed retrieval technique.

6.3.1 Theoretical background

Based on the results of the CYCLES (CYCLonic Extratropical Storms) project, HOUZE (1993) summarized the conceptual model of rainbands dominated by different rainfall processes and leading to differing rainfall intensities within extra-tropical cyclones. According to this conceptual model, the rainfall area is separated into the following subareas of different precipitation processes and rainfall intensities:

- Precipitation from convective cores in connection with narrow cold-frontal rainbands (very high precipitation intensities from Cb).
- Convective-stratiform precipitation from Ns in connection with convective cores (Cb) within narrow cold-frontal rainbands (moderate to high precipitation intensities).
- Enhanced advective-stratiform precipitation from Ns with ice particles from embedded shallow generating cells, that fall from above ("seeder-feeder" effect) in connection with wide cold-frontal rainbands and warm-frontal rainbands (moderate precipitation intensities).
- Precipitation from clouds of intermediary character between convectively dominated and advective-stratiform background precipitation areas (light to moderate precipitation intensities).
- Advective-stratiform background precipitation (light precipitation intensities).

Following the conceptual model of rainbands in connection with extra-tropical cyclones it can be stated that narrow cold-frontal, wide

cold-frontal and warm-frontal rainbands are dominated by convective precipitation processes. On the other hand the advective-stratiform background and the intermediary precipitation area are of advective-stratiform character. The advective-stratiform background precipitation area, which spatially dominates the frontal system, is the result of widespread rising processes (cf. HOUZE 1993). The intensification of the advective-stratiform background rainfall intensities in the envelope of the frontal precipitation systems is caused by a locally confined strengthening of the buoyancy in the upper cloud levels (cf. HOUZE 1993). The associated "seeder-feeder" effect leads to slightly intensified rainfall rates. These precipitation areas are of intermediary character between convectively dominated and advective-stratiform background precipitation areas.

Table 6.1: Overview of the subareas of differing precipitation processes and rainfall intensities according to the conceptual model of rainbands introduced by HOUZE (1993).

conceptual model	Radar	Radar reflectivity [dBZ]	Rainfall rate [mm/h]
precipitation from convective cores in connection with narrow cold-frontal rainbands	very high rainfall intensities with thunderstorms	> 46.0	> 35.0
convective stratiform precipitation in connection with convective cores within narrow cold-frontal rainbands	moderate to high rainfall intensities possibly with thunderstorms	37.0 to 45.9	8.1 to 34.9
enhanced advective-stratiform precipitation produced by embedded generating cells in connection with wide cold-frontal rainbands and warm-frontal rainbands	moderate rainfall intensities	28.0 to 36.9	1.9 to 8.0
intermediary precipitation from clouds of intermediary character between convectively and advectively dominated precipitation areas	light to moderate rainfall intensities	19.0 to 27.9	0.4 to 1.8
advective-stratiform background precipitation from clouds within the frontal rainband	light rainfall intensities	7.0 to 18.9	0.06 to 0.4

The above mentioned five subareas of differing precipitation processes and rainfall intensities can also be identified in the radar product of the German Weather Service (DWD 2005). Table 6.1 gives an overview of the five subareas of differing precipitation processes and intensities according to the conceptual model of rainbands

introduced above together with the corresponding radar reflectivity and the characteristic rainfall intensity.

6.3.2 Conceptual design

According to the precipitation processes in connection with extra-tropical cyclones, convectively dominated precipitation areas are characterized by a large vertical extension and a cloud top rising high into the atmosphere. As a result, the established relationship between CTT and rainfall probability and intensity can be applied for the detection and classification of these precipitation areas. However, it becomes also visible that the advective-stratiform precipitation areas, that form a major part of the precipitating cloud areas in connection with extra-tropical cyclones are not necessarily connected to cold CTT. As a consequence, a CTT threshold does not seem to be effective for the detection and classification of these areas. For this reason, several authors used a_{ef} and τ derived from multispectral data of new generation satellite systems for an improved detection of this precipitation areas (e.g. NAUSS & KOKHANOVSKY 2007, 2006; LENSKY & ROSENFELD 2003a,b). The basic assumption of these techniques is that precipitating clouds are characterized by a combination of large droplets (presented by a_{ef}), that can fall against the updraft winds within the cloud and a large vertical cloud extension (presented by τ), that favours the growth of precipitation droplets and prevents them from evaporation below the cloud bottom (see also LENSKY & ROSENFELD 2003b). Based on the improved rain area delineation attained by these techniques, THIES et al. (2008a,b) introduced a new technique for the detection of precipitating cloud areas, which relies on information about the CWP and the CP in the upper parts. The CWP, which is calculated by multiplying a_{ef} and τ following equation (6.1), represents the column amount of water in the cloud and is used to characterize precipitation clouds.

$$CWP = \frac{2}{3} \cdot \tau \cdot a_{ef} \tag{6.1}$$

Furthermore, the CP in the upper cloud regions is considered, because effective rain formation processes in connection with extra-tropical cyclones are mainly coupled to ice particles in the upper parts of the clouds and the "seeder-feeder" effect (HOUZE 1993). As a consequence, precipitating cloud areas are characterized by a sufficiently large CWP and the existence of ice particles in the upper cloud parts. Concerning the advective-stratiform precipitation areas it is therefore assumed that areas with a higher CWP and a higher amount of ice particles in the upper cloud regions are characterized by

higher rainfall intensities. Concerning the convective precipitation areas, it is assumed that convective rain clouds with higher rainfall intensities are characterized by a larger vertical extension and a cloud top reaching higher into the atmosphere. Therefore, it is expected that information about the CWP, the CP in the upper cloud parts and the cloud top height (CTH) enable the separation of the rainfall area into subareas of different precipitation processes and rainfall intensities.

6.3.3 Theoretical approach

For the detection of the convective precipitation areas the Advective Convective Technique (ACT; REUDENBACH et al. 2007) has been chosen. It was especially developed for convective precipitation processes in the mid-latitudes and allows a proper detection of convective precipitation areas. Additionally, it enables the differentiation of the convective rain area into the following subsections (see also section 6.3.1):

- convective cores areas
- regions of convective-stratiform precipitation
- regions of enhanced advective-stratiform precipitation.

The technique represents an extension of the Enhanced Convective Stratiform Technique (ECST; REUDENBACH et al. 2001; REUDENBACH 2003) an improved version of the well-known Convective Stratiform Technique (CST; ADLER & NEGRI 1988). The ACT additionally considers the brightness temperature difference between a water vapour and an infrared channel for a more reliable identification of deep convective clouds and the associated convective-stratiform precipitating cloud areas (see also TJEMKES et al. 1997; SCHMETZ et al. 1997). The use of the WV-IR-brightness temperature differences ($\Delta T_{WV\text{-}IR}$) for the detection of high rain clouds is described in detail by REUDENBACH et al. (2001, 2007) and REUDENBACH (2003). Generally, positive $\Delta T_{WV\text{-}IR}$ indicate high rain clouds. This phenomenon is caused by the presence of water vapour in the lower stratosphere above the cloud (FRITZ & LASZLO 1993), which is transported there by deep convection with overshooting tops (e.g. PAGE 1982; KLEY et al. 1982). When the cloud top approaches the tropopause, it blocks lower tropospheric radiation from escaping into space and hence, the received signal at the satellite level originates from the cloud top and the atmosphere aloft. As the temperature in the stratosphere increases with height, the water vapour above the cloud absorbs outgoing radiation from the cloud top and emits radiation at higher temperatures. Because of the stronger water vapour absorption lines in the WV channel compared to the IR channel this results in higher

brightness temperatures in the WV channel (SCHMETZ et al. 1997; TJEMKES et al. 1997).

As the ACT as well as the ECST have been developed for Meteosat First Generation (MFG) Meteosat Visible and Infra-Red Imager radiometer (MVIRI), THIES et al. (2007, 2008c) transferred the techniques to MSG SEVIRI. Because of the higher spectral resolution of MSG SEVIRI, they investigated the four possible WV-IR combinations in detail by means of radiative transfer calculations. Distinct differences in $\Delta T_{WV\text{-}IR}$ for a convective cloud whose top rises consistently into higher atmospheric levels were calculated between $\Delta T_{WV6.2\text{-}IR10.8}$ and $\Delta T_{WV7.3\text{-}IR12.1}$. The different $\Delta T_{WV\text{-}IR}$ values can be explained by the channels spectral range, their spectral response function and the resulting influence of water vapour absorption lines on the cloud signal detected by the satellite sensor (THIES et al. 2007, 2008c). As a result, the four WV-IR combinations show different sensitivities to the CTH at different levels, which provide useful information for the detection and classification of convectively dominated precipitation areas.

The CWP necessary for rainfall intensity differentiation within the advective-stratiform precipitation areas can be retrieved on a pixel basis during day-time using a combination of two solar channels (e.g., NAKAJIMA & NAKAJIMA 1995; KAWAMOTO et al. 2001; KOKHANOVSKY et al., 2003, 2005; PLATNICK et al. 2003). This is due to the fact that the reflection of solar light by a cloud in a non-absorbing wavelength (i.e., a visible channel between 0.4 and 0.8 μm) is strongly correlated to τ while the reflection of solar light in a slightly absorbing wavelength (i.e., a near-infrared channel between 1.6 and 3.9 μm) is mainly a function of a_{ef}.

Since the cloud microphysical and optical properties are strongly related to the reflection of solar light but not to the emission of the cloud, there is no operational retrieval for MSG SEVIRI at hand, that can explicitly compute a_{ef} and τ during night-time. Anyhow, several case studies have shown that implicit information about a_{ef} and τ is available in the emissive channels during night-time (e.g. HUANG et al. 2004; LENSKY & ROSENFELD 2003a,b; GONZALEZ et al. 2002; ACKERMAN et al. 1998; BAUM et al. 1994; OU et al. 1993). Based on the findings of these case studies, THIES et al. (2008a) used radiative transfer calculations to demonstrate that implicit information about the CWP is available from the four channel differences $\Delta T_{3.9\text{-}7.3}$, $\Delta T_{3.9\text{-}10.8}$, $\Delta T_{8.7\text{-}10.8}$, $\Delta T_{10.8\text{-}12.1}$, that can be used to separate raining from non-raining cloud areas.

Information about the CP can be gained by considering the brightness temperature difference between the 8.7 μm channel

(8.3-9.1 µm) and the 10.8 µm channel (9.8-10.8 µm) ($\Delta T_{8.7\text{-}10.8}$) together with the brightness temperature difference between the 10.8 µm channel and the 12.1 µm channel (11-13 µm) ($\Delta T_{10.8\text{-}12.1}$) (refer to STRABALA et al. 1994).

6.4 Process separation and rainfall intensity differentiation with MSG SEVIRI

Based on the theoretical background presented in section 6.3 together with the conceptual design and the theoretical approach, the following section describes the implementation of the precipitation process separation and rainfall intensity differentiation technique for MSG SEVIRI. Since the focus of the present study lies on the differentiation of an already identified precipitation area and not on the initial discrimination between raining and non-raining clouds itself, the rain area detected from the radar network of the German Weather Service is taken for this investigation.

For the differentiation of the rainfall area a stepwise classification algorithm similar to the "cascade method" proposed by CAPACCI et al. (2008) is applied (see figure 6.1). After the separation of the convective and advective-stratiform precipitation processes (section 6.4.1) both subareas are divided into regions of differing rainfall intensities (section 6.4.2). First, the convective cores together with the convective-stratiform areas are separated from the cloud fields of enhanced advective-stratiform precipitation. Then the convective cores are distinguished from the convective-stratiform precipitating cloud areas (section 6.4.2.1). Finally, the intermediary precipitation fields are separated from the advective-stratiform background precipitation area (section 6.4.2.2).

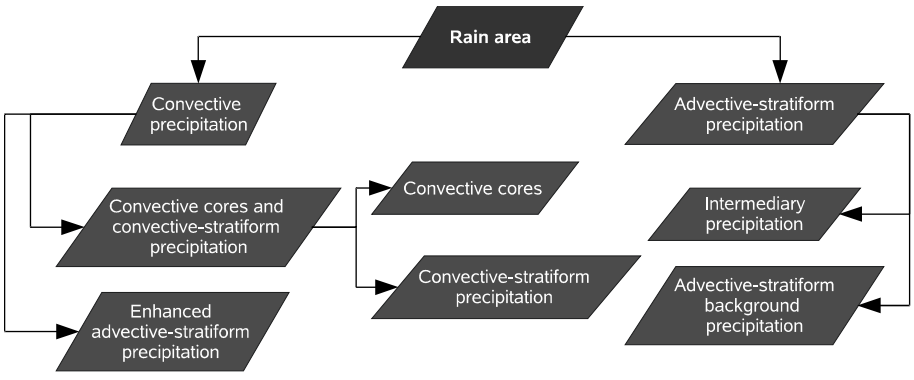

Figure 6.1: Overview of the stepwise classification scheme for precipitation process and rainfall intensity differentiation.

6.4.1 Precipitation process separation

First, the rainfall area is divided into convective and advective-stratiform precipitation areas. The technique follows the suggestion of HOUZE (1997) and STEINER et al. (1995) to detect the convective rain area and denote the remaining subarea as stratiform plus intermediary.

As introduced in section 6.3.3, the detection of convective precipitation areas by the ACT is based on the brightness temperature difference between a WV and an IR channel. However, based on the results of THIES et al. (2007, 2008c; see section 6.3.3), a modified technique is proposed here. To incorporate the different sensitivities of the WV-IR channel combinations of SEVIRI into the detection scheme, the two channel differences $\Delta T_{WV6.2\text{-}IR10.8}$ and $\Delta T_{WV7.3\text{-}IR12.1}$ have been chosen (see section 6.3.3). To gain information about the CTT in the the $IR_{10.8}$ channel ($BT_{10.8}$) is also included. This was done to consider the maximum possible information content concerning the rising top of a convective cloud within the troposphere and the interaction of the emitted radiation with the water vapour above cloud top level.

To use the information about CTH from the two WV-IR channel differences and $BT_{10.8}$ for the process separation, the confidences of the convectively dominated rainfall areas are computed as a function of the combined values of the three parameters $\Delta T_{WV6.2\text{-}IR10.8}$, $\Delta T_{WV7.3\text{-}IR12.1}$, and $BT_{10.8}$. The use of confidences has been successfully applied for rain area delineation (e.g. CHENG et al. 1993; KURINO 1997; NAUSS & KOKHANOVSKY 2007; THIES et al. 2008a,b) and is employed here to separate the different precipitating cloud areas. Figure 6.2 gives an overview of the introduced scheme for the separation of the two precipitation processes, that is described in the following.

The computation of the pixel based confidences of the convective rain areas is done by a comparison of $\Delta T_{WV6.2\text{-}IR10.8}$, $\Delta T_{WV7.3\text{-}IR12.1}$, and $BT_{10.8}$ with the ground-based radar for the training data set (altogether 1559 scenes, see section 6.2). For the calculation of the confidences of the convective precipitation areas the radar classes between 7.0 and 27.9 dBZ are considered as advective-stratiform and the radar classes with a reflectivity higher than 28.0 dBZ are considered as convectively dominated (see Table 6.1).

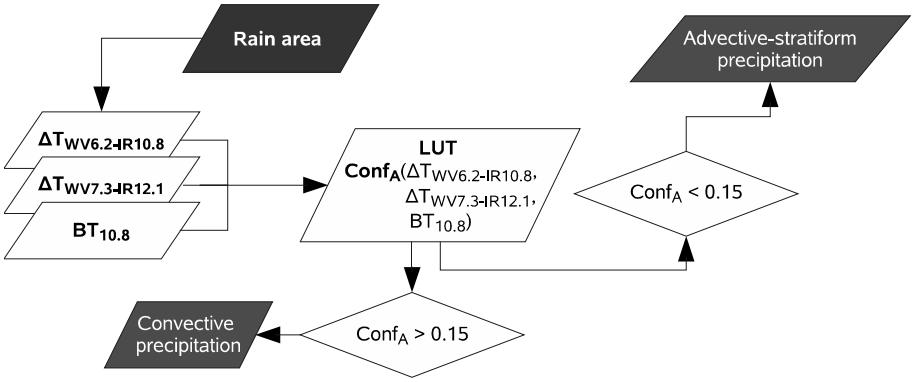

Figure 6.2: Overview of the introduced scheme for precipitation process separation as part of the stepwise classification.

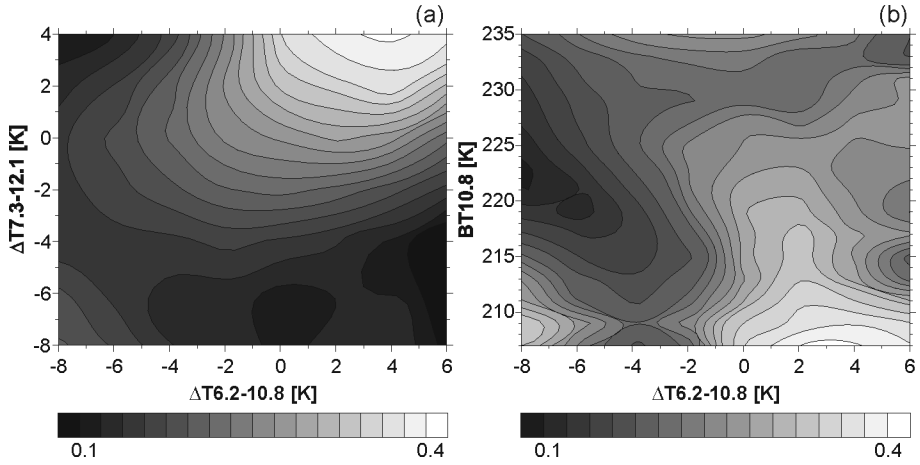

Figure 6.3: Calculated confidences of the convective precipitation areas in contrast to the advective-stratiform precipitation areas as a function of two variables; $\Delta T_{WV6.2\text{-}IR10.8}$ versus $\Delta T_{WV7.3\text{-}IR12.1}$ (a), $\Delta T_{WV6.2\text{-}IR10.8}$ versus $BT_{10.8}$ (b).

Figure 6.3 shows the confidences of the convective precipitation areas as a function of the two WV-IR differences as well as of $BT_{10.8}$ calculated with equation (6.2).

$$Confidence_A(x_1, x_2) = \frac{N_A(x_1, x_2)}{N_A(x_1, x_2) + N_B(x_1, x_2)} \qquad (6.2)$$

where $Confidence_A$ denotes the confidences of the convectively dominated precipitation area. N_A and N_B are the frequencies of the convectively dominated pixels and the advective-stratiform pixels, respectively. x_1 and x_2 denote the respective channel differences ($\Delta T_{WV6.2\text{-}IR10.8}$, $\Delta T_{WV7.3\text{-}IR12.1}$) and $BT_{10.8}$ combined for the calculation of the confidences.

As can be seen in figure 6.3 a high $\Delta T_{WV6.2\text{-}IR10.8}$ values together with high $\Delta T_{WV7.3\text{-}IR12.1}$ values reveal high convective rainfall confidences. The same holds true for low $BT_{10.8}$ together with high $\Delta T_{WV6.2\text{-}IR10.8}$ values (figure 6.3 b). This corroborates the findings of THIES et al. (2007, 2008c) that $\Delta T_{WV6.2\text{-}IR10.8}$ and $\Delta T_{WV7.3\text{-}IR12.1}$ increase with increasing CTH. At the same time, the higher the cloud reaches into the atmosphere the lower becomes $BT_{10.8}$. Thus, to make use of the combined information content about CTH available from the two WV-IR channel differences and $BT_{10.8}$ for the separation of convective precipitation fields, the confidences of convective rain areas are computed as a function of the combined values of the three parameters as shown in equation (6.3):

$$Confidence_A(x_1, x_2, x_3) = \frac{N_A(x_1, x_2, x_3)}{N_A(x_1, x_2, x_3) + N_B(x_1, x_2, x_3)} \qquad (6.3)$$

where $Confidence_A$ denotes the confidences of the convective precipitation areas. N_A and N_B are the frequencies of the convectively dominated pixels and the advective-stratiform pixels, respectively, and x_1, x_2 and x_3 denote the three variables $\Delta T_{WV6.2\text{-}IR10.8}$, $\Delta T_{WV7.3\text{-}IR12.1}$, and $BT_{10.8}$ combined for the calculation of the confidences of the convective precipitation areas. The confidence threshold appropriate for the separation of the convective precipitation fields is determined by optimizing the ETS (see section 6.2). Different confidence threshold values between 0.1 and 0.7 were used to separate the satellite-based convective rain area. The ETS for the separated convective fields based on the different confidence levels were calculated in comparison with ground-based radar data. The detected convective rain area using a confidence threshold of 0.15 yields the maximum ETS of 0.0868, which is chosen as the minimum threshold. Pixels with value combinations possessing a confidence higher than the minimum threshold are classified as convectively dominated. The remaining area is referred to as advective-stratiform precipitating cloud area.

6.4.2 Intensity differentiation

After the separation of the rain area into convective and advective-stratiform precipitation areas, the division into subareas of different rainfall intensities is described in the following.

6.4.2.1 Subdivision of the convective precipitation areas

As for the detection of the convective precipitation area the classification into the three subareas of different rainfall intensities (precipitation from convective cores, convective-stratiform

precipitation, enhanced advective-stratiform precipitation; see section 6.3.1) is accordingly done by means of confidences of the respective subarea and an appropriate minimum threshold. Figure 6.4 gives an overview of the introduced scheme for the division of the convective rain areas into subareas of differing rainfall intensities.

The differentiation of the convective precipitation area into subareas of differing rainfall intensities also relies on the WV and IR channels available during day-time and night-time. For that reason, the computation of the pixel based confidences by comparing the two WV-IR channel differences and $BT_{10.8}$ with ground-based radar data is applied for the whole training data set consisting of 1559 precipitation scenes from January to August 2004 (see section 6.2).

The classification is based on the conceptual model that convective rain clouds with higher rainfall intensities are characterized by a larger vertical extension and a cloud top reaching higher into the atmosphere (see section 6.3.2). First the convective cores together with the convective-stratiform precipitation areas are separated from the areas of enhanced advective-stratiform precipitation. The calculation of the confidences of convective cores together with the convective-stratiform precipitation areas in contrast to the areas of enhanced advective-stratiform precipitation is done in a comparison with the ground-based radar data, where radar classes with reflectivities greater than 37.0 dBZ are contrasted to the radar classes with reflectivities between 28.0 to 36.9 dBZ (refer to table 6.1).

Figure 6.5 shows the calculated confidences of convective cores together with convective-stratiform precipitation areas in contrast to the enhanced advective-stratiform precipitation cloud fields as a function of the two WV-IR differences and $BT_{10.8}$, respectively, calculated in analogy with equation (6.2). As can be seen the combinations of high $\Delta T_{WV6.2\text{-}IR10.8}$ and high $\Delta T_{WV7.3\text{-}IR12.1}$ values possess high confidence levels (figure 6.5 a). The same holds true for low $BT_{10.8}$ together with high $\Delta T_{WV6.2\text{-}IR10.8}$ (figure 6.5 b). This is in accordance with the assumption introduced above that higher values of $\Delta T_{WV6.2\text{-}IR10.8}$ and $\Delta T_{WV7.3\text{-}IR12.1}$ as well as low values of $BT_{10.8}$ signify higher rainfall intensities.

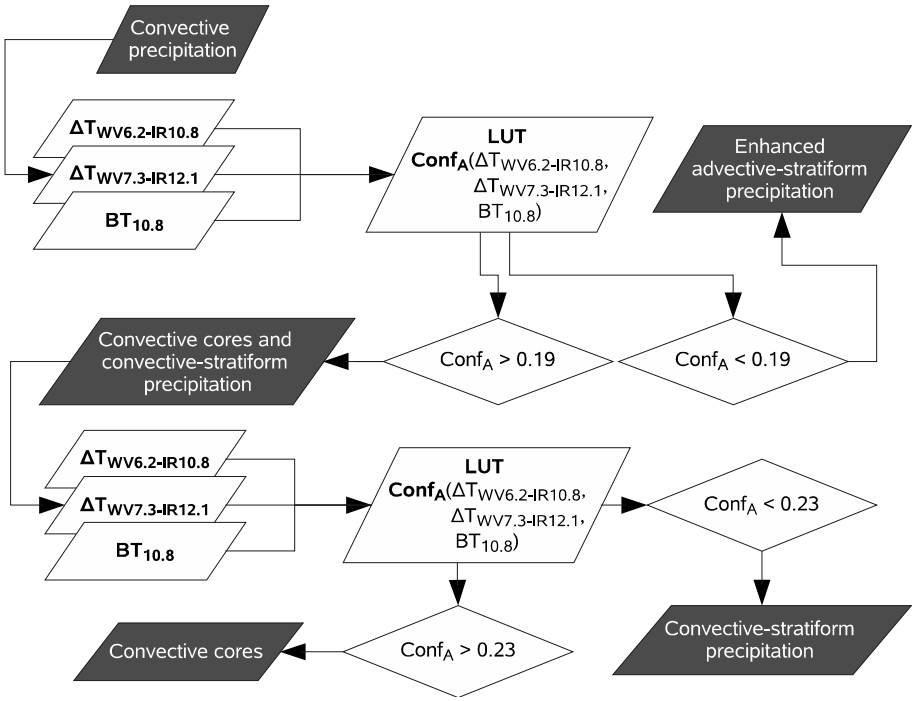

Figure 6.4: Overview of the rainfall intensity differentiation within the convective precipitation areas as part of the stepwise classification.

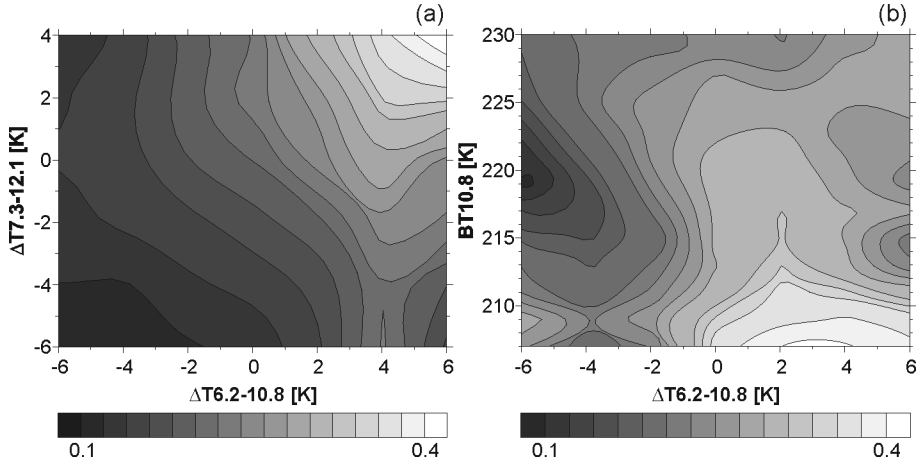

Figure 6.5: Calculated confidences of the convective cores together with convective-stratiform precipitation areas in contrast to the enhanced advective-stratiform precipitation cloud fields as a function of two variables; $\Delta T_{WV6.2-IR10.8}$ versus $\Delta T_{WV7.3-IR12.1}$ (a), $\Delta T_{WV6.2-IR10.8}$ versus $BT_{10.8}$ (b).

To make use of the combined information content available from $\Delta T_{WV6.2\text{-}IR10.8}$, $\Delta T_{WV7.3\text{-}IR12.1}$, and $BT_{10.8}$ the confidences of convective cores together with convective-stratiform precipitation areas are computed in contrast to the enhanced advective-stratiform precipitation areas as a function of the combined values of the three parameters analogously to equation (6.3).

The determination of the appropriate confidence threshold to separate the areas of convective cores and convective-stratiform precipitation from the enhanced advective-stratiform precipitation areas is done by maximizing the ETS (refer to section 6.4.1). The confidence threshold of 0.19 yields to the maximum ETS of 0.1004 and is used as the minimum threshold. Pixels with value combinations possessing a confidence higher than the minimum threshold are classified as convective cores and convective-stratiform precipitating cloud fields. The remaining convective rain areas are classified as enhanced advective-stratiform precipitation.

In the next step the convective cores are separated from the convective-stratiform precipitation areas. For this purpose the confidences of convective cores (radar reflectivity greater than 46.0 dBZ) are calculated in contrast to the convective-stratiform precipitation areas (radar reflectivities between 37.0 and 45.9 dBZ) following equation (6.2) analogously to the procedure presented above. Figure 6.6 shows the calculated confidences of the convective cores in contrast to the convective-stratiform precipitation areas as a function of the two WV-IR differences and $BT_{10.8}$ respectively. In accordance to the assumption introduced above, the combination of high $\Delta T_{WV6.2\text{-}IR10.8}$ and high $\Delta T_{WV7.3\text{-}IR12.1}$ values possess high confidence levels (figure 6.6 a). The same holds true for low $BT_{10.8}$ values together with high $\Delta T_{WV6.2\text{-}IR10.8}$ values (figure 6.6 b).

To make use of the combined information content available from the two WV-IR channel differences and $BT_{10.8}$, the confidences of convective cores are computed as a function of the combined values of the three parameters as shown in equation (6.3).

The determination of the appropriate confidence threshold to separate the convective cores from the convective-stratiform precipitation areas is done by maximizing the ETS again (refer to section 6.4.1). The confidence threshold of 0.23 yields to the maximum ETS of 0.1958 and is used as a minimum threshold. Pixels with value combinations possessing a confidence higher than the minimum threshold are classified as convective cores. The remaining rain areas are classified as convective-stratiform precipitating cloud fields.

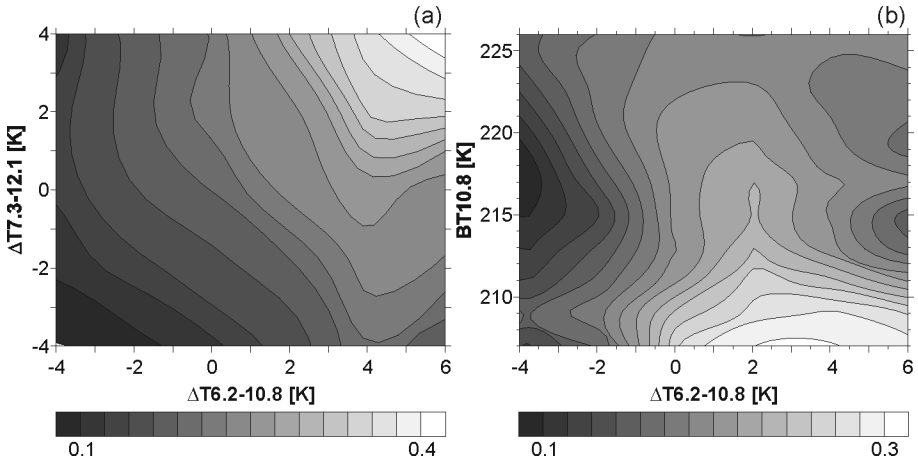

Figure 6.6: Calculated confidences of convective cores in contrast to the convective-stratiform precipitation area as a function of two variables; $\Delta T_{WV6.2\text{-}IR10.8}$ versus $\Delta T_{WV7.3\text{-}IR12.1}$ (a), $\Delta T_{WV6.2\text{-}IR10.8}$ versus $BT_{10.8}$ (b).

6.4.2.2 Subdivision of the advective-stratiform precipitation areas

After the differentiation of the convective precipitation areas the further division of the advective-stratiform precipitation areas is described in the following. Because of the differing information content about the CWP and the different retrieval approaches between day-time and night-time (refer to section 6.3.3) the subdivision of the advective-stratiform precipitation areas is separated into a day-time and a night-time algorithm. Figure 6.7 gives an overview of the proposed scheme for the division of the advective-stratiform precipitation areas into the subareas of intermediary and advective-stratiform background precipitation during day-time and night-time.

(a) day-time algorithm

The CWP (i.e., values of a_{ef} and τ) considered for a rainfall intensity differentiation can be retrieved on a pixel basis during day-time using a combination of two solar channels (i.e., a VIS and a NIR channel; see section 6.3.2). However, because no operational retrieval technique is currently available for MSG SEVIRI, that is applicable to water and ice clouds, and that is fast enough concerning the 15 minute scan cycle, the authors decided to use the original reflectance of the 0.56 - 0.71 µm ($VIS_{0.6}$) and 1.5 - 1.78 µm ($NIR_{1.6}$) SEVIRI channels, instead of computed values of a_{ef} and τ.

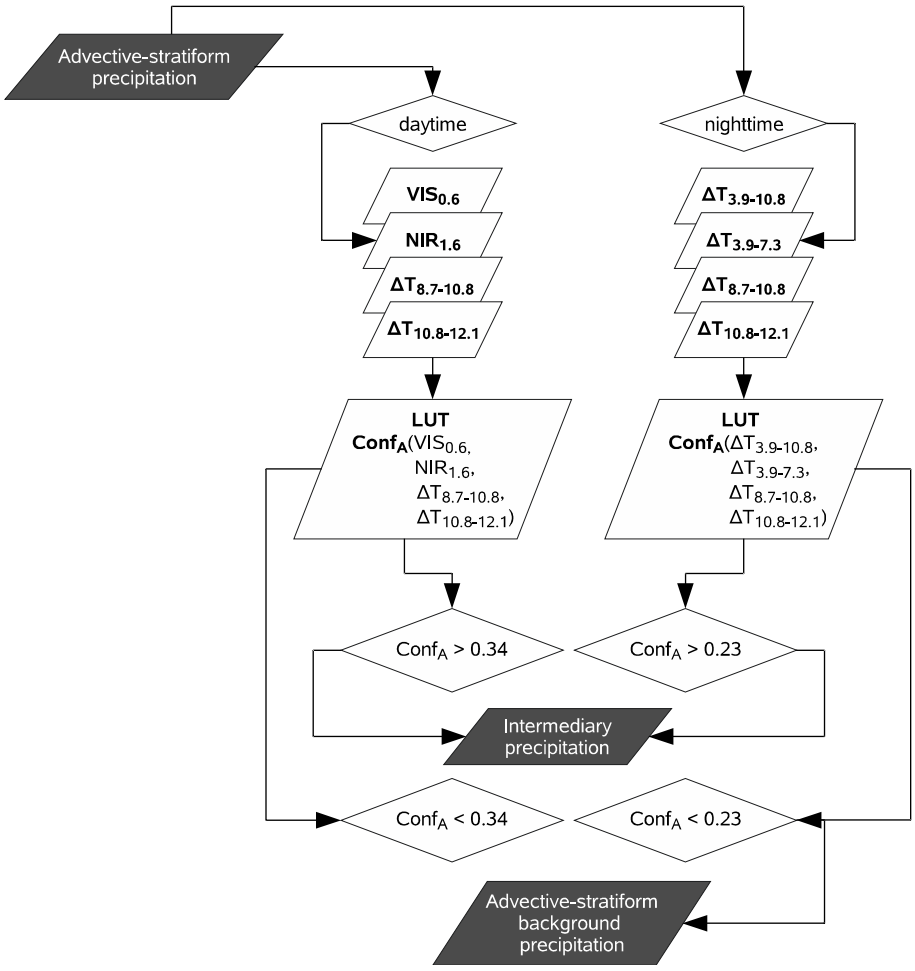

Figure 6.7: Overview of the rainfall intensity differentiation within the advective-stratiform precipitation areas as part of the stepwise classification.

To use the information about the CWP and the CP for a division of the advective-stratiform precipitation area the confidences of the intermediary precipitating cloud fields (radar reflectivity between 19.0 and 27.9 dBZ) are calculated in contrast to the advective-stratiform background precipitation areas (radar reflectivity between 7.0 and 18.9 dBZ) as a function of the value combinations of the four variables $VIS_{0.6}$, $NIR_{1.6}$, $\Delta T_{8.7\text{-}10.8}$, and $\Delta T_{10.8\text{-}12.1}$. The computation of the pixel based confidences is done by a comparison of the four value combinations with ground-based radar data for day-time precipitation events (altogether 850 scenes, see section 6.2).

Figure 6.8 shows the calculated confidences of the intermediary rain areas as a function of $VIS_{0.6}$ and $NIR_{1.6}$ (a), as well as a function of $\Delta T_{8.7\text{-}10.8}$ and $\Delta T_{10.8\text{-}12.1}$ (b) computed analogously to equation

(6.2). As can be seen in figure 6.8 a high confidences coincide with high values of $VIS_{0.6}$ and low values of $NIR_{1.6}$, indicating a higher CWP. High values of $VIS_{0.6}$ are characteristic for higher τ and lower values of $NIR_{1.6}$ are the result of larger a_{ef} as the absorption increases with increasing particle size. Figure 6.8b shows that ice clouds, where $\Delta T_{8.7\text{-}10.8}$ values are greater than coincident $\Delta T_{10.8\text{-}12.1}$ values, are characterized by high confidence levels. On the other hand, for water clouds $\Delta T_{10.8\text{-}12.1}$ values are greater than $\Delta T_{8.7\text{-}10.8}$ values (cf. STRABALA et al. 1994). These areas are characterized by lower confidence levels.

To summarize, value combinations representative for large CWP and ice particles in the upper cloud parts are characterized by higher confidence levels for the intermediary rain area. This corroborates the assumption, formulated above, that raining cloud areas characterized by a higher CWP and the existence of more ice particles in the upper regions produce higher rainfall intensities.

To make use of the combined information about the CWP and the CP provided by the parameters $VIS_{0.6}$, $NIR_{1.6}$, $\Delta T_{8.7\text{-}10.8}$, $\Delta T_{10.8\text{-}12.1}$, the confidences of the intermediary precipitation areas are computed as a function of the combined values of the four variables as shown in equation (6.4) using the above mentioned 850 scenes.

$$Confidence_A(x_1, x_2, x_3, x_4) = \frac{N_A(x_1, x_2, x_3, x_4)}{N_A(x_1, x_2, x_3, x_4) + N_B(x_1, x_2, x_3, x_4)} \quad (6.4)$$

were $Confidence_A$ denotes the confidences of the intermediary rain area. N_A represents the frequencies of intermediary precipitating pixels, while N_B stands for the frequencies of the pixels with advective-stratiform background precipitation. x_1, x_2, x_3 and x_4 denote the four variables $VIS_{0.6}$, $NIR_{1.6}$, $\Delta T_{8.7\text{-}10.8}$, $\Delta T_{10.8\text{-}12.1}$ combined for the calculation of the confidences of the intermediary rain areas.

The threshold of the calculated confidences appropriate for a delineation of the intermediary precipitation fields is determined by optimizing the ETS (refer to section 6.4.1). The confidence threshold of 0.34 yields the to maximum ETS of 0.0971, which is therefore used as minimum threshold. Pixels with value combinations possessing a confidence higher than the minimum threshold are classified as intermediary precipitation. The remaining areas are classified as advective-stratiform background precipitation.

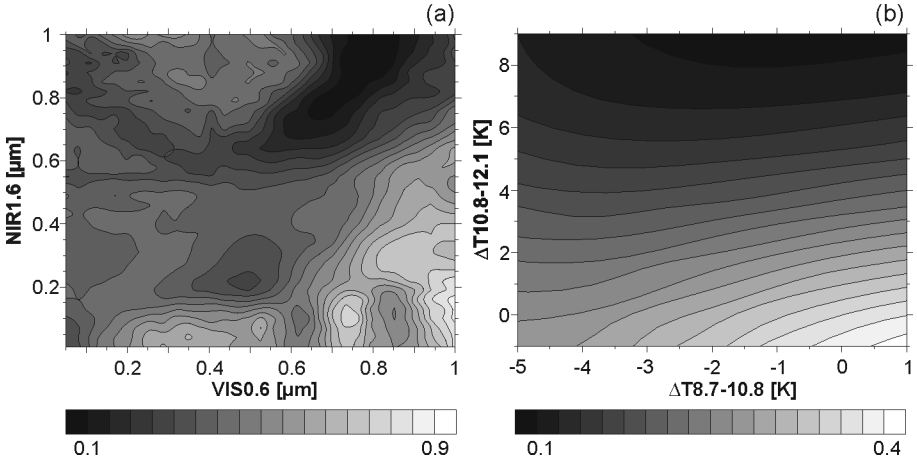

Figure 6.8: Calculated confidences of the intermediary precipitation areas in contrast to the advective-stratiform background precipitation areas as a function of two variables; $VIS_{0.6}$ versus $NIR_{1.6}$ (a), $\Delta T_{8.7\text{-}10.8}$ versus $\Delta T_{10.8\text{-}12.1}$ (b).

(b) night-time algorithm

As mentioned in section 6.3.3 there is no operational retrieval scheme available for MSG SEVIRI, that can explicitly compute a_{ef}, τ and CWP during night-time. However, THIES et al. (2008a) demonstrated that implicit information about the CWP is available from the four channel differences $\Delta T_{3.9\text{-}10.8}$, $\Delta T_{3.9\text{-}7.3}$, $\Delta T_{8.7\text{-}10.8}$, $\Delta T_{10.8\text{-}12.1}$ during night-time and successfully used this information for rain area delineation.

To make use of the implicit information about the CWP and the CP for the division of the advective-stratiform precipitation areas during night-time, the confidences of the intermediary precipitation areas are calculated in contrast to the advective-stratiform background precipitation areas as a function of the four channel differences ($\Delta T_{3.9\text{-}10.8}$, $\Delta T_{3.9\text{-}7.3}$, $\Delta T_{8.7\text{-}10.8}$, $\Delta T_{10.8\text{-}12.1}$) by using equation (6.2). The computation of the pixel based confidence of the intermediary precipitation areas is analogous to the day-time scheme and is done by a comparison of the SEVIRI channel differences with ground-based radar data for night-time precipitation events (altogether 709 scenes, see section 6.2).

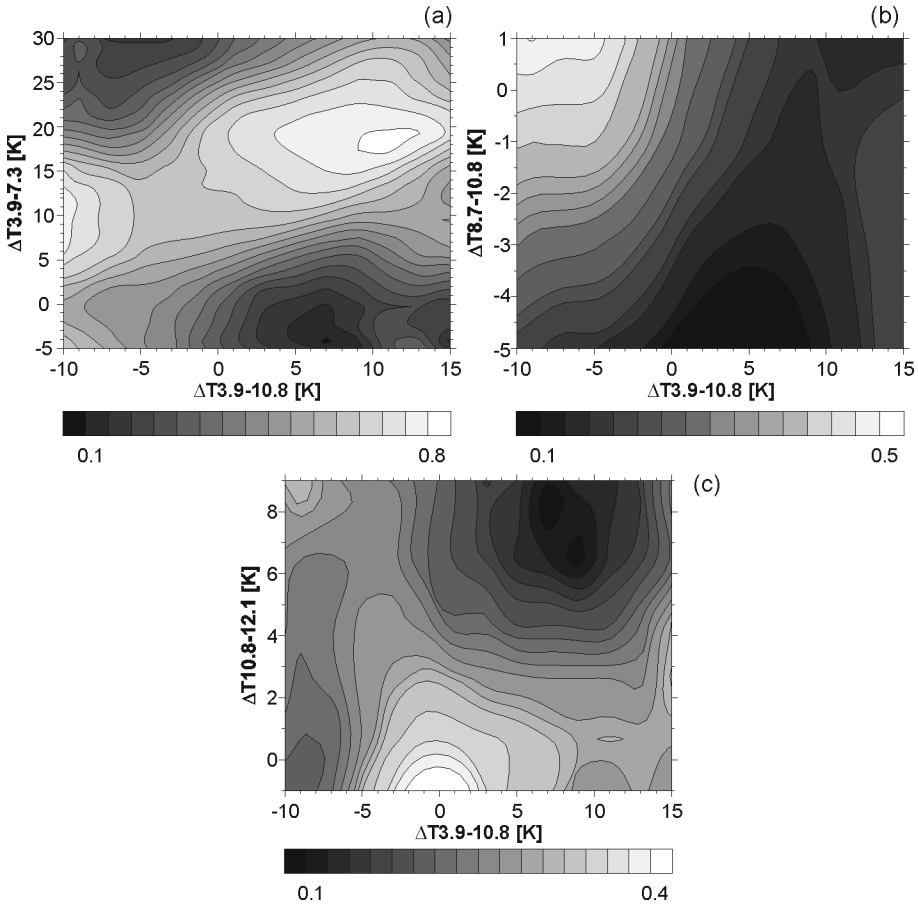

Figure 6.9: Calculated confidences of the intermediary precipitation areas in contrast to the advective-stratiform background precipitation area as a function of two channel differences; $\Delta T_{3.9\text{-}10.8}$ versus $\Delta T_{3.9\text{-}7.3}$ (a), $\Delta T_{3.9\text{-}10.8}$ versus $\Delta T_{8.7\text{-}10.8}$ (b), $\Delta T_{3.9\text{-}10.8}$ versus $\Delta T_{10.8\text{-}12.1}$ (c).

The confidences of the intermediary precipitation areas as a function of two different channel differences calculated with equation (6.2) are depicted in figure 6.9. For the combination of $\Delta T_{3.9\text{-}10.8}$ versus $\Delta T_{3.9\text{-}7.3}$ (figure 6.9 a) higher confidences can be found for medium $\Delta T_{3.9\text{-}10.8}$ and medium $\Delta T_{3.9\text{-}7.3}$ values. These intervals coincide with those for a larger CWP. Lower confidences are characterized by high $\Delta T_{3.9\text{-}10.8}$ and high $\Delta T_{3.9\text{-}7.3}$, which correspond to a lower CWP (refer to THIES et al. 2008a). Regarding the combination of $\Delta T_{3.9\text{-}10.8}$ versus $\Delta T_{8.7\text{-}10.8}$ (figure 6.9 b), higher confidences are indicated for medium $\Delta T_{3.9\text{-}10.8}$ and large $\Delta T_{8.7\text{-}10.8}$ values. These intervals correspond to a larger CWP. Lower confidences can be found for high $\Delta T_{3.9\text{-}10.8}$ and small $\Delta T_{8.7\text{-}10.8}$ values, which coincide with a lower CWP (refer to THIES et al. 2008a). Concerning the combination of $\Delta T_{3.9\text{-}10.8}$ and $\Delta T_{10.8\text{-}12.1}$ (figure 6.9

c) higher confidences are indicated for medium $\Delta T_{3.9\text{-}10.8}$ and small $\Delta T_{10.8\text{-}12.1}$ values, which coincide with a larger CWP. Lower confidences can be found for high $\Delta T_{3.9\text{-}10.8}$ and high $\Delta T_{10.8\text{-}12.1}$ values, which correspond to a lower CWP (refer to THIES et al. 2008a).

To summarize it can be stated that value combinations indicating higher CWP values are characterized by higher confidence levels for the intermediary precipitation area. This corroborates the conceptual model that rain areas with a higher CWP are characterized by higher rainfall intensities and possess higher confidence levels.

To make use of the combined information content in each channel difference, the confidences of the intermediary rain area are computed as a function of the combined values of the four channel differences as shown in equation (6.4) using the above mentioned 709 night-time scenes. The confidence threshold appropriate for rain area separation is determined analogously to the day-time scheme leading to a confidence threshold of 0.23 (ETS of 0.0873), that is chosen as the minimum threshold.

Table 6.2 shows the calculation of the confidences of the respective subareas together with the threshold values, the optimized ETS value as well as the corresponding radar reflectivity thresholds.

Table 6.2: Overview of the calculation of the confidences and the thresholds used for the separation of the respective subarea, together with the optimized ETS and the corresponding radar reflectivities.

$Confidence_A$	N_A	N_B	N_A (dBZ)	N_B (dBZ)	Confidence threshold	ETS
Convectively dominated precipitation area	Convectively dominated precipitation area	Advective-stratiform precipitation area	> 28.0	7.0 to 27.9	0.15	0.0868
Convective cores and convective-stratiform precipitation area	Convective cores and convective-stratiform precipitation area	Enhanced advective-stratiform precipitation area	> 37.0	28.0 to 36.9	0.19	0.1
Convective cores	Convective cores	Convective-stratiform precipitation area	> 46.0	37.0 to 45.9	0.23	0.2
Intermediary rain area	Intermediary rain area	Advective-stratiform background precipitation area	19.0 to 27.9	7.0 to 18.9	0.34 (daytime) 0.23 (nighttime)	0.0971 (daytime) 0.0873 (nighttime)

6.5 Appraisal of the introduced rain area differentiation technique

For an appraisal of the new proposed technique for precipitation process and rainfall intensity differentiation, the new scheme is applied to a validation data set consisting of precipitation events from January to August 2004 (altogether 1396 scenes, see section 6.2). The precipitation events chosen for the evaluation study are independent from the above mentioned precipitation events used for algorithm development.

Because of the differing information content concerning the CWP between day and night (see section 6.3.1), the comparison study for is done separately for the 720 day-time and the 676 night-time scenes.

The comparison is realized by calculating standard verification scores for dichotomous data sets (see section 6.2) on a pixel basis for each scene in comparison with corresponding ground-based radar data from the German Weather Service without any spatio-temporal aggregation. The statistics were calculated separately for each area of different precipitation processes and rainfall intensities classified by the new scheme (see table 6.1).

First the results for the convectively dominated precipitation subareas are presented, starting with the areas of enhanced advective-stratiform precipitation (28.0 to 36.9 dBZ, see table 6.1) followed by the convective-stratiform precipitation areas (37.0 to 45.9 dBZ, see table 6.1) and the convective cores (> 46.0 dBZ, see table 6.1). After that, the calculated indices for the advective-stratiform background precipitation areas (7.0 to 18.9 dBZ, see table 6.1) are presented, followed by the intermediary precipitating cloud fields (19.0 to 27.9 dBZ, see table 6.1).

(a) enhanced advective-stratiform precipitation

The indices calculated for the areas of enhanced advective-stratiform precipitation for day- and night-time scenes are depicted in table 6.3. The area percentage of the enhanced advective-stratiform precipitating cloud fields detected by the proposed scheme is in good accordance with those identified in the radar data during day-time as well as during night-time. Overall, the detected area is slightly overestimated by the satellite technique for day-time scenes. In contrast, the detected area is underestimated somewhat during night-time. Altogether, this precipitation area covers about 10% of the whole rain area for the day-time scenes compared to about 5% for the night-time scenes. The POD indicates that on average about 30% of the pixels classified as enhanced advective-stratiform precipitation by the radar are

consistently identified by the satellite scheme together with a very low percentage of wrongly classified pixels indicated by the POFD. On the other hand, the FAR average value is relatively high. This holds true for both data sets. Despite the low area fraction of the enhanced advective-stratiform precipitation area the CSI indicates a good degree of correctly classified pixels. In this context the ETS value can also be considered as satisfying, which applies for day-time as well as for night-time schemes. The positive impression concerning the classified area of enhanced advective-stratiform precipitation is further supported by the good values of the HSS and the HKD, again for both data sets.

The Relative operation characteristic (ROC) plots (JOLLIFFE & STEPHENSON 2003, MASON 1982) displayed in figure 6.10 underline the good results concerning the detected precipitation area. For the main part of the classified scenes the calculated POD is greater than the corresponding POFD signifying that the scheme has skill. Moreover, the results for the classified scenes show a convenient combination of medium POD values together with a low POFD values. Here, the day-time scheme is somewhat superior to the night-time scheme. Altogether, the performance of the proposed scheme concerning the detection of enhanced advective-stratiform precipitating cloud areas on a 15 minute basis with a spatial resolution of 3 by 3 km can be denoted satisfactory.

Table 6.3: Results of the standard verification scores applied to the enhanced advective-stratiform precipitation subareas for day-time and for night-time scenes by the proposed satellite technique. The scores are based on 720 day-time and the 676 night-time precipitation scenes from January to August 2004.

	Area [%] Radar	Area [%] Satellite	Bias	POD	POFD	FAR	CSI	ETS	HSS	HKD
Day										
Mean	10.18	10.31	1.02	0.31	0.12	0.69	0.19	0.08	0.14	0.13
Std	6.41	10.07	0.44	0.15	0.08	0.12	0.08	0.04	0.06	0.09
Min	0.18	0.16	0.22	0.02	0.00	0.32	0.01	-0.02	-0.04	-0.02
Max	27.63	40.63	2.20	0.76	0.51	0.99	0.35	0.20	0.33	0.40
Night										
Mean	4.92	4.09	0.85	0.28	0.09	0.76	0.15	0.08	0.15	0.15
STD	7.55	10.54	0.56	0.16	0.10	0.14	0.09	0.04	0.11	0.12
Min	0.06	0.03	0.20	0.08	0.00	0.36	0.01	-0.02	-0.06	-0.10
Max	33.67	47.83	2.17	0.79	0.46	0.98	0.40	0.28	0.44	0.52

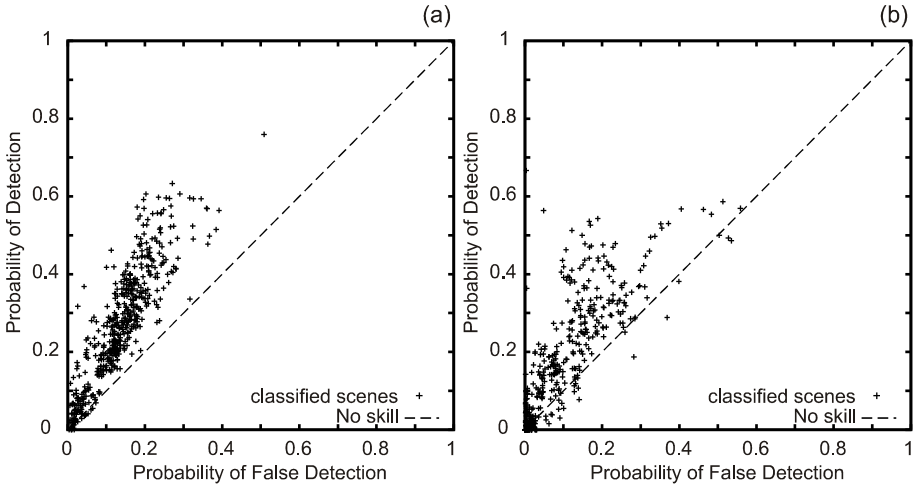

Figure 6.10: Relative operation characteristic (ROC) plot for the enhanced advective-stratiform precipitation subareas for day-time (a) and for night-time (b) scenes.

(b) convective-stratiform precipitation

Concerning the convective-stratiform precipitation area the percentage detected by the satellite based technique is in good accordance with those identified in the radar data (table 6.4). Overall the detected area is slightly overestimated by the introduced method. The convective-stratiform precipitation area covers about 4% of the whole rain area for the day-time scenes compared to about 1% for the night-time scenes. Bearing in mind the low area fraction of this precipitation subarea proportional to the whole rain area the POD value can be considered as satisfying. On average 19% of the pixels classified as convective-stratiform precipitation by the radar are consistently identified by the satellite scheme during day-time and 13% during night-time. The very low percentage of wrongly classified pixels indicated by the POFD underlines this good impression. At the same time, the FAR average value is relatively high. Despite the low area fraction the CSI indicate a satisfying degree of correctly classified pixels. In this context the ETS value can also be considered as satisfactory. The good values of the HSS and the HKD further support the positive impression concerning the classified area of convective-stratiform precipitation. Apart from the POD, the FAR and the CSI, that indicate a slightly better performance of the day-time scheme, there is no distinct difference between both data sets.

Table 6.4: As table 6.3 but for the convective-stratiform precipitation subareas for day-time and for night-time scenes.

	Area [%] Radar	Area [%] Satellite	Bias	POD	POFD	FAR	CSI	ETS	HSS	HKD
Day										
Mean	3.70	4.25	1.14	0.19	0.03	0.79	0.11	0.05	0.09	0.12
STD	2.66	5.02	0.53	0.11	0.02	0.10	0.06	0.03	0.05	0.10
Min	0.00	0.02	0.21	0.01	0.00	0.45	0.01	-0.02	-0.04	-0.02
Max	11.28	19.79	2.19	0.61	0.13	1.00	0.36	0.12	0.21	0.50
Night										
Mean	0.84	0.96	1.15	0.13	0.02	0.89	0.06	0.05	0.10	0.11
STD	2.76	3.05	0.61	0.09	0.02	0.08	0.07	0.06	0.12	0.12
Min	0.01	0.01	0.20	0.01	0.00	0.50	0.01	-0.05	-0.11	-0.11
Max	16.96	13.61	2.47	0.67	0.20	0.99	0.42	0.40	0.59	0.68

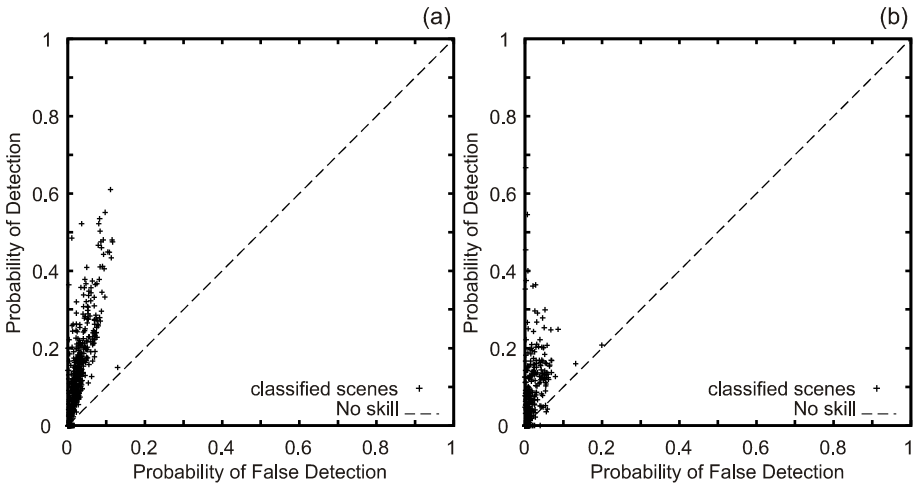

Figure 6.11: Relative operation characteristic (ROC) plot for the convective-stratiform precipitation subareas for day-time (a) and for night-time (b) scenes.

The ROC plots displayed in figure 6.11 show that for the major component of the classified scenes the calculated POD is greater than the corresponding POFD signifying that the satellite-based technique has skill. Moreover, the results for the classified scenes show a convenient combination of medium POD values together with a low POFD. Accordingly to the POD and the CSI both plots indicate a slightly better performance of the day-time scheme.

(c) convective cores

The area percentage of the convective cores with high rainfall intensities classified by the proposed algorithm is almost consistent with those detected by the ground-based radar (table 6.5). This statement holds true for both data sets. Despite the very low fraction of this classified subarea the calculated indices reveal a positive performance of the new differentiation scheme. The good POD value is accompanied by a very low POFD value and the high FAR is even lower than for the convective-stratiform precipitation area. The CSI indicates a good degree of correctly classified pixels and the ETS value can also be considered as satisfying. The overall positive impression for the classified convective-stratiform precipitation area is underlined by the good values of the HSS and the HKD. Apart from the two indices accounting also for correctly classified pixels by chance (ETS) as well as for pixels correctly identified by chance as no convective cores (HSS) the calculated indices point to a slightly better performance of the day-time scheme regarding the classified convective cores.

Table 6.5: As table 6.3 but for the convective cores for day-time and for night-time scenes.

	Area [%] Radar	Area [%] Satellite	Bias	POD	POFD	FAR	CSI	ETS	HSS	HKD
Day										
Mean	0.72	0.70	0.98	0.15	0.00	0.76	0.10	0.05	0.10	0.11
Std	0.92	1.11	0.59	0.14	0.00	0.15	0.09	0.04	0.06	0.14
Min	0.01	0.01	0.11	0.01	0.00	0.00	0.01	-0.01	-0.01	-0.01
Max	4.82	6.42	2.50	1.00	0.02	0.99	1.00	0.33	0.50	1.00
Night										
Mean	0.08	0.08	0.99	0.09	0.00	0.84	0.07	0.07	0.10	0.09
Std	0.33	0.23	0.58	0.19	0.00	0.29	0.15	0.15	0.19	0.19
Min	0.01	0.01	0.06	0.01	0.00	0.00	0.01	0.00	-0.01	-0.01
Max	1.80	1.69	2.50	1.00	0.01	0.98	1.00	1.00	1.00	1.00

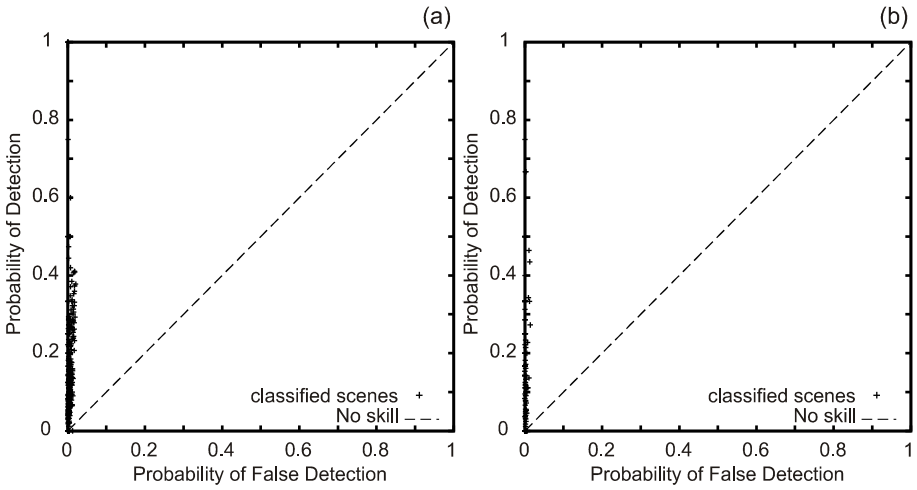

Figure 6.12: Relative operation characteristic (ROC) plot for convective cores for day-time (a) and for night-time (b) scenes.

The ROC plots in figure 6.12 signify that the results for the classified scenes show a convenient combination of medium to low POD values together with a low corresponding POFD values. The calculated POD is always greater than the corresponding POFD.

(d) advective-stratiform background precipitation

The area fraction of the advective-stratiform background precipitation classified by the satellite-based technique is in good agreement with the corresponding area detected by the radar during day-time as well as during night-time (table 6.6). Altogether this precipitation process covers about 60% of the whole rain area for the day-time scenes compared to about 75% for the night-time scenes. The slight underestimation by the satellite technique is a bit more pronounced for day-time scenes. The POD indicates that on average about 65% of the pixels classified as advective-stratiform background precipitation by the radar are consistently identified by the proposed scheme during day-time and about 75% during night-time. Compared to the FAR the POFD indicates a higher percentage of wrongly classified convective pixels. The high CSI value further supports the overall good performance of the technique with a better value for night-time scenes. However, because of the high fraction of the advective-stratiform precipitation area proportional to the whole rain area, a correct classification by the introduced technique is more probable. When accounting for pixels classified correctly by chance the very good CSI value is relativized somewhat by the lower ETS, which indicate a better performance of the day-time scene. Anyhow, when

the pixels correctly identified by chance as not advective-stratiform background precipitation are considered additionally to pixels correctly classified as advective-stratiform background precipitation by chance the good HSS value signifies a good performance of the proposed separation scheme. Accordingly the HKD indicates a satisfying ability of the satellite technique to separate the area of advective-stratiform background precipitation from the other subareas within the rain area. Again the HSS and HKD values point to a more advantageous performance of the day-time scene.

The ROC plots displayed in figure 6.13 support the overall good impression of the performance gained from table 6.6. The results for the main part of the classified scenes show a good combination of medium to high POD values together with low to medium values of the corresponding POFD during day-time as well as during night-time. Moreover, for the major component of the classified scenes the calculated POD is greater than the corresponding POFD signifying that the scheme has skill. The few classification results lying below the no-skill line are characterized by a POD just slightly lower than the corresponding POFD.

Table 6.6: As table 6.3 but for the advective-stratiform background precipitation subareas for day-time and for night-time scenes.

	Area [%] Radar	Area [%] Satellite	Bias	POD	POFD	FAR	CSI	ETS	HSS	HKD
Day										
Mean	58.18	56.64	0.98	0.63	0.43	0.32	0.49	0.11	0.20	0.21
Std	15.68	19.27	0.24	0.18	0.20	0.14	0.16	0.04	0.08	0.09
Min	33.18	20.76	0.50	0.26	0.16	0.00	0.19	-0.04	-0.09	-0.25
Max	100.00	98.13	1.79	0.98	0.99	0.64	0.89	0.33	0.50	0.48
Night										
Mean	74.06	73.61	1.00	0.73	0.58	0.23	0.60	0.08	0.15	0.16
Std	16.87	17.38	0.21	0.16	0.20	0.13	0.17	0.04	0.12	0.13
Min	24.20	22.61	0.50	0.22	0.13	0.00	0.17	-0.06	-0.03	-0.11
Max	97.73	96.58	1.77	0.97	0.93	0.63	0.89	0.22	0.46	0.55

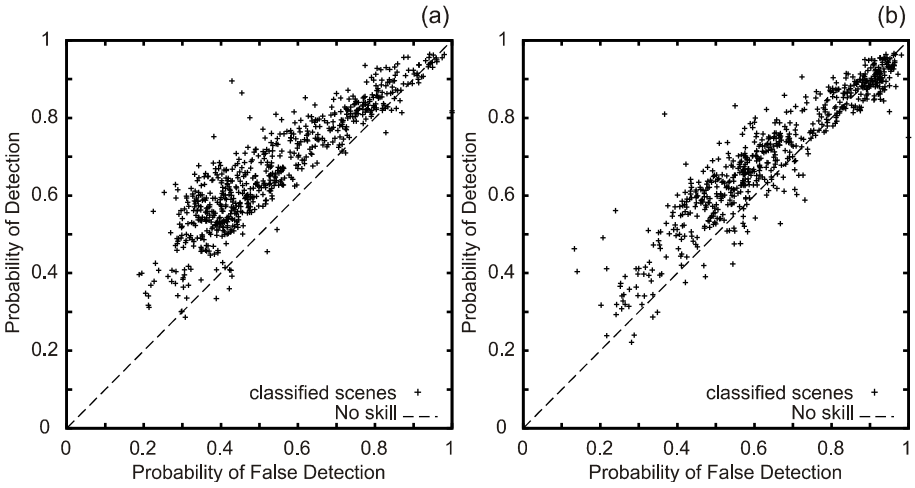

Figure 6.13: Relative operation characteristic (ROC) plot for the advective-stratiform background precipitation subareas for day-time (a) and for night-time (b) scenes.

(e) intermediary precipitation

The area fraction classified as intermediary precipitation by the satellite-based technique is in good accordance with the corresponding area detected by the radar for day-time scenes as well as for night-time scenes (table 6.7). Altogether this precipitation area covers about 28% of the whole rain area for the day-time scenes compared to about 20% for the night-time scenes. On average about 38% of the pixels classified as intermediary precipitation by the radar are consistently identified by the day-time scheme and about 30% by the night-time scheme. At the same time, the POFD indicates a low percentage of wrongly classified convective pixels, which coincide on the other hand with a relatively high FAR average value. The CSI shows a good value for both data sets and further supports the positive impression regarding the classified intermediary rain area. This is relativized somewhat by the low average value of the ETS. However the HSS average value signifies a satisfying performance concerning the classified subarea. Accordingly the HKD indicates a good ability of the satellite technique to separate the area of intermediary precipitation from the other subareas within the rain area. As for the advective-stratiform background precipitation area the classification performance concerning the intermediary precipitation area is characterized by a slightly higher quality during day-time scenes compared to night-time scenes.

Table 6.7: As table 6.3 but for the intermediary precipitation subareas for day-time and for night-time scenes.

	Area [%] Radar	Area [%] Satellite	Bias	POD	POFD	FAR	CSI	ETS	HSS	HKD
Day										
Mean	27.22	28.10	1.03	0.37	0.25	0.64	0.23	0.06	0.12	0.12
Std	8.17	14.10	0.43	0.16	0.13	0.09	0.08	0.03	0.05	0.06
Min	4.37	3.24	0.22	0.03	0.03	0.33	0.02	-0.02	-0.04	-0.05
Max	43.64	69.54	2.01	0.77	0.71	0.93	0.43	0.36	0.53	0.49
Night										
Mean	20.11	21.27	1.07	0.30	0.18	0.72	0.21	0.04	0.07	0.07
Std	9.45	9.34	0.40	0.14	0.09	0.11	0.13	0.05	0.09	0.10
Min	4.39	2.00	0.20	0.08	0.02	0.47	0.02	-0.02	-0.06	-0.09
Max	46.85	41.64	2.10	0.86	0.43	0.98	0.63	0.17	0.30	0.37

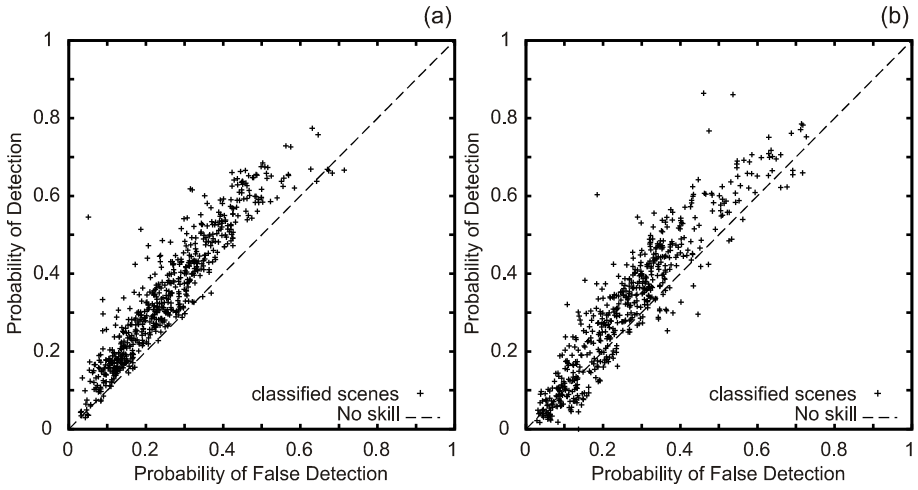

Figure 6.14: Relative operation characteristic (ROC) plot for the intermediary precipitation subareas for day-time (a) and for night-time (b) scenes.

The ROC plots displayed in figure 6.14 give an overview for all classified scenes. The results for the main part of the classified scenes show a good combination of medium to high POD values together with low to medium values of the corresponding POFD. Moreover, for the major component of the classified scenes the calculated POD is greater than the corresponding POFD signifying that the scheme has skill. The few classification results lying below the no-skill line are characterized by a POD just slightly lower than the corresponding POFD.

(f) Summary of the results

To summarize the results of the comparison study an overall good performance of the proposed scheme can be stated, especially concerning the high temporal resolution of 15 minutes and the high spatial resolution of 3 by 3 km. Thus, a process-oriented separation of areas with different rainfall intensities according to the conceptual model of rainbands introduced in section 6.3.1 is possible.

The slightly better performance of the day-time scheme for the advective-stratiform precipitation area is probably due to the higher information content about the CWP inherent in the $VIS_{0.6}$ and $NIR_{1.6}$ channel compared to the four channel differences considered in the night-time scheme (refer to section 6.4.2).

The better results for the convectively dominated precipitation areas for day-time scenes might be a consequence of the higher area percentage of the respective subarea for the day-time data set compared to the night-time data set. In general, the lower area fraction of the convectively dominated precipitation areas makes potential spatial misalignments between radar and satellite data more probable. Furthermore, the lower fraction exerts a higher influence on the quality of the calculated scores. This interpretation is supported by the fact that the fraction of the classified convectively dominated precipitation areas and the bias point to a good accordance between the radar data and the satellite-based technique. Spatial misalignments between both techniques are most probably the result of the differing viewing geometry between the satellite scanning the cloud top and the ground-based radar network scanning the cloud bottom and detecting the rainfall intensities at the surface together with the differing spatial resolution and the projection of the radar data to the SEVIRI viewing geometry. The winds within the cloud and below the cloud bottom can displace the rain drops and also cause spatial misalignments.

The discrepancy between the POD and FAR for the classified areas can be explained by the differing denominator for both indices. The POFD gives the fraction of the wrongly classified pixels proportional to the pixels classified as not belonging to the respective subarea by the radar data. The advective-stratiform precipitation areas covers a great part of the whole rain area leading to a low fraction of the area not belonging to this subarea. This explains the relatively high POFD. In contrast, the FAR gives the fraction of the wrongly classified pixels proportional to all pixels classified as advective-stratiform precipitation areas by the satellite technique. Therefore, the denominator for calculating the FAR is much higher compared to the POFD and leads to low FAR values. Regarding the convective precipitation areas the situation is reversed. The pixels classified as

not belonging to these subareas by the radar cover a large fraction of the whole rain area. As a consequence, the calculated POFD is much lower. In contrast, the amount of all pixels classified as convective by the satellite technique is relatively small causing a higher FAR in this case.

To gain a visual impression of the performance of the introduced retrieval scheme, the classified rain area for a scene from 16 August 2004 10:45 UTC is depicted in figure 6.15. Figure 6.15 a shows the rain area classified by the new developed scheme and figure 6.15 b shows the rain area classified by the radar network. The classified rain area for a scene from 30 May 2004 23:45 UTC is depicted in figure 6.16. Figure 6.16 a shows the rain area classified by the new developed scheme and figure 6.16 b the rain area classified by the radar network.

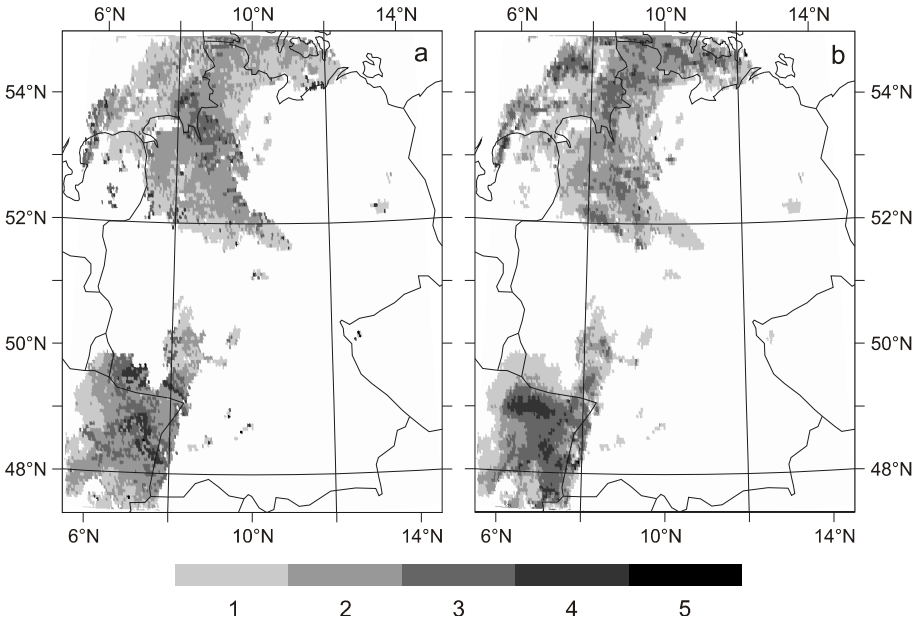

Figure 6.15: Classified rain area for the scene from 16 August 2004 10:45 UTC, by the proposed retrieval scheme (a) and by the radar data (b). 1: Advective-stratiform background precipitation; 2: Intermediary precipitation; 3: Enhanced advective-stratiform precipitation; 4: Convective-stratiform precipitation; 5: Convective cores (see table 6.1).

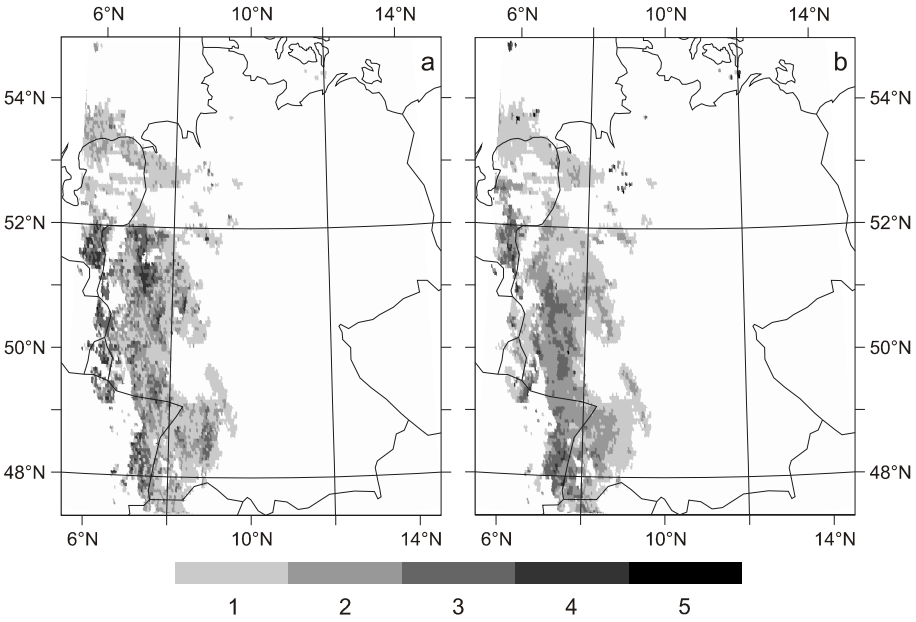

Figure 6.16: Classified rain area for the scene from 30 August 2004 23:45 UTC, by the proposed retrieval scheme (a) and by the radar data (b).1: Advective-stratiform background precipitation; 2: Intermediary precipitation; 3: Enhanced advective-stratiform precipitation; 4: Convective-stratiform precipitation; 5: Convective cores (see table 6.1).

6.6 Conclusions

A new consistent day and night technique for precipitation process separation and rainfall intensity differentiation using Meteosat Second Generation SEVIRI data has been proposed.

In a first step the convectively dominated precipitation area is detected within the rain area delineated by the ground-based radar network and the remaining area is declared as advective-stratiform precipitation. In the following both separated areas are subdivided into areas of differing rainfall intensities according to the conceptual of rainbands.

The detection and differentiation of the convective precipitation area relies on information about the CTH gained from WV-IR differences $\Delta T_{WV6.2\text{-}IR10.8}$, $\Delta T_{WV7.3\text{-}IR12.1}$ and the IR CTT $BT_{10.8}$. It is assumed that cloud areas with a higher WV-IR difference and a lower top temperature are characterized by higher rainfall intensities.

The subdivision of the advective-stratiform precipitation area is based on information about the CWP and the CP in the upper parts. It is assumed that advective-stratiform cloud areas characterized by

higher CWP values and a higher amount of ice particles in the upper parts of the cloud produce higher rainfall intensities. Information about the CP is gained by considering the temperature differences $\Delta T_{8.7\text{-}10.8}$ and $\Delta T_{10.8\text{-}12.1}$ (STRABALA et al. 1994). Information about the CWP is incorporated by considering the $VIS_{0.6}$ and $NIR_{1.6}$ channel during day-time and the temperature differences $\Delta T_{3.9\text{-}10.8}$, $\Delta T_{3.9\text{-}7.3}$, $\Delta T_{8.7\text{-}10.8}$ and $\Delta T_{10.8\text{-}12.1}$ during night-time.

The results of the new proposed technique are validated against ground-based radar data and indicate an encouraging performance of the new algorithm concerning process separation and intensity differentiation and support the possibility of process-oriented classification of the detected rain area by means of MSG SEVIRI.

Such a process separation and intensity differentiation is of valuable benefit for now-casting purposes, because of deficiencies regarding the assignment of instantaneous precipitation rates at the ground. A separation of the rain area into subareas of different rainfall intensities offers the potential for an improved rainfall rate assignment in a next step, which can be done by applying distinct regression functions for each of the classified subareas. Concerning this topic, comprehensive research efforts have just been started in order to develop a new method for the assignment of rainfall rates based on the differentiated areas of differing rainfall intensities and on information about CWP, CP and CTH.

The good validation results for the proposed scheme that are obtained on a 15 minute basis without any spatial and temporal aggregation, suggest that the achieved accuracies are sufficient for the proposed applications. This is especially true, as for similar comparison studies the data are generally temporally aggregated over 3h or 24h, (e.g. validation web page of the international precipitation working group (IPWG; *http://www.bom.gov.au/bmrc/SatRainVal/validation-intercomparison.html*)). However, for a comprehensive appraisal of the proposed retrieval technique extensive and detailed validation studies are still necessary.

Acknowledgements

The current study is funded by the German Ministry of Research and Education (BMBF) in the framework of GLOWA-Danube project (G-D/2004/TP-10, precipitation/remote sensing) as well as by the German Research Council DFG (BE 1780/18-1) within the SORT project.

The authors are grateful to the German weather service (DWD) for providing the radar data sets within the Eumetsat/DWD Advanced Multisensor Precipitation Experiment (AMPE).

References

ACKERMAN, S. A., C. C. MOELLER, K. I. STRABALA, H. E. GERBER, L. E. GUMLEY, W. P. MENZEL & S. C. TSAY (1998): Retrieval of effective microphysical properties of clouds: a wave cloud case study. - *Geophysical Research Letters, 25*: 1121–1124.

ADLER, R. F. & R. A. MACK (1984): Thunderstorm cloud height-rainfall rate relations for use with satellite rainfall estimation techniques. - *Journal of Climate and Applied Meteorology, 23*: 280 – 296.

ADLER, R. F. & A. J. NEGRI (1988): A satellite technique to estimate tropical convective and stratiform rainfall. - *Journal of Applied Meteorology, 27*: 30–51.

AMINOU, D. M. A. (2002): MSG's SEVIRI instrument. - *ESA Bulletin, 111*: 15–17.

BA, M. B. & A. GRUBER (2001): GOES Multispectral Rainfall Algorithm (GMSRA). - *Journal of Applied Meteorology, 40*: 1500-1514.

BARNES, W. L., T. S. PAGANO & V. V. SALOMONSON (1998): Prelaunch characteristics of the Moderate Resolution Imaging Spectroradiometer (MODIS) on EOS-AM1. - *IEEE Transactions on Geoscience and Remote Sensing, 36:* 1088–1100.

BAUM, B. A., R. F. ARDUINI, B. A. WIELICKI, P. MINNIS & S. C. TSAY (1994): Multilevel cloud retrieval using multispectral HIRS and AVHRR data: night-time oceanic analysis. - *Journal of Geophysical Research – Atmospheres, 99*: 5499–5514.

BENDIX, J., C. REUDENBACH & R. ROLLENBECK (2003): The Marburg Satellite Station. *Proceedings of the 2002 Meteorological Satellite Users' Conference. Dublin, EUMETSAT:* 139–146.

BENNARTZ, R. (2007): Passive microwave precipitation measurements at mid- and high-latitudes. In: LEVIZZANI, V., P. BAUER, & F. J. TURK (Ed.): Measuring precipitation form space. - *Advances in global change research, 28*. Springer: Netherlands.

CAPACCI, D., F. PORCÙ & F. PRODI (2008): Rain-rate estimation from SEVIRI/MSG and AMSR-E/AQUA. Validation and comparison by using U.K. Weather radars. *Proceedings of the Joint 2007 EUMETSAT Meteorological Satellite Conference and the 15th*

Satellite Meteorology & Oceanography Conference of the American Meteorological Society. Amsterdam, EUMETSAT: P.50.

CERMAK, J., J. BENDIX & M. DOBBERMANN (2007): FMet - An Integrated Framework for Meteosat Data Processing for Operational Scientific Applications. - *Computers and Geosciences,* accepted.

CHENG, M., R. BROWN & C. G. COLLIER (1993): Delineation of precipitation areas by correlation of METEOSAT visible and infrared data in the region of the United Kingdom. - *Journal of Applied Meteorology, 32*: 884–898.

DWD (2005): Weather radar network. - Available online at http://www.dwd.de/en/Technik/Datengewinnung/Radarverbund/Radarbroschuere_en.pdf, 10 November 2007.

EBERT, E. E., J. E. JANOWIAK & C. KIDD (2007): Comparison of near-real-time precipitation estimates from satellite observations and numerical models. - *Bulletin of the American Meteorological Society, 88*: 47–64.

FRITZ, S. & I. LASZLO (1993): Detection of water vapour in the stratosphere over very high clouds in the tropics. - *Journal of Geophysical Research, 98*: D12: 22959-22967.

FRÜH, B., J. BENDIX, T. NAUSS, M. PAULAT, A. PFEIFFER, J. W. SCHIPPER, B. THIES & H. WERNLI (2007): Verification of precipitation from regional climate simulations and remote-sensing observations with respect to ground-based observations in the upper Danube catchment. - *Meteorologische Zeitschrift, 16*: 275–293.

GONZÁLEZ, A., J. C. PÉREZ, F. HERRERA, F. ROSA, M. A. WETZEL, R. D. BORYS & D. H. LOWENTHAL (2002): Stratocumulus properties retrieval method from NOAA-AVHRR data based on the discretization of cloud properties. - *International Journal of Remote Sensing, 23*: 627–645.

HOUZE, R. A. (1993): Cloud Dynamics, Vol. 53. of International Geophysics Series, Academic Press, San Diego.

HOUZE R. A. (1997): Stratiform precipitation in regions of convection: A meteorological paradox? - *Bulletin of the American Meteorological Society, 78*: 2179-2196.

HUANG, H.L., P. YANG, H. L. WEI, B. A. BAUM, Y. X. HU, P. ANTONELLI & S. A. ACKERMAN (2004): Inference of ice cloud properties from high spectral resolution infrared observations. - *IEEE Transactions on Geoscience and Remote Sensing, 42*: 842–853.

JOLLIFFE, I. T. & D. B. STEPHENSON (2003): Forecast verification. A Practitioner's Guide in Atmospheric Science. John Wiley and Sons, Chichester.

JOYCE, R. J., J. E. JANOWIAK, P. A. ARKIN & P. XIE (2004): CMORPH: A method that produces global precipitation estimates from passive microwave and infrared data at high spatial and temporal resolution. - *Journal of Hydrometeorology, 5:* 487–503.

KÄSTNER, M., F. TORRICELLA & S. DAVOLIO (2006): Intercomparison of satellite-based and model-based rainfall analyzes. - *Meteorological Applications, 13*: 213-223.

KAWAMOTO, K., T. NAKAJIMA & T. Y. NAKAJIMA (2001): A global determination of cloud microphysics with AVHRR remote sensing. - *Journal of Climate, 14*: 2054–2068.

KIDD, C., D. R. KNIVETON, M. C. TODD & T. J. BELLERBY (2003): Satellite Rainfall Estimation Using Combined Passive Microwave and Infrared Algorithms. - *Journal of Hydrometeorology, 4*: 1088-1104.

KLEY, D., A. SCHMELTEKOPF, K. KELLY, R. WINKLER, T. THOMPSON & M. MCFARLAND (1982): Transport of water vapour through the tropical tropopause. Geophysical Research Letters, 9, 617-624.

KOKHANOVSKY, A. A. & V. V. ROZANOV (2003): The reflection function of optically thick weakly absorbing turbid layers: a simple approximation. - *Journal of Quantitative Spectroscopy and Radiative Transfer, 77*: 165–175, 2003.

KOKHANOVSKY, A. A., V. V. ROZANOV, T. NAUSS, C. REUDENBACH, J. S. DANIEL, H. L. MILLER & J. P. BURROWS (2005): The semianalytical cloud retrieval algorithm for SCIAMACHY. I: The validation. - *Atmospheric Chemistry and Physics, 6*: 1905–1911.

KURINO, T. (1997): A satellite infrared technique for estimating 'deep/shallow' precipitation. - *Advances in Space Research, 19*: 511–514.

LENSKY, I. M. & D. ROSENFELD (2003a): A night-time delineation algorithm for infrared satellite data based on microphysical considerations. - *Journal of Applied Meteorology, 42*: 1218–1226.

LENSKY, I. M. & D. ROSENFELD (2003b): Satellite-based insights into precipitation formation processes in continental and maritime convective clouds at night-time. - *Journal of Applied Meteorology, 42*: 1227–1233.

LENSKY, I. M. & D. ROSENFELD (2006): The time-space exchangeability of satellite retrieved relations between cloud top temperature and particle effective radius. - *Atmospheric Chemistry and Physics, 6*: 2887-2894.

LEVIZZANI, V., J. SCHMETZ, H. J. LUTZ, J. KERKMANN, P. P. ALBERONI & M. CERVINO (2001): Precipitation estimations from geostationary orbit

and prospects for Meteosat Second Generation. - *Meteorological Applications, 8:* 23–41.

LEVIZZANI, V. (2003): Satellite rainfall estimations: new perspectives for meteorology and climate from the EURAINSAT project. - *Annales Geophysicae-Italy, 46*: 363–372.

MASON, I. (1982): A model for assessment of weather forecasts. - *Australian Meteorological Magazine*, 30: 291–302.

MILLER, S. W., P. A. ARKIN & R. J. JOYCE (2001): A combined microwave/infrared rain rate algorithm. - *International Journal of Remote Sensing, 22:* 3285 – 3307.

NAKAJIMA, T. Y. & T. NAKAJIMA (1995): Wide-area determination of cloud microphysical properties from NOAA AVHRR measurements for FIRE and ASTEX regions. - *Journal of the Atmospheric Sciences, 52*: 4043–4059.

NAUSS, T. & A. A. KOKHANOVSKY (2006): Discriminating raining from non-raining clouds at mid-latitudes using multispectral satellite data. - *Atmospheric Chemistry and Physics, 6*: 5031–5036.

NAUSS, T. & A. A. KOKHANOVSKY (2007): Assignment of rainfall confidence values using multispectral satellite data at mid-latitudes: first results. - *Advances in Geosciences, 10*: 99–102.

OU, S. C., K. N. LIOU, W. M. GOOCH & Y. TAKANO (1993): Remote sensing of cirrus cloud parameters using advanced very-high-resolution radiometer 3.7- and 10.9-µm channels. - *Applied Optics, 32*: 2171–2180.

PAGE, W. (1982): NASA experiment on tropospheric-stratospheric water vapour transport in the intertropical convergence zone. - *Geophysical Research Letters, 9*: 599-624.

PLATNICK, S., M. D. KING, S. A. ACKERMAN, W. P. MENZEL, B. A. BAUM, J. C. RIÉDI & R. A. FREY (2003): The MODIS cloud products: algorithms and examples from Terra. - *IEEE Transactions on Geoscience and Remote Sensing, 41*: 459–473.

REUDENBACH, C., G. HEINEMANN, E. HEUEL, J. BENDIX & M. WINIGER (2001): Investigation of summertime convective rainfall in Western Europe based on a synergy of remote sensing data and numerical models. - *Meteorology and Atmospheric Physics, 76*: 23–41.

REUDENBACH, C. (2003): Konvektive Sommerniederschläge in Mitteleuropa. Eine Kombination aus Satellitenfernerkundung und numerischer Modellierung zur automatischen Erfassung mesoskaliger Niederschlagsfelder. - *Bonner Geographische Abhandlungen, 109*: 152 pp.

REUDENBACH, C., T. NAUSS, J. CERMAK, M. DOBBERMANN, J. BENDIX, W. THEISSEN, P. SCHEIDGEN & O. HARMANN (2004): An integrated receiving and processing unit for MSG, NOAA and Terra/Aqua data. *Proceedings of the 2003 EUMETSAT Meteorological Satellite Conference, Weimar:* 291-297.

REUDENBACH, C., T. NAUSS, & J. BENDIX (2007): Retrieving precipitation with GOES, Meteosat and Terra/MSG at the tropics and mid-latitudes. In: LEVIZZANI, V., P. BAUER, & F. J. TURK (Ed.): Measuring precipitation form space. - *Advances in global change research, 28*. Springer: Netherlands.

ROSENFELD, D. & I. LENSKY (1998): Satellite-based insights into precipitation formation processes in continental and maritime convective clouds. - *Bulletin of the American Meteorological Society, 79*: 2457-2476.

SCHMETZ, J., P. PILI, S. TJEMKES, D. JUST, J. KERKMANN, S. ROTA & A. RATIER (2002): An introduction to Meteosat Second Generation (MSG). - *Bulletin of the American Meteorological Society, 83*: 977–992.

SCHMETZ, J., TJEMKES, S. A., GUBE, M. & VAN DE BERG, L. (1997): Monitoring deep convection and convective overshooting with Meteosat. - *Advances in Space Research, 19*: 433-441.

SELTMANN, J. (1997): Radarforschung im DWD: Vom Scan zum Produkt. - *Promet, 26*: 32-52.

STANSKI, H. R., L. WILSON & W. BURROWS (1989): Survey of common verification methods in meteorology. - *World Weather Watch Technical Report No.8. WMO: Geneva*, WMO/TD No. 358, 114 pp.

STEINER, M., R. A. HOUZE & S. E. YUTER (1995): Climatological characterization of 3-dimensional storm structure from operational radar and rain-gauge data. - *Journal of Applied Meteorology, 34*: 1978-2007

STRABALA, K. I., S. A. ACKERMAN & W. P. MENZEL (1994): Cloud properties inferred from 8-12-µm Data. - *Journal of Applied Meteorology, 33*: 212–229.

THIES, B., T. NAUSS & J. BENDIX (2007): Detection of high rain clouds using water vapour emission – transition from Meteosat First (MVIRI) to Second Generation (SEVIRI). - *Advances in Space Research,* submitted.

THIES, B., T. NAUSS & J. BENDIX (2008a): Discriminating raining from non-raining cloud areas at mid-latitudes using Meteosat Second Generation SEVIRI night-time data. - *Meteorological Applications*, DOI: 10.1002/met.56.

THIES, B., T. NAUSS & J. BENDIX (2008b): Discriminating raining from non-raining cloud areas at mid-latitudes using Meteosat Second Generation SEVIRI day-time data. - *Atmospheric Chemistry and Physics: 8*, 1-9.

THIES, B., T. NAUSS & J. BENDIX (2008c): First results on a process-oriented rain area classification technique using Meteosat Second Generation SEVIRI night-time data. - *Advances in Geosciences, 16*: 63-72.

TJEMKES, S. A., L. VAN DE BERG & J. SCHMETZ (1997). Warm water vapour pixels over high clouds as observed by Meteosat. - *Contributions to Atmospheric Physics, 70*: 15–21.

TURK, J. & P. BAUER (2006): The International Precipitation Working Group and Its Role in the Improvement of Quantitative Precipitation Measurements. - *Bulletin of the American Meteorological Society*, 87: 643–647.

WENG, F. Z., L. M. ZHAO & R. R. FERRARO (2003): Advanced microwave sounding unit cloud and precipitation algorithms. - *Radio Science, 38*: Art. No. 8068.

WORLD WEATHER RESEARCH PROGRAM/WORKING GROUP ON NUMERICAL EXPERIMENTATION JOINT WORKING GROUP ON VERIFICATION (WWRP/WGNE): Forecast Verification – Issues, Methods and FAQ. - Available online at http://www.bom.gov.au/bmrc/wefor/staff/eee/verif/verif web page.html, 11 May 2007.

CHAPTER 7

Summary and Outlook

7 Summary and Outlook

7.1 Summary

Knowledge of the spatio-temporal precipitation distribution is of great value in agriculture, water engineering, climatology and risk management. So far, no adequate method existed for the detection and monitoring of precipitation at high temporal and spatial resolutions in most parts of the world where radar networks are not available.

Due to spectral constraints, existing retrieval techniques rely on a relationship between rainfall probability and intensity and the cloud top temperature measured in an infrared channel. These techniques show considerable drawbacks concerning precipitation processes in the mid-latitudes. Improved techniques for rain area identification based on spectral enhancements of new generation satellite systems used to be only available on polar orbiting platforms with poor temporal resolutions. Furthermore, these algorithms are only applicable during day-time. With the advent of Meteosat Second Generation (MSG) Spinning-Enhanced Visible and InfraRed Imager (SEVIRI) in 2004, a geostationary satellite system with significantly improved spectral and spatial resolutions has become available.

The central aim of the present study therefore was to develop a novel method for operational precipitation detection during day- and night-time based on MSG SEVIRI data. The focus of the newly developed scheme lies on precipitation processes in the mid-latitudes in connection with extra-tropical cyclones. It is therefore not only applicable to convectively dominated rain areas but also to precipitating cloud areas of advective-stratiform character.

The main hypotheses of this study were:

- MSG SEVIRI allows the discrimination of the rain area based on information about the cloud water path and the cloud phase.
- MSG SEVIRI allows the separation of subareas of differing precipitation processes and rainfall intensities based on a information about the cloud water path, the cloud phase and the cloud top height.
- The discrimination of the rain area and the separation into subareas of differing precipitation processes and rainfall intensities can be performed with comparable accuracy during day- and night-time.

The approach taken to explore this presumptions rests upon the following conceptual model, which forms the basis of the newly

developed rainfall retrieval scheme based on the advanced second-generation GEO system MSG SEVIRI:

- Precipitating cloud areas are characterized by a sufficiently high cloud water path and ice particles in the upper part.
- Cloud areas with higher rainfall intensities are characterized by a higher cloud water path and a higher amount of ice particles in the upper part.
- Convective clouds with very high rainfall intensities are characterized by a large vertical extension and a high rising cold cloud top.

Based on this conceptual design, the new retrieval scheme consists of an entirely new methodology compiling novel and innovative algorithms and approaches. The following three components are the focal parts of the novel technique:

- A new algorithm for the identification of the rain area during day- and night-time was developed for SEVIRI. The method allows not only a proper detection of mainly convective rain areas but also enables the detection of advective-stratiform precipitation (e.g. in connection with mid-latitude frontal systems). It is based on information about the CWP and the cloud phase in the upper cloud regions. The day-time technique considers the $VIS_{0.6}$ and the $NIR_{1.6}$ channel to gain information about the cloud water path. The night-time approach considers the channel differences $\Delta T_{3.9\text{-}10.8}$, $\Delta T_{3.9\text{-}7.3}$, $\Delta T_{8.7\text{-}10.8}$, and $\Delta T_{10.8\text{-}12.1}$ to gain implicit knowledge about the CWP. Additionally, the day-time and night-time technique consider the channel differences $\Delta T_{8.7\text{-}10.8}$ and $\Delta T_{10.8\text{-}12.1}$ to gain information about the cloud phase (chapter 4 and 5).
- An infrared retrieval technique appropriate for convective precipitation processes in the mid-latitudes was successfully transferred and adapted to MSG SEVIRI. The phenomenon of positive brightness temperature differences between the WV and IR channels ($\Delta T_{WV\text{-}IR}$), which enables the detection and classification of convectively dominated raining cloud areas was investigated for the WV and IR channels of SEVIRI. Based on radiative transfer calculations, which revealed the existence of positive $\Delta T_{WV\text{-}IR}$ for all SEVIRI WV-IR differences, the $\Delta T_{WV\text{-}IR}$ technique could be applied and transferred to SEVIRI (chapter 3).
- A new technique for precipitation process and rainfall intensity separation was developed for SEVIRI. The process separation

and the further subdivision relies on information about the cloud top height, the cloud water path and the cloud phase in the upper parts. The subdivision is realized in a stepwise manner. In a first step the rain area is separated into the subareas of convective and advective-stratiform precipitation processes. In the following both separated process areas are divided into subareas of differing rainfall intensities. The process separation and the subdivision of the convective precipitation area relies on information about the cloud top height gained from the WV-IR differences $\Delta T_{WV6.2\text{-}IR10.8}$ and $\Delta T_{WV7.3\text{-}IR12.1}$ together with the cloud top temperature in the $IR_{10.8}$ channel. The subdivision of the advective-stratiform precipitation area is based on information about the CWP and the particle phase in the upper parts of the cloud. Information about the particle phase is gained by considering the temperature differences $\Delta T_{8.7\text{-}10.8}$ and $\Delta T_{10.8\text{-}12.1}$. Information about the CWP is incorporated by considering the $VIS_{0.6}$ and $NIR_{1.6}$ channel during day-time and the temperature differences $\Delta T_{3.9\text{-}10.8}$, $\Delta T_{3.9\text{-}7.3}$, $\Delta T_{8.7\text{-}10.8}$, and $\Delta T_{10.8\text{-}12.1}$ during night-time (chapter 6).

The rain area and the process-oriented rainfall intensities detected and classified by the newly developed retrieval technique were validated against corresponding ground-based radar data of Germany, representative for mid-latitude precipitation processes. The results of the validation study indicate persuading performance of the new algorithm concerning rain area identification as well as process and intensity differentiation and indicate the stability of the introduced conceptual design.

Based on the successful implementation of the three components and the good performance of the developed precipitation retrieval scheme indicated by the validation results the main hypotheses can be verified:

> MSG SEVIRI allows identification of the rain area and its further separation into subareas of different precipitation processes and rainfall intensities based on information about the cloud water path, the cloud phase in the upper parts and the cloud top height. The detection of the rain area and its intensity differentiation can be performed with comparable accuracy during day- and night-time.

A solid, reliable and physically founded approach is thus at hand for the detection and monitoring of precipitation in a quasi-continuous manner at high spatial and temporal resolutions using MSG SEVIRI data. The proposed technique presents an important contribution in the

context of satellite based quantitative precipitation measurement in near-real-time. Beside its applicability in climatological studies analyzing the spatio-temporal precipitation distribution it can also provide valuable input for data assimilation for the initialization of numerical weather and climate models but also for hydrological models. Concerning now-casting and risk management purposes the high spatial and especially temporal resolution provided by SEVIRI, which allows to consider short-time precipitation dynamics, is of great benefit. To all these applications of great social, hydrological and climatological relevance, the new scheme provides valuable information.

7.2 Outlook

As an outlook and a demonstration of the potential of the new precipitation retrieval scheme, its applicability for climatological studies is briefly demonstrated. Climatological studies concerning the spatio-temporal precipitation distribution represent a major application of the proposed technique. While the short time series of MSG SEVIRI data available so far does not allow for climatologically significant conclusions, the potential for such studies can nonetheless be highlighted on this basis.

In order to demonstrate the potential of the new scheme, the results have been aggregated for some sample time series. Figure 7.1 shows the relative frequency of precipitation events between January and August 2004. Figure 7.1a is based on 1570 day-time scenes and figure 7.1b is based on 1385 night-time scenes. Figure 7.2 displays the mean rainfall intensity based on the same data sets for day and night. The presented maps should not be interpreted as a precipitation climatology. Anyhow, some typical characteristics of the spatial precipitation distribution in Central Europe can be identified, that are in accordance with those presented by WEISCHET & ENDLICHER (2000) and the hydrological atlas of Germany (BUNDESMINISTERIUM FÜR UMWELT, NATURSCHUTZ, UND REAKTORSICHERHEIT 2003).

According to the climatological situation and the dominant atmospheric conditions in Central Europe high frequencies of precipitation events together with high rainfall intensities are connected to the higher locations of the mountain ranges. At the same time the larger valleys and basins are characterized by lesser precipitation frequencies and intensities. For example the Upper Rhein Valley in the south western part shows lower frequencies and intensities than the Vogesen Mountains and the Schwarzwald. Further maxima can be identified in the area of the Schwäbische Alb, in the Eifel region, the Westerwald, the Rothaargebirge and the Sauerland.

Concerning the maxima in the region of the Alpine foothills the blocking effect of the Alps leading to enhanced precipitation frequencies can be recognized. Other centres of precipitation activities can be found along the line Schwäbische Alb, Fränkische Alb, Fichtel Gebirge, Erzgebirge and Thüringer Wald. Generally the spatial precipitating frequency and intensity is characterized by small locally confined variations. These variations are amongst others due to local luv-lee effects. An example are the frequency and intensity differences between the western declivity and the eastern declivity of the Taunus and the Harz mountain ranges. On a large scale the dominant influence of extra-tropical cyclones crossing Central Europe from the west, which decreases to the north eastern parts becomes obvious. This leads to lesser precipitation frequencies and intensities in the north eastern regions. But also the great basins with lower frequencies and intensities can be identified.

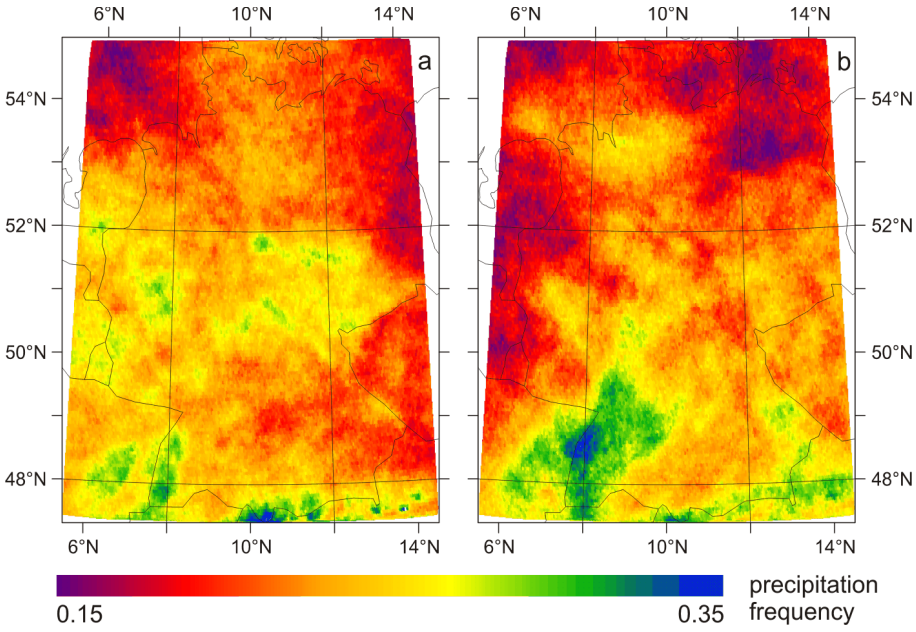

Figure 7.1: Relative frequency of precipitation events between January and August 2004, based on 1570 day-time scenes (a) and on 1385 night-time scenes (b).

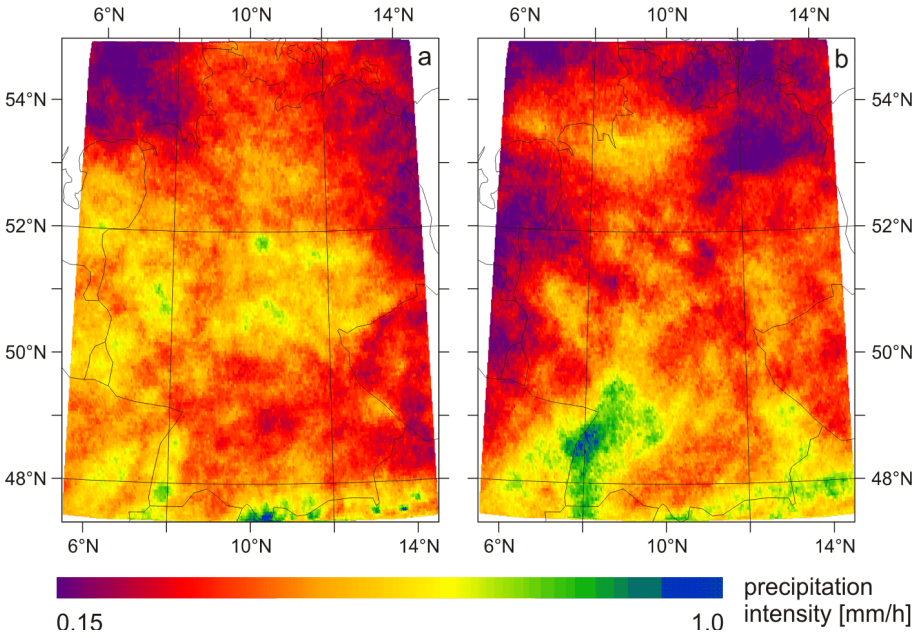

Figure 7.2: Mean rainfall intensity between January and August 2004, based on 1570 day-time scenes (a) and on 1385 night-time scenes (b).

In general, the day-time maps show a spatially more differentiated precipitation structure than the night-time maps. The lower frequencies and intensities in the Upper Rhein Valley are not so distinct in the night-time maps. The same holds true for the maxima in the area around the Rothaargebirge and the Thüringer Wald as well as for the Hunsrück and the Eifel. On the other hand, the regions Schwäbische and Fränkische Alb are characterized by higher frequencies and intensities, which are not so distinct in the day-time map. The same applies to the Bayrische Wald. An interesting feature is the area of higher frequencies and intensities around the north western cost depicted in the night-time maps but not in the day-time maps.

The described differences between the day- and night-time maps might be due to differing precipitation processes dominant during day and night and should be analyzed in more detail. For a final statement a climatological time period of the precipitation frequency and intensity maps for both data sets has to be analyzed. Concerning the high spatial and temporal resolution of MSG SEVIRI, such climatological analyzes are now possible with the introduced retrieval scheme.

In the previous paragraphs, the applicability of the new scheme, and the feasibility of an operational quasi-continuous precipitation

detection based on MSG SEVIRI data have been shown. The maps presented give an outlook on the potential of the new retrieval technique for climatological studies. Thereby, valuable climatological information about the spatio-temporal precipitation distribution in the mid-latitudes can be obtained. Because of the high temporal and spatial resolution provided by MSG SEVIRI, the new scheme opens new perspectives in climatological studies, e.g. concerning the diurnal precipitation variations, the separation into different meteorological conditions and the influences of different precipitation processes.

Based on the reliable and physically founded discrimination of the rain area and its further subdivision into subareas of differing precipitation processes and rainfall intensities the next step, an improved instantaneous rainfall rate assignment can be tackled. Regarding the deficiencies associated with the assignment of instantaneous precipitation rates at the ground, the separation of the rain area into different rainfall intensity classes marks a valuable contribution. The rainfall rate assignment is generally based on a regression function between the rainfall rate measured at ground level and cloud properties derived from optical satellite data. In general low rainfall intensities occur over a much longer time period compared to high rainfall intensities from short-living convection clouds. As a consequence, low rainfall intensities dominate the data set in the sense, that the resulting regression function used to assign the rainfall rate yields an underestimation of high rainfall rates. A regression function derived separately for each detected intensity class can improve the accuracy and the representativeness of the retrieved regression function.

Another application field, to which the new scheme can make a considerable contribution are hybrid techniques intending to merge passive microwave (PMW) based retrieval techniques with data from GEO satellite systems in order to overcome the low spatial and especially the low temporal resolution of the PMW sensors aboard low earth orbits (LEO) systems (e.g. Joyce et al. 2004; Kidd et al. 2003; Kuligowski 2002; Miller et al. 2001; Turk et al. 2000; Hsu et al. 1999; Kummerow & Giglio 1995). As these hybrid techniques still rely on infrared brightness temperatures from the GEO system, the new developed retrieval technique for MSG SEVIRI offers the potential to enhance the quality and reliability of the merged rainfall products.

References

BUNDESMINISTERIUM FÜR UMWELT, NATURSCHUTZ UND REAKTORSICHERHEIT (Hrsg., 2003): Hydrologischer Atlas von Deutschland. Freiburger Verlagsdienste, Freiburg.

HOUZE, R. A. (1993): *Cloud Dynamics*, Vol. 53. of *International Geophysics Series*, Academic Press, San Diego.

HSU, K. L., H. V. GUPTA, X. G. GAO & S. SOROOSHIAN (1999): Estimation of physical variables from multichannel remotely sensed imagery using a neural network: Application to rainfall estimation. - *Water Resources Research, 35*: 1605-1618.

JOYCE, R. J., J. E. JANOWIAK, P. A. ARKIN & P. XIE (2004): CMORPH: A method that produces global precipitation estimates from passive microwave and infrared data at high spatial and temporal resolution. - *Journal of Hydrometeorology, 5:* 487–503.

KIDD, C., D. R. KNIVETON, M. C. TODD & T. J. BELLERBY (2003): Satellite Rainfall Estimation Using Combined Passive Microwave and Infrared Algorithms. - *Journal of Hydrometeorology, 4*: 1088-1104.

KULIGOWSKI, R. J. (2002): A self-calibrating real-time GOES rainfall algorithm for short-term rainfall estimates. - Journal of Hydrometeorology, 3: 112-130.

KUMMEROW, C. & L. GIGLIO (1995): A method for combining passive microwave and infrared rainfall observations. - *Journal of Atmospheric and Oceanic Technology, 12*: 33-45.

MILLER, S. W., P. A. ARKIN & R. J. JOYCE (2001): A combined microwave/infrared rain rate algorithm. - *International Journal of Remote Sensing, 22:* 3285 – 3307.

TURK, F. J., J. HAWKINS, E. A. SMITH, F. S. MARZANO, A. MUGNAI & V. LEVIZZANI (2000): Combining SSM/I, TRMM and infrared geostationary satellite data in a near-real-time fashion for rapid precipitation updates: advantages and limitations. *Proceedings of the 2000 Eumetsat Meteorological Satellite Data Users' Conference, EUMETSAT*: 452-459.

WEISCHET, W. & W. ENDLICHER (2000): Regionale Klimatologie. Teil 2. Die Alte Welt. Europa, Afrika, Asien. Teubner, Stuttgart, 626 pp.

CHAPTER 8

Zusammenfassung

8 Zusammenfassung

Informationen über die raum-zeitliche Niederschlagsverteilung sind von großem Nutzen in der Landwirtschaft, im Wasserbau, in der Klimatologie und im Bereich des Risikomanagements. In den meisten Gebieten der Erde ohne bodengebundene Radarnetzwerke existierte bislang keine adäquate Methode zur räumlich und zeitlich hochaufgelösten Erfassung und Beobachtung des Niederschlags.

Aufgrund der spektralen Begrenzung basierten existierende Verfahren zur Niederschlagserfassung mit Satellitendaten auf einem Zusammenhang zwischen der Regenwahrscheinlichkeit und -intensität und der Wolkenoberflächentemperatur in einem Infrarot-Kanal. Diese Verfahren zeigen erhebliche Schwächen hinsichtlich der Niederschlagsprozesse in den Mittelbreiten.

Verbesserte Techniken zur Erfassung der Niederschlagsfläche, die auf der erhöhten spektralen Auflösung von Satellitensystemen der neuesten Generation beruhen, waren auf polar umlaufende Systeme mit einer schlechten zeitlichen Auflösung beschränkt. Darüber hinaus waren diese Verfahren nur bei Tag anwendbar. Mit der Verfügbarkeit des Spinning-Enhanced Visible and InfraRed Imager (SEVIRI) an Bord von Meteosat Second Generation (MSG) seit Anfang 2004 steht ein geostationäres Satellitensystem mit einer deutlich verbesserten spektralen und räumlichen Auflösung zur Verfügung.

Das zentrale Ziel der vorliegenden Studie war daher die Entwicklung einer neuen Methode zur operationellen Niederschlagserfassung bei Tag und Nacht basierend auf MSG SEVIRI Daten. Der Fokus der neu entwickelten Methode lag dabei auf Niederschlagsprozessen im Zusammenhang mit außertropischen Zyklonen in den Mittelbreiten. Daher ist es nicht nur zur Erfassung konvektiv dominierter Niederschlagssituationen geeignet, sondern darüber hinaus auch für die Erfassung advektiv-stratiform regnender Wolkenbereiche einsetzbar.

Die grundlegenden Hypothesen der vorliegenden Studie waren:

- MSG SEVIRI gestattet die Erfassung der Niederschlagsfläche basierend auf Informationen über den Wolkenwasserweg und die Wolkenphase.
- MSG SEVIRI gestattet die Differenzierung von Bereichen unterschiedlicher Niederschlagsprozesse und -intensitäten.
- Die Erfassung der Niederschlagsfläche und die Differenzierung von Bereichen unterschiedlicher

Niederschlagsprozesse und -intensitäten kann bei Tag und Nacht in vergleichbarer Genauigkeit erfolgen.

Der Ansatz zur Untersuchung der Hypothesen beruht auf folgendem Konzeptmodell, welches die Grundlage für das neu entwickelte Verfahren zur Erfassung und Differenzierung der Niederschlagsfläche basierend auf MSG SEVIRI darstellt:

- Regnende Wolkenbereiche sind durch einen ausreichend hohen Wolkenwasserweg und das Vorhandensein von Eispartikeln in den oberen Bereichen gekennzeichnet.
- Wolkenbereiche erhöhter Niederschlagsintensität sind durch einen höheren Wolkenwasserweg sowie einen höheren Gehalt an Eispartikeln in den oberen Bereichen gekennzeichnet.
- Konvektive Wolken mit sehr hohen Niederschlagsintensitäten sind durch eine große vertikale Mächtigkeit und eine hochreichende kalte Wolkenobergrenze gekennzeichnet.

Basierend auf diesem Konzeptmodell besteht die neu entwickelte Technik aus einer völlig neuen Methodik, bestehend aus einer Vielfalt neuer und innovativer Algorithmen und Ansätze. Die folgenden drei Komponenten bilden den Schwerpunkt der neuen Technik:

- Ein neues Verfahren zur Erfassung der Niederschlagsfläche bei Tag und Nacht wurde für MSG SEVIRI entwickelt. Dieses gestattet nicht nur die Erfassung von konvektiv dominierten Regenflächen, sondern darüber hinaus auch die Erfassung von advektiv-stratiformen Niederschlagsfeldern (z.B. im Zusammenhang mit Frontensystemen in den Mittelbreiten). Das Verfahren beruht auf Informationen über den Wolkenwasserweg und die Wolkenphase in den oberen Wolkenbereichen. Das Tag-Verfahren verwendet den VIS_0.6 und den NIR_1.6 Kanal, um Informationen über den Wolkenwasserweg zu erhalten. Das Nacht-Verfahren berücksichtigt die Kanaldifferenzen dT_3.9_10.8, dT_3.9-7.3, dT_8.7_10.8 und dT_10.8_12.1, um implizite Informationen über den Wolkenwasserweg zu gewinnen. Zusätzlich werden sowohl bei Tag als auch bei Nacht die Kanaldifferenzen dT_8.7_10.8 und dT_10.8_12.1 zur Gewinnung von Informationen über die Wolkenphase herangezogen (Kapitel 4 und 5).
- Ein für konvektive Niederschlagsprozesse in den Mittelbreiten geeignetes Infrarot-Verfahren wurde erfolgreich auf MSG SEVIRI übertragen und angepasst. Das Phänomen positiver Temperaturdifferenzen zwischen den Wasserdampf – und Infrarotkanälen (dT_WV_IR), welches die Erfassung und

Klassifikation konvektiv dominierter Niederschlagsbereiche gestattet, wurde für die Wasserdampf (WV)- und Infrarotkanäle (IR) von MSG SEVIRI untersucht. Basierend auf Strahlungstransferrechnungen, die die Existenz von positiven dT_WV_IR für alle SEVIRI WV-IR Differenzen belegten, konnte die dT_WV_IR-Technik auf MSG SEVIRI angewendet und übertragen werden (Kapitel 3).

- Ein neues Verfahren zur Differenzierung von Bereichen unterschiedlicher Niederschlagsprozesse und -intensitäten wurde für MSG SEVIRI entwickelt. Die Prozess- und Intensitätsunterscheidung beruht auf Informationen über die Höhe der Wolkenobergrenze, den Wolkenwasserweg und die Wolkenphase in den oberen Bereichen. Die Klassifikation erfolgt schrittweise. In einem ersten Schritt wird die Niederschlagsfläche in die beiden Bereiche konvektiver und advektiv-stratiformer Niederschlagsprozesse aufgeteilt. Anschließend werden beide Bereiche in Gebiete unterschiedlicher Niederschlagsintensitäten untergliedert. Die Erfassung und Differenzierung der konvektiv dominierten Niederschlagsflächen basiert auf Informationen über die Höhe der Wolkenobergrenze, abgeleitet aus den WV-IR Differenzen dT_WV6.2_IR10.8 und dT_WV7.3_IR12.1 sowie der Temperatur der Wolkenobergrenze im IR_10.8 Kanal. Die Differenzierung der advektiv-stratiformen Niederschlagsflächen beruht auf Informationen über den Wolkenwasserweg und die Wolkenphase in den oberen Bereichen. Informationen über die Wolkenphase werden anhand der Kanaldifferenzen dT_8.7_10.8 und dT_10.8_12.1 gewonnen. Zur Gewinnung von Informationen über den Wolkenwasserweg werden bei Tag der VIS_0.6 und der NIR_1.6 Kanal, bei Nacht die Kanaldifferenzen dT_3.9_10.8, dT_3.9-7.3, dT_8.7_10.8 und dT_10.8_12.1 herangezogen (Kapitel 6).

Die durch das neu entwickelte Verfahren erfasste Niederschlagsfläche und die differenzierten Bereiche unterschiedlicher Niederschlagsprozesse und -intensitäten wurden mithilfe von bodengebundenen Radardaten über Deutschland (stellvertretend für Niederschlagsprozesse in den Mittelbreiten) validiert. Die Ergebnisse der Validierungsstudie zeigten eine überzeugende Performanz der neuen Technik sowohl hinsichtlich der identifizierten Niederschlagsfläche als auch bezüglich der differenzierten Niederschlagsprozesse und -intensitäten und konnten die Stabilität des vorgestellten Konzeptmodells belegen. Basierend auf der

erfolgreichen Implementierung der drei Komponenten und der guten Performanz des neu entwickelten Verfahrens können die grundlegenden Hypothesen als bestätigt angesehen werden:

MSG SEVIRI gestattet die Erfassung der Niederschlagsfläche und ihre Differenzierung in Bereiche unterschiedlicher Niederschlagsprozesse und -intensitäten basierend auf Informationen über den Wolkenwasserweg, die Wolkenphase in den oberen Bereichen und die Höhe der Wolkenobergrenze. Die Erfassung und Differenzierung der Niederschlagsfläche erfolgt bei Tag und Nacht mit vergleichbarer Genauigkeit.

Somit ist ein solider, verlässlicher und physikalisch begründeter Ansatz für die quasi-kontinuierliche Erfassung und Beobachtung des Niederschlags mit einer hohen zeitlichen und räumlichen Auflösung, basierend auf MSG SEVIRI, gegeben. Die vorgestellte Technik stellt einen wichtigen Beitrag im Kontext Satelliten basierter quantitativer Niederschlagserfassung in Nah-Echtzeit dar. Abgesehen von ihrer Anwendbarkeit im Zuge klimatologischer Studien zur Analyse der raum-zeitlichen Niederschlagsverteilung kann sie wertvollen Input für die Datenassimilierung zur Initialisierung numerischer Wetter-, Klima- sowie hydrologischer Modelle liefern. Die hohe räumliche und besonders die hohe zeitliche Auflösung von SEVIRI, die die Berücksichtigung der kurzzeitigen Niederschlagsdynamik gestattet, ist hinsichtlich der Kurzfristvorhersage sowie des Risikomanagements von großem Nutzen. Für all diese Anwendungen von großer gesellschaftlicher, hydrologischer und klimatologischer Relevanz stellt das neue Verfahren Informationen von außerordentlichem Wert bereit.